ÇUKUROVA UNIVERSITY
INSTITUTE OF NATURAL AND APPLIED SCIENCES

MSc THESIS

Arda YENİÇUN

THE USE OF SHROUDED CYLINDER AND SPLITTER PLATE ON CONTROLLING THE VORTEX SHEDDING IN THE ANNULAR REGION

DEPARTMENT OF MECHANICAL ENGINEERING

ADANA-2018

ÇUKUROVA UNIVERSITY

INSTITUTE OF NATURAL AND APPLIED SCIENCES

THE USE OF SHROUDED CYLINDER AND SPLITTER PLATE ON CONTROLLING THE VORTEX SHEDDING IN THE ANNULAR REGION

Arda YENİÇUN

MSc THESIS

DEPARTMENT OF MECHANICAL ENGINEERING

We certify that the thesis titled above was reviewed and approved for the award of degree of the Master of Science by the board of jury on 07/09/2018.

Asst. Prof. Dr. Engin PINAR	Prof. Dr. Beşir ŞAHİN	Assoc.Prof.Dr.Cuma KARAKUŞ
SUPERVISOR	MEMBER	MEMBER

This MSc Thesis is written at the Department of Institute of Natural and Applied Sciences of Çukurova University.

Registration Number:

Prof. Dr. Mustafa GÖK

Director

Institute of Natural and Applied Sciences

This MSc Thesis was supported financially by the Scientific and Technological Researched Council of Turkey under contract no:114R087.

ABSTRACT

MSc THESIS

THE USE OF SHROUDED CYLINDER AND SPLITTER PLATE ON CONTROLLING THE VORTEX SHEDDING IN THE ANNULAR REGION

Arda YENİÇUN

ÇUKUROVA UNIVERSITY
INSTITUTE OF NATURAL AND APPLIED SCIENCES
DEPARTMENT OF MECHANICAL ENGINEERING

Supervisor : Asst. Prof. Dr. Engin PINAR
Year:2018, Pages:111
Jury : Asst. Prof. Dr. Engin PINAR
: Prof. Dr. Beşir ŞAHİN
: Assoc. Prof. Dr. Cuma KARAKUŞ

The purpose of this work was to control flow structures in the area between the inner and outer cylinders, fluctuations of velocity components and the vibration generated by this flow structure on the cylinder. This study has three main components. The first component was inner cylinder which has D_i = 50mm diameter which kept constant for all experiments. The second component was perforated outer cylinder which has three different porosities such as, β_c =0.3, 0.5, 0.7. The third component was splitter plate which has also three different porosities, β_p =0.3, 0.5, 0.7. The splitter plate had five different plate angles as α = 60°, 90°, 120°, 150°, 180° taking the flow direction as a reference line. The Reynolds number was kept constant at Re = $5x10^3$ based on the inner cylinder diameter. Quantitative and qualitative outcomes were obtained by dye visualization and PIV measurements to define the best combination of cylinders and splitter plate for controlling flow structure. The results showed that β_c =0.3 outer cylinder causes a significant decrease in the TKE_{max} value and also the number of vortices in annular region decreased to one instead of two, because this outer cylinder caused a reduction in the amount of flow which goes into this inner region. In general, the outer cylinder with low porosities such as β_c = 0.3 and β_c = 0.5 cylinder were found to be better for diminishing the TKE_{max} than βc = 0.7 outer cylinder. The results indicated that the time average vorticity magnitudes increase by increasing porosity ratios of splitter plate and outer cylinder. It was concluded that α = 150° was the most effective plate angle for control flow structure when used with β_c =0.5 cylinder and β_p =0.5 plate.

Key Words: Cylinder, Passive control, PIV, Turbulent kinetic energy

ÖZ

YÜKSEK LİSANS TEZİ

SİLİNDİR ÇİFTİ ARA BÖLGESİNDEKİ GİRDAPLARIN DELİKLİ SİLİNDİR VE AYIRICI PLAKA İLE KONTOLÜ

Arda YENİÇUN

ÇUKUROVA ÜNİVERSİTESİ
FEN BİLİMLERİ ENSTİTÜSÜ
MAKİNA MÜHENDİSLİĞİ ANABİLİM DALI

Danışman : Dr. Öğr. Üyesi. Engin PINAR
Yıl:2018, Sayfa:111
Jüri : Dr. Öğr. Üyesi. Engin PINAR
: Prof. Dr. Beşir ŞAHİN
: Doç. Dr. Cuma KARAKUŞ

Bu çalışmanın amacı, iç ve dış silindirler arasındaki bölgedeki akış yapılarını, hız bileşenlerinin dalgalanmalarını ve silindir üzerinde bu akış yapısının oluşturduğu titreşimi kontrol etmektir. Bu çalışmanın üç ana bileşeni vardır. İlk bileşen, D_i = 50 mm çapa sahip olan ve tüm deneyler için sabit tutulan iç silindirdir. İkinci bileşen üç farklı açıklık oranına (β_c = 0.3, 0.5, 0.7) sahip delikli dış silindirdir. Üçüncü bileşen de üç farklı açıklık oranına (β_p = 0.3, 0.5, 0.7) sahip olan ayırıcı plakadır. Ayırıcı plaka akış yönüne göre α = 60°, 90°, 120°, 150°, 180° olarak beş farklı açıya sahiptir. Reynolds sayısı iç silindir çapına göre Re = 5000 değerinde sabit tutulmuştur. Akış yapısını kontrol etmek için boya görselleştirme ve PIV deneyleri ile nicel ve nitel sonuçlar elde edilmiştir. Sonuçlar, β_c = 0.3 dış silindirin, TKE_{maks} değerinde önemli bir azalmaya neden olduğunu ve ayrıca ara bölgedeki döngü sayısının iki yerine bire düşürdüğünü göstermiştir. Çünkü bu dış silindir ara bölgeye giren akış miktarında azalmaya neden olmuştur. Genel olarak, düşük açıklık oranlarının TKE_{maks} değerlerini düşürmedeβ_c = 0,7 dış silindirden daha iyi olduğu tespit edilmiştir. Sonuçlar, zaman ortalama eş düzey konturlarının, ayırıcı plakanın ve dış silindirin artan açıklık oranları ile arttığını göstermiştir. α = 150° plaka açısının, βc =0.5 dış silindir ve βp =0.5 plaka ile uygulandığında, akış yapısının kontrolü için en etkili bir parametre olduğu ve TKE_{maks} değerini yüksek oranda azalttığı sonucuna varılmıştır.

Anahtar Kelimeler: Silindir, Pasif kontrol, PIV, Türbülans kinetik enerji

EXPANDED ABSTRACT

There are several factors that affect the flow characteristics cylinder, particularly fluctuations of velocity components and the vibration of the cylinder generated by this flow structure. Here, the main factor is the Reynolds number (Re), In general, flow characteristics and velocity fluctuations can cause vortex formation, flow separation and vortex induced vibration (VIV) on the circular cylinder. The flow separation phenomena and the vortex formation at downstream of the cylinder causes undesirable effects on the cylinder consequently resulting the vibration, sounds caused from that vibration and even failure of a body under a certain period of time. The occurrence of flow separation from the surface of the submerged cylinder is due to the pressure recovery or adverse pressure that occurs along the halfway of the cylinder. Swirl flow formation starts with flow separation leading to the vortex shedding. When these swirling vortices are discontented from the surface of the cylinder they apply forces to the cylinder. That is to say, vortex shadings occur on both sides of the cylinder at different times and apply forces in opposite directions to the cylinder when those vortices roll away from the cylinder surface. Under a high rate of forces applied the cylinder may start vibrating the cylinder. When the frequency of vortex shedding is high enough, for example having wind storm the cylinder may generate sound due to the high rate of vibrations. It is substantially important to control the aggressive vortical flow structure around the cylinder and hence it is better to avoid these undesirable flow effects. Because there are a lot of engineering applications that experiences these effects such as turbine blades, bridges, high tower constructions etc. There are also underwater applications like underwater pipelines and marine cables. Underwater applications and researches on bluff bodies are the motivation for the present work.

Among all bluff bodies, the circular cylinder take important place and are preferred (Gabbai & Benaroya, 2005; Williamson, 1996) due to its simple geometry and its easy implementation. There are two different strategies in literature to control the flow characteristics of the circular cylinder. These are active flow control and

passive flow control strategies. Passive flow control techniques were examined in more detail than the active flow controls because this work encloses the passive flow control. The passive flow control technique does not need any external energy source. The passive flow control techniques could be classified into two categories. Affecting the shear layer of body and separation of flow lines with some external devices are considered as the first category. The second category is to try stopping the momentum transfer of the layers using perforated coating or shroud elements (Zdravkovich, 1981). In this study, both shrouded cylinder and splitter plate were used as a control element.

The experiments were carried out in a large-scale water channel located in the Fluid Mechanics Laboratory at Çukurova University. The experiments were carried out using two different test setups. Firstly, the dye-injection flow visualization experiments carried out in order to demonstrate the flow behavior in the annular region. Qualitatively information about the flow behavior were obtained from the dye experiments. The second test setup was performed using the particle image velocimetry (PIV) technique. Quantitative measurements were obtained from PIV experiments.

In general, the dye-injection flow visualization experiments provide information about the instantaneous vortical flow, for example, the formation of vorticity concentrations and the interactions between these concentrations. It can be easily seen the splitting of large-scale vortices into small pieces when these dye visualizations are observed with the necked eye. The solid cylinder with diameter of D_i = 50 mm was manufactured from acetyl polymer called Delrin. The outer meshed cylinders (control elements) with diameter of D_o =125 mm was manufactured from chrome-nickel screens. The Reynolds number was kept constant as Re =5000 based on the inner cylinder diameter. The method applied in the dye-injection flow visualization experiments was based on the light sensitive dye (Fluorescent Paint, Rhodamine 6G or Rhodamine B) illuminated with a continuous type laser in the dark environment. The instantaneous images were taken and organized for all experimental parameters.

Increasing technological developments provide new measuring techniques. All measurement techniques have some advantages and disadvantages associated with the specific method. The Particle Image Velocimetry method (PIV) is a non-intrusive

technique used to measure an instantaneous two-dimensional velocity vector field over a specified flow field. The velocity was determined by measuring the displacement of particles in the flow field that is illuminated by a laser light sheet.

Although there was an abundant investigation about the passive flow control technique by using the shrouded cylinder and the splitter plate around the circular cylinder, studies up to now did not focus on the annular region which was defined as the region between the inner and the outer cylinder. In this present work, the aim was controlling the vortices generated by the inner cylinder in the annular region. Shrouded cylinders and splitter plate were used for this purpose and these plates were placed at different angles taking the flow direction as a reference line. The diameter ratio of the cylinders is kept constant as $D_i/D_o = 0.4$ throughout the whole study such as the Reynolds number. During the experiments, the inner cylinder and the perforated outer cylinder were positioned concentrically. The effects of the porosity of the outer cylinders β_c, the porosity of the splitter plate, β_p and the plate angle, α on vortical flow behavior were investigated experimentally in deep water. For the porosity, three different values were chosen as $\beta = 0.3$, 0.5 and 0.7 both the outer cylinder and the splitter plate. The other parameter was the plate angle α. There were five different values for the plate angle as $\alpha = 60°, 90°, 120°, 150°, 180°$.

The use of the outer cylinder alone (no inner cylinder and the splitter plate) caused the circulation in the upper and lower side of the outer cylinder at the cylinder with low porosities such as $\beta_c = 0.3$ and $\beta_c = 0.5$. Thus, it was understood that the circulation which indicated by F_3 in Figure 4.6 originated from the outer cylinder.
On the other hand, the outer cylinder had a significant effect on decreasing the turbulence intensity of flow in the annular region as seen in Figure 4.7.

The dye visualization experiments showed that when the inner cylinder use with the porosity of the outer cylinder, which is $\beta_c = 0.3$ act like nearly a non-perforated cylinder. Therefore, it does not allow the sufficient flow into the annular region from the outer cylinder holes. It was found that from the streamline topologies for the outer cylinder with the porosity of $\beta c = 0.3$, a large focal point, F_1 formed instead of the focal points, F_1 and F_2 in the annular region when we use the perforated plate with the

porosity βp = 0.3 at plate angles of α = 60°, 90°, 120°, 150° as seen in Figure 4.8. Therefore, it was determined that the outer cylinder with porosity of β_c = 0.3 was not successful in controlling vortical flow structures and fluctuations of velocity components in the annular region. The maximum value of TKE in the annular region was evaluated for the outer cylinder with the porosity of β_c = 0.5 as 0.0247. On the other and the TKE_{max} values were found to be 0.0274 and 0.0323 for the porosities of the outer cylinder β_c = 0.3 and β_c = 0.7 respectively. These values of TKE_{max} showed that the outer cylinder with the porosity of β_c = 0.5 is the most successful porosity, β_c for decreasing the fluctuations flow data in the near wake which is an indication of effective suppression of vortex shedding. In general, the perforated outer cylinder with low porosities, β_c such as β_c = 0.3 and β_c = 0.5 were better for diminish the TKE_{max} value. On the other hand, the porosity of the plate was less effective in reducing the TKE_{max} value than the porosity of the outer cylinder. But, it could be said that the splitter plate succeeded in influencing the interaction of the vorticity concentrations with each other. A reduction of 52% in TKE_{max} values was achieved when the porosity of the plate, β_p = 0.5 at the plate angle of α = 150° with the porosity of the outer cylinder β_c = 0.5 is used. According to this reduction the above case was the most effective case for decreasing the TKE_{max} value and the fluctuations in the near wake. Furthermore, the plate angle α = 150° had a trend as decreasing the maximum value of TKE for the outer cylinder with the porosities of β_c = 0.5 and 0.7. Thus, the plate angle, α = 150° also can be advised within the aid of a complete elimination of upper and lower vorticity layer interactions in the annular region.

Although previous studies using the perforated outer cylinders and the plates could be found in the literature, there were not many studies investigating the annular region like the present study. In addition to the results obtained from this research, this study could be expanded to specify better control method on the control of vortex formation and turbulence intensity and possibly the more appropriate combination might be found by using different control elements and porosities, β_c.

GENİŞLETİLMİŞ ÖZET

Dairesel silindir ardındaki akış karakteristiklerini, özellikle hız bileşenlerinin dalgalanmaları ve silindir üzerindeki bu akış yapısı tarafından üretilen titreşimlerini etkileyen bazı faktörler vardır. Örneğin, Reynolds sayısı, Re ve suyun durumu vb. gibi. Bu akış karakteristikleri ve hız dalgalanmaları, dairesel silindir ardında girdap oluşumuna, akış ayrışmasına ve girdap kaynaklı titreşime (VIV) neden olabilir. Akış ayrılma fenomeni ve silindirin arkasındaki girdap oluşumuna bağlı düşük basınç, silindir üzerinde istenmeyen etkilere neden olur ve sonuç olarak titreşimlere, bu titreşimden kaynaklanan seslere ve belirli bir zaman sonunda bir yapının kırılmasına neden olur. Bu nedenlerden dolayı silindirin arkasındaki akış oluşumunu kontrol etmek çok önemlidir. Ayrıca türbin kanatları, ısı değiştirici tüpleri gibi bu etkileri yaşayan çok sayıda mühendislik uygulaması vardır. Sualtı boru hatları ve deniz kabloları gibi su altı uygulamaları da yine bu etkilerin altında varlıklarını sürdürmektedir. Sualtı uygulamaları ve dairesel şekilli yapılar üzerine yapılan araştırmalar bu tez için motivasyon olmuştur.

Tüm katı gövdeler arasında, basit geometrisi ve kolay uygulanması nedeniyle dairesel silindir önemli bir yer tutmuş ve tercih edilmiştir (Gabbai & Benaroya, 2005; Williamson, 1996). Dairesel silindirin ardındaki akış karakteristiklerini kontrol etmek için literatürde iki farklı strateji vardır. Bunlar aktif akış kontrolü ve pasif akış kontrol stratejileridir. Pasif akış kontrol teknikleri, aktif akış kontrollerinden daha ayrıntılı olarak incelenmiştir, çünkü bu çalışma pasif akış kontrolünü uygulaması alanına girmektedir. Pasif akış kontrol tekniği uygulamaları herhangi bir harici enerji kaynağına ihtiyaç duymamaktadır. Pasif akış kontrol teknikleri iki kategoriye ayrılabilir. Bir vücudun kayma tabakasını etkilemek ve bazı harici cihazlar kullanarak akış hatlarının ayrılmasını kontrol etmek ilk kategori olarak kabul edilebilir. İkinci kategori, delikli kaplama veya örtü elemanları kullanılarak akım çizgilerinin momentum transferini durdurmayı

denemektir (Zdravkovich, 1981). Bu çalışmada hem delikli dış silindir hem de ayırıcı plaka kontrol elemanı olarak kullanılmıştır.

Deneyler Çukurova Üniversitesi Akışkanlar Mekaniği Laboratuvarı'nda bulunan büyük ölçekli bir su kanalında gerçekleştirilmiştir. Deneyler iki farklı test düzeni kullanılarak gerçekleştirilmiştir. İlk olarak, boya-enjeksiyon akış görselleştirme deneyleri, iç ve dış silindir ara bölgesinde akış davranışını görselleştirmek için gerçekleştirilmiştir. Ara bölgedeki akış davranışı hakkında niteliksel olarak bilgi, boya deneylerinden elde edilmiştir. İkinci test kurulumu ise PIV tekniği kullanılarak yapılmıştır. Kantitatif ölçümler PIV deney düzeneğinde yapılan ölçümlerle elde edilmiştir. Genel olarak, boya-enjeksiyon akış görselleştirme deneyleri, örneğin, girdap konsantrasyonlarının oluşumu ve bu konsantrasyonlar arasındaki etkileşimler gibi anlık girdaplı akış hakkında bilgiler verir.

Çıplak gözle bu boya görselleri incelendiğinde, büyük ölçekli girdapların küçük parçalara bölünmesi kolayca görülebilir. İç silindir modeli (D_i = 50 mm), çok yönlü bir mühendislik polimeri olan Delrin adlı bir tür asetil polimerinden üretilmiştir. Farklı açıklık oranlarına sahip ve çapı 125 mm olan delikli dış silindirler (kontrol elemanları) krom-nikel malzemeden imal edilmişlerdir. Reynolds sayısı iç silindir çapına göre Re = 5000 olarak sabit tutulmuştur. Boya-enjeksiyon akış görselleştirme deneylerinde uygulanan yöntem, karanlık ortamda sürekli tipte bir lazerle aydınlatılan ışığa duyarlı boyaya (Floresan Boya, Rhodamine 6G veya Rhodamine B) dayanmaktadır. Boya deneylerinden bütün deney parametreleri için anlık akış görselleri alınmış ve bu görseller organize edilerek sunulmuştur.

Artan teknolojik gelişmeler, yeni ölçüm teknikleri de sağlamıştır. Tüm ölçüm tekniklerinin, belirli yöntemle ilişkili bazı avantajları ve dezavantajları vardır. Parçacık Görüntü yöntemi, PIV, incelenen alan altındaki anlık iki boyutlu hız vektör alanını ölçmek için kullanılan bir tekniktir. Hız, bir lazer tabakası ile

aydınlatılan bir akış alanında parçacıkların yer değiştirmesinin ölçülmesiyle belirlenmiştir.

Dairesel silindir etrafında delikli silindir ve ayırıcı plaka kullanılarak pasif kontrol tekniği konusunda bol miktarda araştırma yapılmasına rağmen, şimdiye kadar yapılan çalışmalar, iç ve dış silindir arasındaki bölge olarak tanımlanan ara bölgeye odaklanmamıştır. Mevcut çalışmada amaç, iç silindir tarafından oluşturulan girdapları kontrol etmektir. Bu amaçla delikli silindirler ve ayırıcı plaka kullanılmış ve bu plakalar akış yönünü referans alarak farklı açılarda yerleştirilmiştir. Silindirlerin çap oranı, Reynolds sayısı gibi tüm çalışma boyunca Di / Do = 0.4 olarak sabit tutulmuştur. Deneyler sırasında, iç silindir ve delikli dış silindir eş merkezli olarak konumlandırılmıştır. Dış silindirlerin açıklık oranı, β_c plaka açıklık oranı, β_p ve plaka açısının, α girdaplı akış yapısı üzerindeki etkileri derin suda deneysel olarak incelenmiştir. Hem delikli dış silindir hem de ayırıcı plaka için belirlenen açıklık oranları β = 0.3, 0.5, 0.7 olarak üç farklı değerden oluşmaktadır. Ayrıca plakanın akış yönüne göre konumlandırıldığı beş farklı plaka açısı mevcuttur. Bunlar; α = 60°, 90°, 120°, 150°, 180° olarak sıralanabilir.

Dış silindirin tek başına kullanılması (iç silindir ve ayırıcı plaka kullanılmadan), βc = 0.3 ve βc = 0.5 gibi düşük gözeneklere sahip dış silindirlerin üst ve alt tarafında girdapların oluşmasına neden olmuştur. Bu durum F_3 ile gösterilen sirkülasyonun dış silindirden kaynaklandığını ortaya çıkarmıştır. (Figure 4.6). Diğer taraftan, dış silindirin iç ve dış silindir ara bölgesindeki akış türbülans değerlerini azaltmada önemli bir etkisi olmuştur. (Figure 4.7).

Boya görselleştirme deneyleri, iç silindirin, dış silindir açıklık oranı β_c = 0.3 ile kullanıldığında neredeyse gözeneksiz bir silindir gibi davrandığını göstermiştir. Bu nedenle, dış silindir deliklerinden ara bölgeye yeterli akışın girmesine izin vermemiştir. Açıklık oranı β_c = 0.3 olan dış silindir için çizilen ortalama akım çizgilerinden, açıklık oranı β_p = 0.3 olan plaka ve plaka açıları α = 60°, 90°, 120°, 150° ile kullanıldığında, iç ve dış silindir ara bölgesinde odak notaları F_1 ve F_2 yerine tek ve büyük bir odak nokta F_1 oluştuğu görülmüştür

(Figure 4.8). Bu nedenle, açıklık oranı β_c = 0.3 olan dış silindirin, girdaplı akış yapısının kontrol edilmesinde ve ara bölgedeki hız bileşenlerinin dalgalanmalarını sönümlemede başarılı olmadığı tespit edilmiştir. TKE_{max} değeri, açıklık oranı β_c = 0.5 olan dış silindir için 0.0247 olarak ölçülmüştür. Diğer tarafta ise açıklık oranı β_c = 0.3 ve β_c = 0.7 olan dış silindirler için TKE_{max} değerleri sırasıyla 0.0274 ve 0.0323 olarak bulunmuştur. Bu TKE_{max} değerleri, açıklık oranı β_c = 0.5 olan dış silindirin, girdap dökülmelerini bastırmada ve yakın art izinde meydana gelen dalgalanmaları azaltmada en etkili parametre olduğunu göstermiştir. Genel olarak, β_c = 0.3 ve β_c = 0.5 gibi düşük açıklık oranına sahip delikli dış silindirler TKE_{max} değerini azaltmada daha başarılı olmuşlardır. Diğer taraftan, plaka açıklık oranının TKE_{max} değerlerini düşürmede dış silindir açıklık oranına göre daha az etkili olduğu görülmüştür. Ancak ayırıcı plakanın iç silindirin hemen ardında oluşan girdapların birbirleri ile etkileşimini engellemede başarılı olduğu söylenebilir. Açıklık oranı β_c = 0.5 olan dış silindir ile birlikte açıklık oranı β_p = 0.5 olan plaka α = 150° ye ayarlanmış olarak kullanıldığında, TKE_{max} değerinde 52% oranında bir azalma elde edilmiştir. TKE_{max} değerindeki bu azalmaya göre, yukarıda açıklanan parametre, iç silindir art izindeki dalgalanmaları düşürmede en iyi kombinasyon olmuştur. Dahası, plaka açısı α = 150° için açıklık oranı β_c = 0.5 ve β_c = 0.7 olan dış silindir ile kullanıldığında, TKE_{max} değerini düşürme eğilimi gösterdiği tespit edilmiştir. Bu yüzden, plaka açısı α = 150°, hem TKE_{max} değerini düşürmedeki başarısı hem de ara bölgede, iç silindirin alt ve üst tarafında oluşan girdapların etkileşimi tamamen ortadan kaldırması dolayısıyla önerilebilir bir parametre olmuştur.

Literatürde delikli dış silindir ve plakaların kullanıldığı önceki çalışmalara sıkça rastlanmasına rağmen, bu çalışmadaki gibi iç ve dış silindir arasında kalan bölgeyi araştıran pek çalışma yoktur. Bu araştırmadan elde edilen sonuçlara ek olarak, bu çalışma en etkili kontrolü sağlamak için genişletilebilir ve muhtemelen farklı kontrol elemanlar ve açıklık oranları kullanılarak daha uygun bir kombinasyon bulunabilir.

ACKNOWLEDGEMENTS

First of all, I would like to express my sincere gratitude to my advisor, Asst. Prof. Dr. Engin PINAR for his great guidance, support and encouragement to develop myself and my studies. Beginning and starting of this work would not have been possible without his long-sightedness and supervision.

Secondly, I would like to thank with a deep sense of gratitude to Prof. Dr. Beşir ŞAHİN who established the fluid mechanics laboratory in Çukurova University and causing this thesis possible.

I sincerely thank Prof. Dr. Hüseyin AKILLI as a Head of Mechanical Engineering Department for his continuous and effective advices to improve myself.

My heartfelt thanks go to Asst. Prof. Dr. Tahir DURHASAN and Asst. Prof. Dr. Göktürk M. ÖZKAN who provided their invaluable time to train me in using experimental facilities in the lab. They always have been with me throughout the study. Without their moral and support it might be so difficult to finish this investigation.

I also thank Mehmet Oğuz TAŞCI, Mehmet Can PEKTAŞ and Sefa MERAL for their company and help during my experiments.

I would like to acknowledge the financial support of the Scientific and Technological Research Council of Turkey (TUBITAK) for funding this thesis under contract No: 114R087.

Although the words are not sufficient to imply their importance, lastly and most importantly I would like to thank my fiancé Yeşer SAMUR, my mother Tümay YENİÇUN, my father İbrahim E. YENİÇUN and my sister Cemre YENİÇUN for their trust, patience and encouragement throughout this study.

CONTENTS **PAGE**

LIST OF FIGURE **PAGE**

LIST OF ABBREVIATONS

D_i	: Inner cylinder diameter
D_o	: Perforated outer cylinder diameter
β	: Porosity
β_c	: Outer cylinder porosity
β_p	: Splitter plate porosity
α	: Splitter plate angle
h_L	: Distance between the plate surface and the laser sheet in plan view
h_W	: Water level
H	: Depth of the water in the channel
<y >	: Time averaged streamline
<w>	: Time averaged vorticity
U	: Free stream velocity
u	: Instantaneous velocity
TKE_{max}	: Maximum turbulent kinetic energy
Re	: Reynolds number
ν	: Kinematic viscosity

1. INTRODUCTION

The phenomenon of vortex formation around a circular cylinder is worth investigating problem for engineers and also still one of the attractive unknown problems in fluid dynamics. When an obstacle encountered vortex shedding, a significant wake flow fluctuations and hence fluctuating time varying forces can happen due to vortex shedding which causes structural vibrations. That is to say, it is commonly encountered that undesired flow induced vibration, noise generated from this vibration results in noise generation, vibration in various types bluff bodies such as bridges, submarines, automobiles and a high-rise structure. Furthermore, if the vortex shedding frequency coincides with the natural frequency of the bluff body, this structural type bluff body starts to resonate under fluctuating pressure forces generated by shedding vortices emanating from the shoulders of bluff bodies. Finally, the time varying pressure forces vibrates the body with a amplitude resulting in failures and considerable reduction in the life span of even huge structures.

1.1. Flow Around a Circular Cylinder

The flow structures especially that form around the circular cylinder, the resulting flow separation and vortex shedding have attracted many attentions of researchers for many years. The vortex shedding behaviors downstream of the circular cylinder have found itself a place in many articles because it gave useful information for the actual engineering application. The circular cylinder has wide range of working area due to its easy handling. Mechanical application of circular cylinder such as heat exchanger tubes, civil engineering applications such as chimneys, bridges and offshore structure and underwater applications such as underwater pipelines, marine cables can be an example of working areas that uses principles of flow over the circular cylinder both in water and air. The reason for the flow behavior over the circular cylinder studies draws such interest on itself is

that both the aerodynamic and the hydrodynamic data are useful for the applications mentioned above.

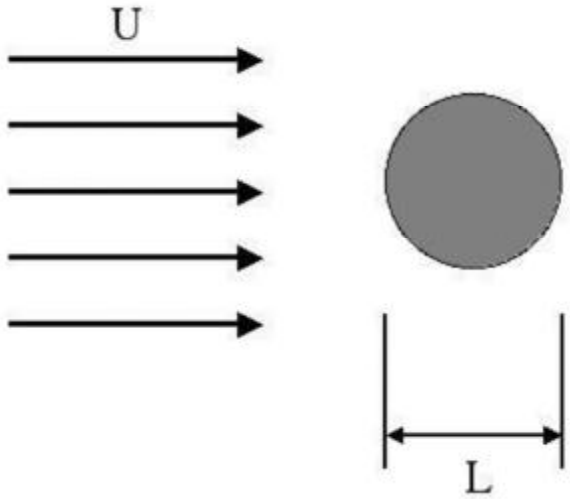

Figure 1.1 Top view of flow field with a circular cylinder

As you can see in Figure 1.1, when a fluid flow encounters the circular cylinder, complex flow behavior such as vortex shedding, flow separation and shear layer instability can be occurred in different Reynolds number and as a result of these flow structures there would be unavoidable lift and drag forces exerted to the cylinder. In the absence of external forces, the dynamics of the flow around a cylinder depends only on the Reynolds number ($Re = U_\infty D / \nu$ where U_∞ is the free-stream velocity far from the cylinder, D the cylinder diameter and ν the kinematic viscosity). That's why the Reynolds number, Re was an indispensable parameter to determine the flow pattern. In Figure 1.2 it is possible to see the flow downstream of the cylinder at high and low Re values.

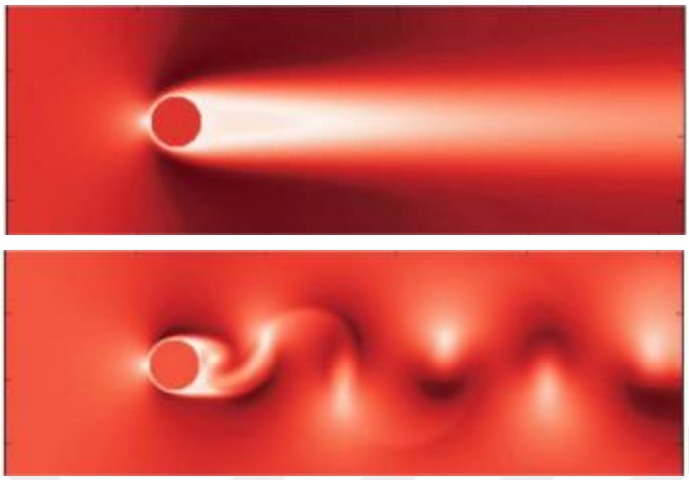

Figure 1.2 Vortex shedding downstream of a circular cylinder for low Re number (top) and high Re number (bottom)

The flow over a body called the laminate, turbulent, and critical named according to the Reynolds number, Re. In the 1996, Williamson (1996) explained these flow regimes with a clear picture as shown in Figure 1.3. The steady and two-dimensional flows occur at $Re \leq 6$. At this value only one separation point occurs and if the Reynolds number is increased up to value of 49, ($6 \leq Re \leq 49$), the flow continues to flow steady and two-dimensional. But further increase in Reynolds number, the vortex pair starts to form in downstream of the circular cylinder.

At the critical Reynolds number, Re = 49 the formation Von Karman vortex street takes place downstream of an obstacle. The instability of vortical flow structure suddenly increases causing the formation of this Von Karman Street even keeping the flow condition constant. The length of the wake flow region increases as this critical Reynolds number increases.

According the study performed by Williamson (1996), the field flow bounded by A-B, in other word for the Reynolds number in the range of $49 < Re < 194$ the flow regime is laminar. The laminar flow structure is illustrated in Figure 1.4. When Reynolds number increase, the wake flow instability increases. The term, which is known as the Strouhal instability and is described as the obstructive

separation of one of the two vortices formed downstream of a body, occurs between these intervals of Re number because of the high oscillations. As a result of this situation, Reynolds stresses increases. For the flow field bounded by B-C (190 < Re < 260) called wake transition regime. If the Reynolds number increases up to Re = 200, 2-D flow transformed 3-D and also the flow regime became turbulent.

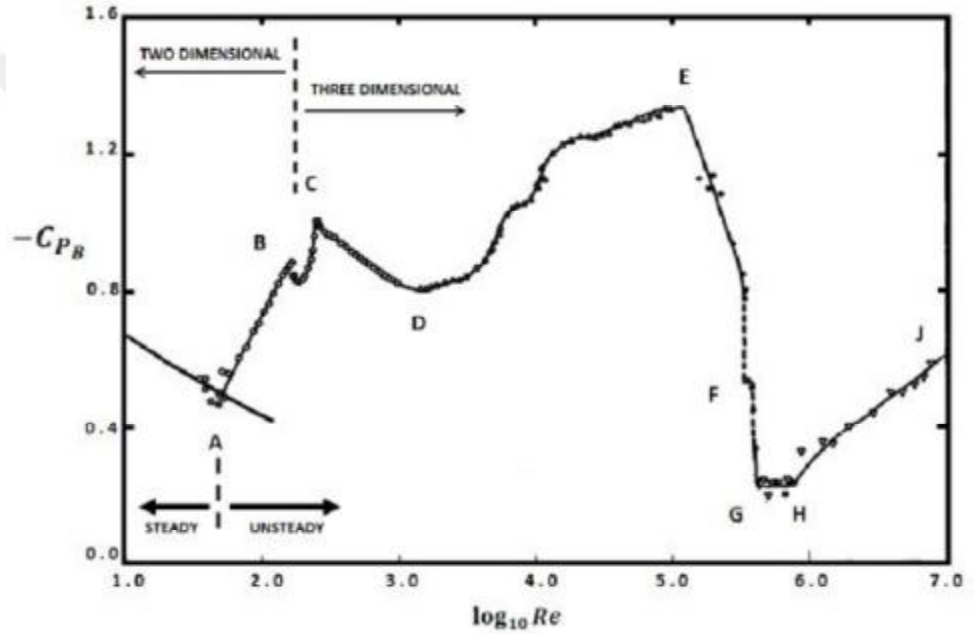

Figure 1.3 Classification of flow regimes according to the plot of base suction coefficients (C_{PB}) over a large range of Reynolds numbers (Williamson, 1996)

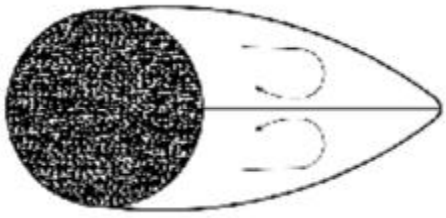

Figure 1.4 Schematic of Steady Wake

For the area bounded by C-D ($260 \leq Re \leq 1000$), the peak value of Reynolds stresses and a particular ordered 3-D streamwise vortex structure in the near wake were effective on the base section. As the Reynolds number, Re is increased towards point D, three dimensionality of the flow starts to be disordered. Hence, the reduction in the two-dimensional Reynolds stresses, a consistent reduction in base section and an increasing length of the wake formation region were observed. Other flow regimes can be classified as D-E, E-G, G-H, H-J flow field and if it is needed to be explained, area bounded by D-E flow regime embrace interval of $10^3 < Re < 2x10^5$, E-G flow regime named critical transition, G-H flow regime called supercritical regime and finally flow regime H-J called boundary layer transition regime or post critical regime.

1.1.1. Boundary Layer Theory and Flow Separation

Prandtl was able to unite two quite separate groups that existed in fluid mechanics prior to 1904 and basically what existed was a split between the theoreticians and the experimental fluid mechanics. These two different group were really quite separate from one another. it wasn't until Ludwig Prandtl came along with the boundary layer concept enabled was a coupling between the potential flow or the mathematical treatment with the viscous flow. The boundary layer theory enable was acknowledgement of the fact that viscosity really only important very close to the wall and is examined by the effect of viscous forces, in this layer called the boundary layer and outside of that region for the most part the fluid be treated as being inviscid and what Prandtl said was that viscosity is important but it's mainly confined to the layer right next to the wall and consequently that was the origin of boundary layer theory. Theoretically, the flow velocity is zero and the momentum of the fluid is very low inside the boundary layer. If the pressure decreases in the direction of the flow, the pressure gradient is said to be favorable. In this position, the pressure force does not affect the flow negatively and can help the fluid movement. On the other hand, while the pressure is increasing in the

direction of the flow, opposite the pressure gradient condition as so it is called exist. In addition to the presence of a strong viscous force, the fluid particles have to move against the increasing pressure force. Therefore, the fluid particles could be stopped or reversed, causing the neighboring particles to move away from the surface. This is called the boundary layer separation.

1.1.2. Wake Region and Wake Flow

In fluid dynamics, the wake is the wave pattern of recirculation flow immediately downstream of a bluff body moving through a fluid. The wake region is caused by viscosity which may be accompanied by flow separation and turbulence or caused by the flow of the fluid around the body. This wave pattern which is prevailing for all type of bodies, also preserves its presence for the circular cylinder and Figure 1.5 shows the wake region and flow separation of shear layer at downstream of the circular cylinder.

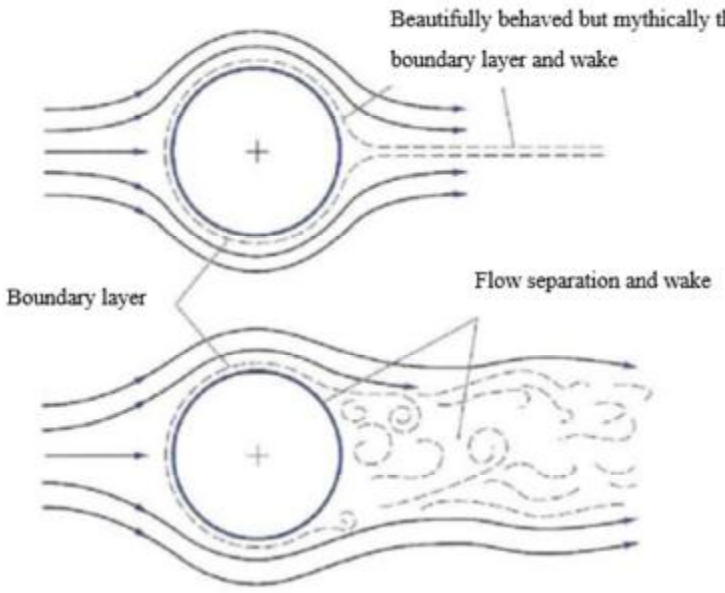

Figure 1.5 The wake flow downstream of the circular cylinder

In fluid dynamics, turbulent flow or wake flow is any pattern of fluid motion characterized by chaotic changes in pressure and flow velocity. It is exactly opposite term of a laminar flow regime, which occurs when a fluid flows in parallel layers, with no interaction between those layers. Turbulence as well as wake flow is caused by excessive kinetic energy in parts of a fluid flow, which overcomes the damping effect of the fluid's viscosity. For this reason, turbulence is easier to create in low viscosity fluids such as water, but more difficult in highly viscous fluids.
In general terms, in wake flow, unsteady vortices downstream of a body appear of many sizes which interact with each other, consequently drag due to friction effects increases.

1.1.3. Vortex Shedding and Vortex Induced Vibration

In fluid dynamics, when a fluid such as water or air flows past a cylinder at certain velocities depending on the size of the cylinder, vortex shedding takes place at downstream of the cylinder. In this type of flow, vortices are created at the back of the cylinder and these vortices separates at certain frequency at either side of the cylinder. The fluid flow past the object creates alternating low-pressure vortices on the downstream side of the cylinder. The cylinder will tend to move toward the low-pressure zone. This movement produce a vibrational load on the cylinder. If the cylinder or any bluff bodies is mounted freely, the frequency of vortex shedding matches the natural frequency of the body, then the body can begin to resonate. Vibration of the body with harmonic frequency can damage or destroy the body at certain time. This vibration is the cause for overhead power line wires "singing in the wind", and for the fluttering of automobile whip radio antennas at some speeds. Vortex shedding was one of the causes proposed for the failure of the original Tacoma Narrows Bridge (Galloping Gertie) in 1940.

1.2. Flow Control

Studies on wake structure and vortex shedding downstream of bluff bodies and analysis of flow separation and shear layers had been a topic of interest due to their fundamental significance and practical importance in aerodynamics and hydrodynamics applications. In such applications, bluff bodies experience unsteady loadings due to the flow separation and formation of the wake region and vortices, which in some cases, play an important role on their design. Roshko (1954), (C.-H. Bruneau, Mortazavi, & Gilliéron, 2008) and (Pinar et al., 2015) reported that, many academic researchers investigated the near-wake flow of a body and vortex shedding downstream of the bodies and vibration caused by this vortex shedding. Control of wake structures and flow separations in such cases could significantly decrease the unsteady forces on the structure; resulting in less structural vibrations. Many researchers tried to suppress the vortex shedding downstream of a body. Scientists offered many methods for basically suppress the vortex formation and possible effect of this formation. But these methods can be aggregated in two approaches. First approach is passive flow control technique. The passive control techniques are dependent on modifications of the bluff body geometry to manipulate the pressure gradient or adding external geometry such as splitter plate to reduce drag and attenuate the flow fluctuation. These passive flow techniques do not need any external energy input during the application and have a simpler implementation compared to the active flow technique for engineering applications. Active flow control methods need external energy to affect the fluid flow structure in the periphery of the body. Classification of the passive and active flow control approaches can be seen in Figure 1.6.

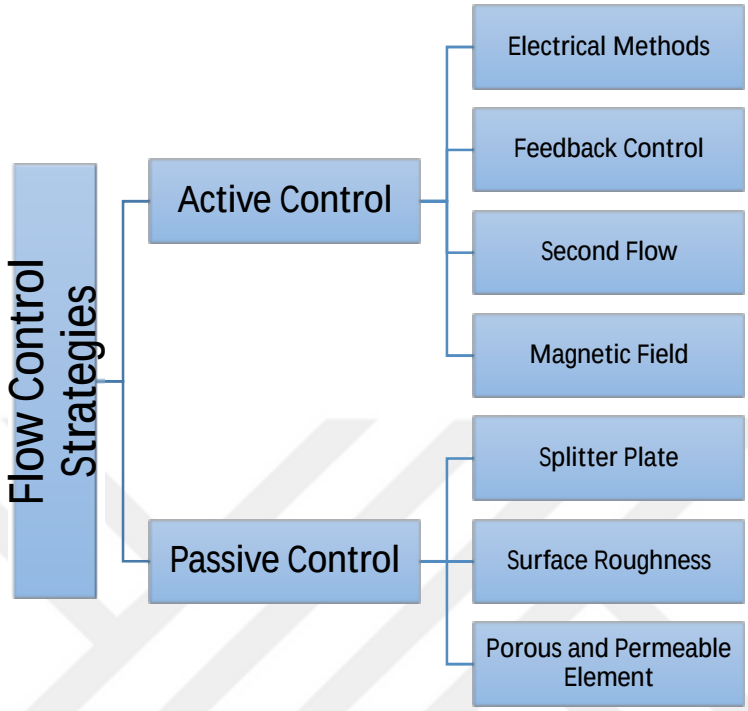

Figure 1.6 Flow control strategies

1.2.1. Active Flow Control Techniques

The ability to manipulate a flow field around a body to enhance the efficiency of the body provides a significant technological advantage in fluid mechanics. The potential benefits of the flow control technique include improved performance and maneuverability and environmental compliance. One of the leading areas of research of many scientists in fluid mechanics is active flow control technique. The energy expenditure was the key word for classification of the flow control methods is based on the illustration given in Figure 1.6. During the last decade, emphasis has been on the development of active control methods in which energy, or auxiliary power, is introduced into the flow.(Mutschke, Shatrov, & Gerbeth, 1998; Sintu Singha, 2011; Weier & Gerbeth, 2004; Williams & Zhao, 1989). Compared to the passive flow control, it is difficult to implement active controls in real engineering applications due to considerably complex actuators as

well as extra energy that is needed. On the other hand, there are also have several advantages of the active flow control technique. The first advantage is to enable the flow stability, drag reduction and flow-induced noise suppression with a small energy input. Secondly, the active flow control can be used for control of the complex flow behavior, dynamical processes like turbulence production in turbulent boundary layers.

1.2.1.1. Feedback Control

Feedback flow control involves the triad of flow phenomena, actuators/sensors, and controls as depicted in Figure 1.7. Flow sensors used in active flow control need to be solid or mounted on a solid surface because noteworthy altering the flow field that is measured due to the sensors is not desired. Actuators that used in active flow control also listed in Figure 1.7. Low energy consumption, fast response and low cost are the desired characteristics of actuators. Early investigation done by Berger (1967). He introduced feedback control to the suppression of wake instability at low Reynolds numbers using an oscillating body. The feedback control strategies has been a area for a lot of studies and attract notice abundance number of investigators (Fujisawa, Kawaji, & Ikemoto, 2001; Leclerc, Sagaut, & Mohammadi, 2006; Park, Ladd, & Hendricks, 1994; Wolfe & Ziada, 2003)

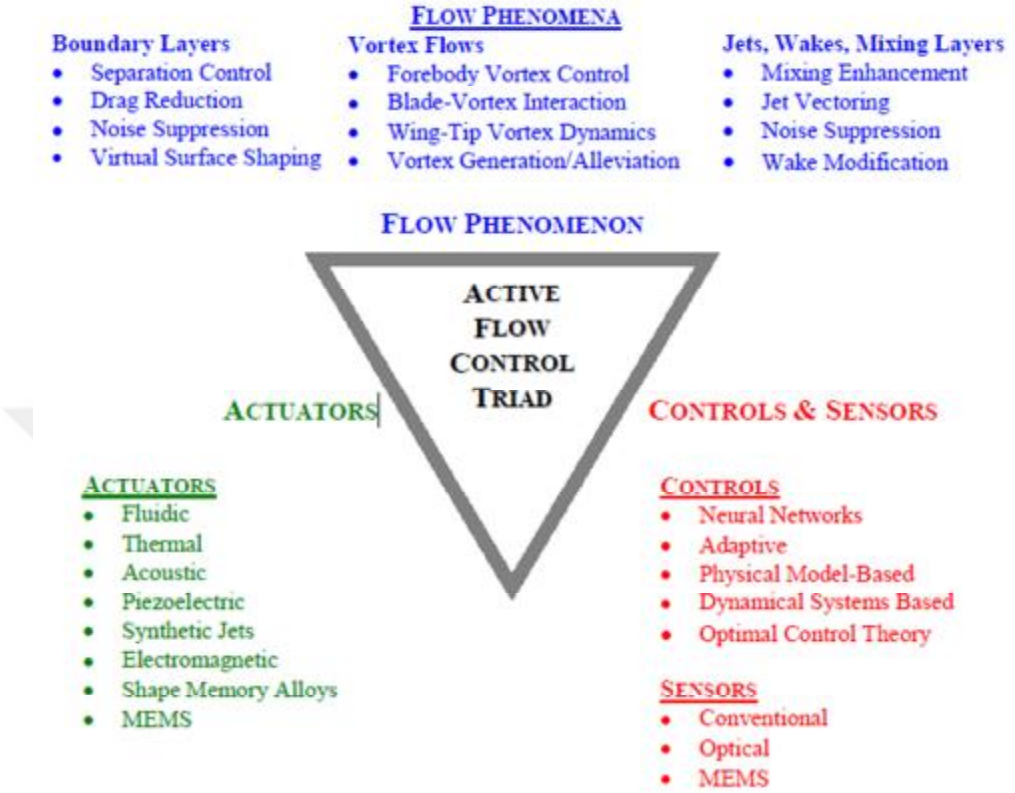

Figure 1.7 The feedback flow control triad (Courtesy D. E. Parekh, Georgia Tech Research Institute)

1.2.1.2. Electro- magnetic control (MHD)

Magnetohydrodynamics (MHD) known as an active flow control method and also classified as a boundary layer control method. Basically; this method is related to the dynamics of magnetic field in medium which is conducted by an electrical current. Any movement occurs in the magnetic field creates an electrical current. In the presence of the magnetic field and the current, the unit volume of liquid is subjected to a fluid force known as Lorentz force. Since this force acts on the opposite direction to the flow, it not only slows down the flow rate and provide a certain balance in the flow but also have significant effect on the drag and lift forces acting on the body. Figure 1.8 shows specifically low and high magnetic

field effect on the vorticity contour in horizontal direction. If you want to change the direction of the Lorentz force, it will be enough to displace the poles of the electrodes.

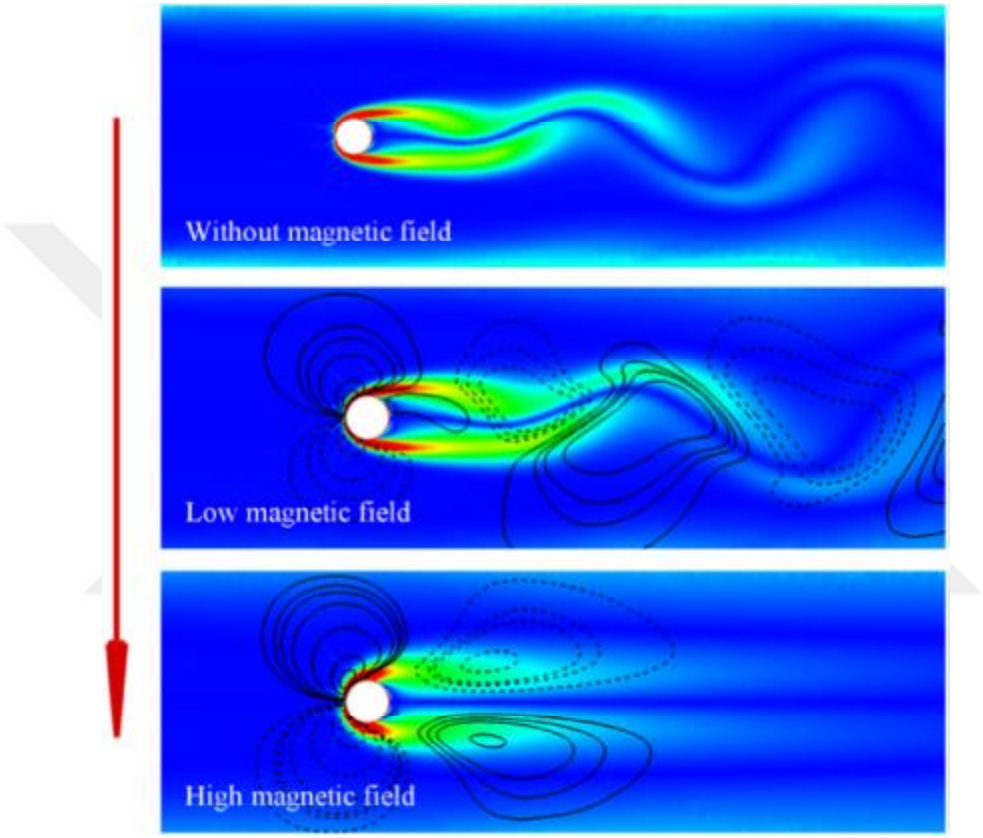

Figure 1.8 Contours of vorticity at different magnetic field strength at Re¼100.Flow is from left to right (Rashidi, Hayatdavoodi, & Esfahani, 2016)

1.2.1.3. Generating a Secondary Flow

This method is classified as active wake control method since it requires an energy input. There were practical examples that use this technique in engineering area such as aircraft, turbine blade, tall buildings with the ground and the cooling flow past computer chips on a circuit board. Creating a secondary flow (suction,

blowing, base bleed) made it possible to solve the problems related to fluid mechanics in these engineering applications. For suction and blowing, the wall of obstacle is penetrable and the suction or blowing velocity is defined. For base bleed method, the wall of obstacle is not penetrable and the secondary flow is injected at the edge of obstacle.

1.2.2. Passive Flow Control Techniques

Passive control technique is a method that can be applied for controlling of vortex shedding in the wake of a bluff body and control of vortex induced motion of a bluff elastic body. This flow control technique can be adaptable in underwater applications such as marine risers and underwater pipelines etc. In underwater engineering application, suppression of vortex shedding is important because of the destructive effect of VIV on bodies. Control of vortex shedding for suppression of VIFM (Vortex Induced Forces and Motion) can be achieved by a passive control. The passive flow control technique can also be applied when the drag coefficient is significant, since changes in drag coefficient are dominated by the location of a separation point. The passive methods are not time depended application and they don't require external energy input. If passive methods do not need external energy, how does it control vortex shedding and suppress them or decrease drag coefficient? The answer to this question is hidden in changing the geometry of the body or adding external devices along the bluff body. Nominally methods such as, utilizing of porous structure, adding perforated cylinders, splitter plates and base bleed and wavy or rough surfaces have been used in the past to weaken vortex shedding and reduce the drag coefficient and hydrodynamic instabilities.

1.2.2.1. Porous Structure and Permeable Cylinders

One of the passive flow control technique is defined here by a flow manipulation using geometrical effects and no extra energy variations. The aim is to use a porous control device easy to set up, low cost and allowing to keep the

geometry unchanged. As an active control device can be hardly implemented in such a case, an efficient passive strategy seems to be a good alternative. Some beneficial effects of passive porous or perforated surfaces on boundary layer characteristics have been reported (Bearman & Harvey, 1993; C. H. Bruneau & Mortazavi, 2004; Mimeau, Mortazavi, & Cottet, 2014; Pinar et al., 2015). The methodology used in this passive technique consists in separating the solid surface from the flow by a porous interface. The idea is to generate an intermediate flow which reduces the boundary layer effects, specially to decrease the vorticity magnitude. This procedure is applied to control vortex flows around a circular cylinder for this work.

1.2.2.2. Splitter Plate

There are numerous techniques to control the vortex shedding downstream of the bluff bodies. Among the passive flow control technique, the splitter plate has been one of the most successful devices for the control of the vortex shedding. The splitter plate has been the topic for a lot of work and attract notice abundance number of investigators (Akilli, Sahin, & Filiz Tumen, 2005; Apelt, West, & Szewczyk, 1973; Bearman, 1965). Their studies show that for sufficiently long splitter plates, the vortex shedding instability in the wake is inhibited, resulting in reducing the drag force on the bluff body. Experiments shows that 20% to 40% drag reduction can be obtained when the splitter plate mounted at right place. The net drags at given Reynolds number reduces when the optimum length of splitter plate is used. Another achievable benefit is disappearing the vortex shedding when the splitter plate length is long enough according to the critical length.

1.2.2.3. Surface roughness

Control of vortex shedding of a bluff bodies and control of vortex induced motion of a bluff elastic body have been topics of research for many years (Zdravkovich, 1997). In underwater engineering application, suppression of vortex

shedding is considerably important because of the destructive effect of VIV on marine risers, underwater pipelines, etc. The control of vortex shedding for suppression of VIFM (Vortex Induced Forces and Motion) can be achieved by surface roughness control actively, passively, or combination thereof (Bernitsas & Raghavan, 2008). The surface roughness has also a great effect on the drag coefficient of a circular cylinder around a critical Reynolds number range, since changes in drag coefficient are dominated by the location of a separation point. The surface roughness causes a shift in a separation point along a body where the section is circular, and this accelerates the transition into a turbulent flow range. The surface roughness modifies the wake structure by changing lines of separation or direction of surface flow. O-rings were fitted on a cylinder as surface protrusions so as to control the flow around the cylinder. For example, Lim and Lee (2002) placed O-rings around a cylinder and they reduced the drag coefficient and frequencies of vortex shedding. Another surface protrusion method is a trip wire which attached to a cylinder surface based on the stagnation point. Ekmekci and Rockwell (2011) studied on the effect of a single wire which was attached on the outer surface and parallel to the span of a stationary circular cylinder. They located on the outer surface and parallel to the span of a stationary circular cylinder at a range of angular positions from $\theta = 40°$ to $120°$.

2. PREVIOUS STUDIES

Although the water tunnel was used in this study, in general, the flow over a bluff body was examined in two different tunnels which are air and water tunnel. Many academic studies carried out to examine the flow behaviors behind the bodies and suppress the vortex shedding downstream of the circular cylinders or square cross-section. The use of these cylinder and square shape bodies was due to the fact that they were the basic forms used in real engineering applications. In the previous studies, although the bodies such as spherical cone and square body were examined, these studies remained less than the ones made with the circular cylinders.

Prior studies similar to this work mostly done with cylindrical bodies. The control methods developed in order to control vortex structures of a body in air and water tunnels are called passive and active flow control strategies. Many techniques have been developed for manipulating the wake flows downstream of bluff bodies, which results in the asymmetric vortex shedding control and suppression of the vortex-induced vibrations. The active flow control methods are based on the use of external energy, while the passive flow control methods include applications in which energy is not used. The principles of the passive flow control depend on the changing the shape of a bluff bodies or protecting the original body by adding with other devices or obstacles.

2.1. Passive Control Methods

The main advantage of the passive control which used to control the vortex shedding on downstream of the cylinder is the fact that the energy free and is often easy to apply. The former control techniques used in passive control include splitter plates, surface protrusions and surface roughness, adding control elements, dimples and grooves.

2.1.1. Control of Vortex Shedding by Surface Roughness

Among the passive flow control techniques, the surface roughness could be counted as a boundary layer control method. The vortex shedding formation and unsteady forces due to shedding of vortices as well as boundary layer separation of the circular cylinder could be manipulated by surface roughness. It was known from the earlier studies; the surface roughness could cause delay in the boundary layer separation. Until now surface roughness was investigated again and again due to its easy manufacturing and simpler installation.

For the studies done with the surface roughness, understanding relations between the drag coefficient and surface roughness in utilize in high building and marine applications was the main aim. In the experiments of Elmar Achenbach (1971), investigated cross flow around a circular cylinder by using surface roughness in wind tunnel which had high pressure with the Reynolds number up to $Re=3x10^6$. He conducted experiments on stationary circular cylinder and sand-grain was chosen for type roughness method. He founded that if surface roughness increases, flow tend to faster change from laminar to turbulent. He defined “drag crisis” which explain as at the critical Reynolds number, the drag coefficient which was affected on the body, experiences a sudden drop when the flow characteristic passes through laminar to turbulence. He noted that this sudden decrease could be eliminated by increasing the surface roughness. When the boundary layer changed from laminar to turbulent, the drag exerted on a cylinder decreased abruptly at a critical value of the Reynolds number. The critical Reynolds number for this “drag crisis” decreased as the surface roughness increases.

In another experimental study was made by E Achenbach and Heinecke (1981) in range of Reynolds number, $Re = 6 \times 10^4 - 5 \times 10^6$ in order to alter the vortex-shedding frequency in the wake of a single cylinder. They used pyramidal roughness method illustrated in Figure 2.1. They measured the local pressure and total drag coefficient from experiments as function of roughness parameter and the Reynolds number in a wind tunnel. They founded that the increasing roughness

parameters cause decreasing the critical Reynolds numbers, Re and therefore a significant decrease in the drag coefficient obtained. They also agreed that these types of roughness had effect at the subcritical Reynolds number but was not very effective at the low Reynolds number.

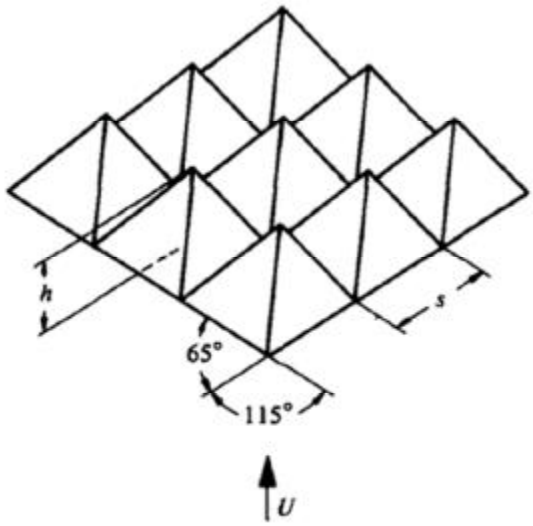

Figure 2.1 Pyramidal surface pattern (E Achenbach & Heinecke, 1981)

Kawamura, Takami, and Kuwahara (1986) researched the effect of the high Reynolds number flows on body which has surface roughness around a circular cylinder. They used experimental and numerical methods for this study and began research at the Reynolds number, Re = $1{,}2x10^3$ and they changed the range of Reynolds number between 10^3 to 10^5. Experimental and numerical approach were used in their study and the results from that approaches were supporting each other. At the Reynolds number, Re = 2×10^4 significant decrease in the drag coefficient was obtained see in Figure 2.2. This reduction of drag was due to the small eddies generated on the surface near the separation points.

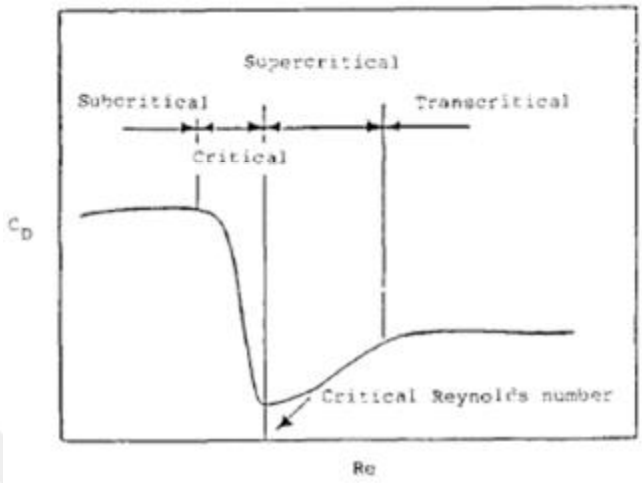

Figure 2.2 Four Reynolds number ranges relevant to the flow a past circular cylinder (Kawamura et al., 1986)

Another experimental study on wind tunnel to reduce drag coefficient of a circular cylinder made by Bearman and Harvey (1993). They used dimpled circular cylinder over the Reynolds number range from Re = 2 x 10^4 to 3 x 10^5. They observed that dimples affect occurrence of critical regime at the lower Reynolds number than the smooth cylinder case. The drag coefficient of smooth and dimples cylinders was almost same in the post critical flow regime. Moreover, over the range of Reynolds number, Re = 4 x 10^4 to 3 x 10^5 dimpled cylinders had a lower drag coefficient than smooth cylinder. Lastly, they did not change design of dimples so they noted that if different design of the dimples or another arrangement of dimples were used, the drag coefficient might be reduced in larger values.

Knowing that the surface roughness's ability on reducing the drag coefficient of a circular cylinder (Merrick & Bitsuamlak, 2008) performed both experimental and numerical study at high Reynolds number, Re in order to control the flow around a circular cylinder by using an artificial surface roughness across the exterior of the cylinder (Figure 2.3). From their experimental results, they could not find optimal roughness pattern for changing the separation point of the cylinder and note that further research must be done for the purpose of scale model testing.

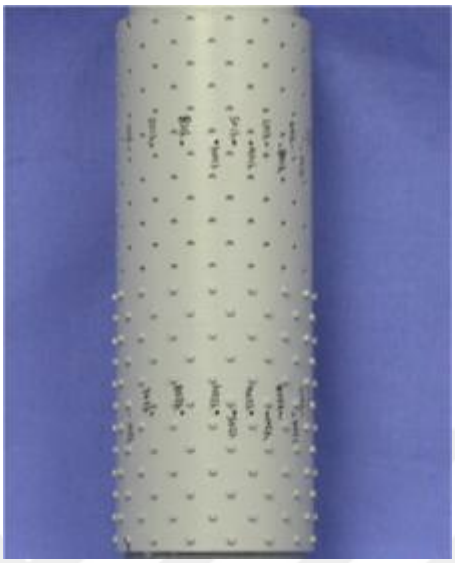

Figure 2.3 Roughness pattern on the resin insert (Merrick & Bitsuamlak, 2008)

All these studies showed that, adding a roughness pattern on a circular cylinder (sandpaper, Pyramidal surface…), the pressure distribution downstream of the cylinder and the drag coefficient around the cylinder could be altered on the positive direction. Thus far, the surface roughness studies that given above were conducted in the wind tunnel and mostly related to the drag reduction. Since, this present study was concerned mostly controlling the vortex shedding immediately downstream of the circular cylinder because of the destructive effect of VIV on the cylinder in deep water, it would be more meaningful to examine studies which had done in a water channel. The former studies used the surface roughness method in order to control vortex shedding frequency were widely examined see e.g.(Allen & Henning, 2001; Bernitsas, Raghavan, & Duchene, 2008; Gao, Fu, Wang, Song, & Chen, 2015; Kiu, Stappenbelt, & Thiagarajan, 2011; Oruç, 2017)

Allen and Henning (2001) performed experimental study in order to figure out the effect of surface roughness on the flow structure with a large aspect ratio on vortex induced vibration and the drag coefficient of the circular cylinder at the critical and supercritical Reynolds number, Re. The Reynolds number, Re and the

surface roughness (k/D, where k was the average peak to trough height of the surface protrusions and D was the diameter of the cylinder) were the two critical parameters for their study. The results of this study showed that in general, the smooth cylinder had better effect on suppressing VIV of a circular cylinder. When the flow was turbulent, the smooth cylinder had low drag coefficient. Another finding from experiments were up to some point if the surface roughness increases, the displacement increases. The drag coefficient and displacement were connected to each other. They noted that surface roughness types could be very essential parameter for these types of studies.

Bernitsas and Raghavan (2008) examined how the surface roughness effects vortex induced vibration (VIV) of a circular cylinder. They achieved roughness on the surface by using sandpaper strip and they executed experiments in a low turbulence free surface water channel. In this study, more than one parameter was investigated independently from each other. The first parameter was the reducing the vortex induced vibration caused from the vortical flow downstream of the circular cylinder. Second parameter was the start and end point of roughness and third parameter was the thickness of the sandpaper base and size of grit. They found that, when the surface roughness distributes properly, the VIV can be reduced or even can be suppressed. They used the similar approach to the above study on (Bernitsas et al., 2008) but the only change was the Reynolds number, Re in order to reduce VIV on the circular cylinder. They concluded almost the same results from these two studies that, the use of the rough surface was helpful on reducing the VIV.

Chang, Ajith Kumar, and Bernitsas (2011) studied on a single circular cylinder in a water channel at high Reynolds number, Re in a range of $3x10^4 < Re < 12x10^4$. The smooth and rough surface condition were investigated in order to understand how surface condition changed the vortex induced vibration and how the surface roughness alter the flow induced motion in a steady flow. They proved that the rough surface were better results for reducing the VIV and vortex induced

motion than the smooth surface. They also showed that rough obstacle inclines five vortices per cycle although smooth obstacle sheds seven vortices per cycle.

Kiu et al. (2011) concentrated on the effect of a uniform surface roughness on the vortex induced vibration of towed cylinder in underwater. They founded from the experiments that, the surface roughness had an important influence on the hydrodynamic effect. The maximum mean drag coefficient tended to decrease as the roughness increased. They also founded from experiments which done with the smooth surface obstacle, the rough surface had a higher Strouhal number, St than the smooth surface.

When a cylinder encounters a flow, it subjects to a time- dependent drag and lift forces over a certain range of the Reynolds number of the flow. If the cylinder is mounted flexibly, these forces may induce vibration on the cylinder. The lift may induce cross-flow (CF) vibration on the other hand the drag may induce in-line (IL) vibration. This is called vortex-induced vibration (VIV). Gao et al. (2015) experimentally studied on these phenomena of VIV by using the surface roughness of a circular cylinder. The displacement response, drag, lift and vibration frequency, were the parameter that they designated for their experimental study. They observed that the displacement response decreased as well as the vibration frequencies and the vortex-shedding frequency increased with increase in the surface roughness. At small surface roughness value beyond their limited Reynolds number range, the drag on the cylinder decreased significantly. In another experimental study related how drag and lift coefficient was affected on different surface roughness was done by Zhou, Wang, Gho, and Tan (2015). They performed experiments using three different kinds of surface roughening methods. Both in these methods, covering the cylinder with a uniformly distributed object was used. These methods could be listed as follows; the sandpaper, netting and dimples as shown in

Figure 2.4. Their results showed that for the cylinder with dimples, the drag coefficient reduces approximately %30 compared to no control case. They

also added that the root mean square lift coefficient of both three different rough surface was calculated lower values than the cylinder that not applied surface roughness.

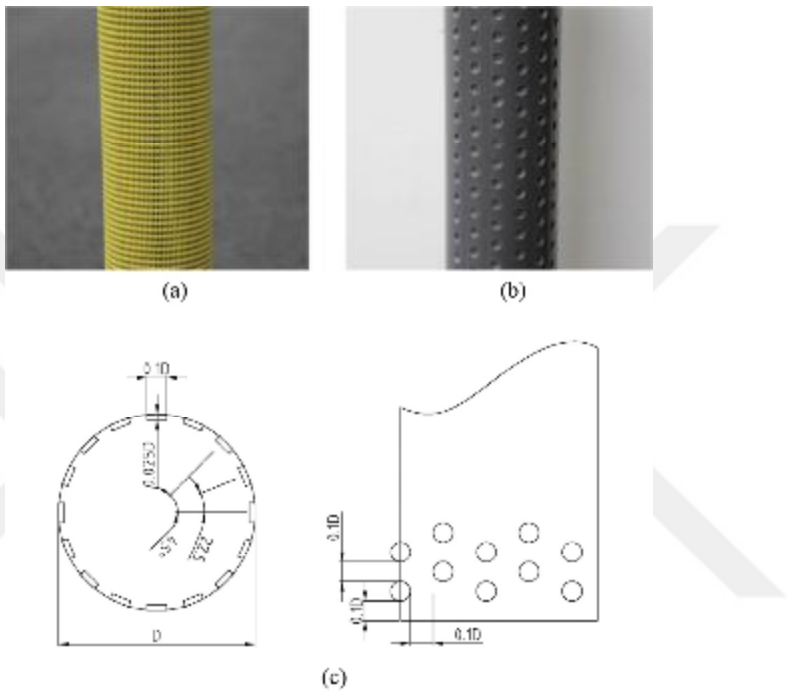

Figure 2.4 The rough cylinders with (a) netting and (b) dimples. (c) Sketch showing details of the dimples (Zhou et al., 2015)

When Rodríguez et al. (2016) numerically simulated flow over a circular cylinder with sand-grain surface roughness, they had intended to find out how the boundary layer of cylinder and wake formation downstream of the cylinder were affected by this surface roughness. They compared the results of the plain cylinder and the cylinder which has the rough surface. The Reynolds number was taken as $Re = 4.2x10^5$. They reported that instabilities caused by the roughness pattern on the circular cylinder, detent an early transition to turbulence. Therefore, the drag coefficient, C_d was found as $C_d = 1.122$ which was higher value than the smooth cylinder.

Lastly; as mentioned in above literatures, the surface roughness leads sharp and observable reduction in the drag coefficient of a circular cylinder at subcritical Reynolds numbers. Beside the reduction in the drag coefficient, delaying in the boundary layer separation could be counted another effect of the surface roughness method. As a result, the surface roughness was important passive flow control method for many application areas. In wide manner it was worth investigation topic in fluid dynamic applications.

2.1.2. Control of Vortex Shedding by Adding Porous Element

This method, which is counted as a passive flow control methods, involved using a replaceable porous control element in order to protect the main body from unwanted vibrations caused from vortical flow and control the effect of the drag forces on the body. (C.-H. Bruneau & Mortazavi, 2006; C. H. Bruneau & Mortazavi, 2004) studied a numerical simulation using the Navier-Stokes equations. The passive flow control of bluff body flows using porous media was investigated by means of the penalization method. They aimed to change the boundary layer behavior and vortex shedding by using porous media between solid square cylinder and fluid. The permeability coefficient K was added Navier-Stokes equation and designated three different Reynolds number so as three different flow regimes for numerical simulation which were Re = $3x10^2$, $3x10^3$ and $3x10^4$. They analyzed all numerical results and concluded that, for the Reynolds number, Re = $3x10^2$, the drag coefficient on the square cylinder decreased drastically because the flow in this Reynolds number, Re value was transition. For bigger Reynolds number, Re was also successful for reducing the drag coefficient on the body and regularization of the flow with well-chosen permeability coefficient (K) but they also noted that not all cases were successful for controlling the vortex shedding downstream of the cylinder and reducing the drag coefficient. Lastly, they agreed that the porous media was efficient as a passive flow control method on reducing

the drag (up to %40 of the global calculated quantities) and altering the vortex formation and regularization of the flow.

Bhattacharyya, Dhinakaran, and Khalili (2006) numerically investigated the flow characteristic and flow concentration around a porous cylinder. They defined a flow field which was governed by four different parameters as follows; Reynolds number (Re), Schmidt number (Sc), Darcy number (Da) and porosity (ε). They analyzed the results and founded that, the drag coefficient, C_d that encountered by the porous cylinder reduced when the Reynolds number, Re increased and also when the Darcy number, Da decreased. At the low Reynolds numbers, Re they observed that the drag coefficient, C_d tended to decrease as the porosity of the cylinder increased. Further analysis showed that If the Darcy number, Da increased, the angle of separation and the wake length reduced.

C.-H. Bruneau et al. (2008) performed a numerical experiment on a square back Ahmed body by adding seven different types of porous layers between a solid body and fluid. The porous layer located at various part of the body shown in Figure 2.5. They evaluated the results in terms of vorticity fields at given time, root mean square of the lift coefficient, C_{Lrms} and drag coefficient, C_d. Different findings were obtained according to numerical results for every diverse case. For example; for the case 1, the end point of the porous layer caused vertical jet so the drag coefficient, C_d increased as well as the vortex shedding frequency. When the flow transient the porous layer to solid body, the pressure differences and the velocity increased. Whereat the total drag increased almost %22.

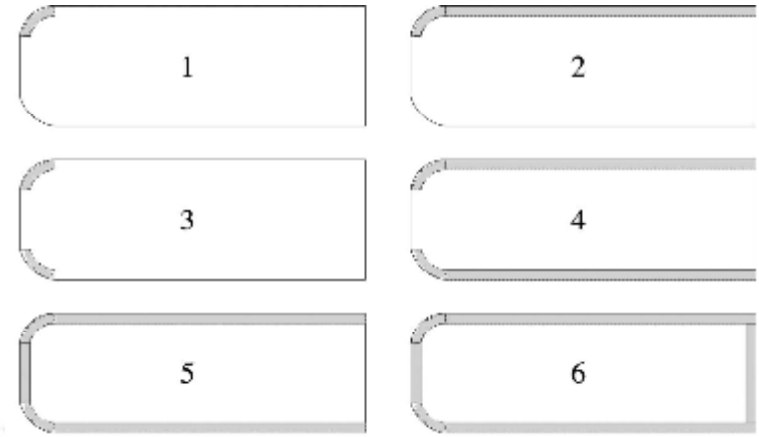

Figure 2.5 Cases 1 (top left), 2 (top right), 3 (middle left), 4 (middle right), 5 (bottom left) and 6 (bottom right) corresponding to various porous device geometries (C.-H. Bruneau et al., 2008)

Zhao and Cheng (2010) conducted a numerical study in order to investigate the effect of a porous layer in reducing the lift coefficient. They used a finite element method to study the flow inside and outside of the porous structure, and they took the Reynolds number as Re = 10^3, 2,5x10^3 and 5x10^3 respectively. It was found that the lift reduction can be achieved by properly choosing the porous material. However, the amount of reduction greatly depended on the Reynolds number, Re the permeability and the Forchheimer coefficient. In addition, they argued that lower lift coefficient would be obtained if the thicker porous structure was used, and that there was a critical Darcy number, Da, which was the minimum RMS lift coefficient, as shown in Figure 2.6.

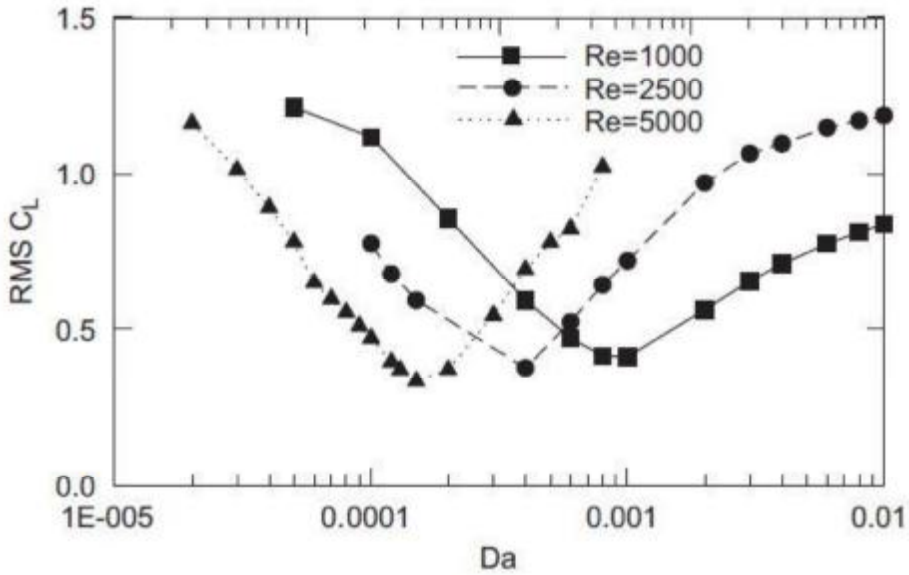

Figure 2.6 Change of RMS lift coefficient with different Darcy number in different Reynolds numbers (Zhao & Cheng, 2010)

Ruck, Klausmann, and Wacker (2012) examined the drag resistance of a cylinders in a wind tunnel using a porous coating at Reynolds number, Re between Re = 10^4 to $13x10^4$. They used the coatings which manufactured from the polyester (Poret-Ester-Foam) with thicknesses of 10mm, 5mm and 3mm. The permeability was defined as Pores per inch, PPI and they used values of PPI in their experiments as follows 30 ppi, 20 ppi and 10 ppi. They also performed experiments with "full coating" and "half coating". They determined that the flow resistance increased when full coating was used. On the contrary, the flow resistance decreased when half coating was used.

Ozkan, Oruc, Akilli, and Sahin (2012) constructed an experimental setup in order to examine the effect of a permeable outer cylinder and its diameter on the flow characteristic downstream of the cylinder. Basically, their set up consisted an inner circular cylinder, which had constant diameter for all experiment (d=50mm), and an outer circular cylinder. The outer permeable cylinder had different diameters as follows D = 60, 70, 80, 90 and 100 mm and the outer cylinder had

different porous values as follows β= 0.4, 0.5, 0.6 and 0.7. The bare cylinder (only inner cylinder) was used for a control case and the turbulence intensity were compared with the bare cylinder. Their investigation of controlling shedding mainly included two parameters, first parameter was the porosity of the outer cylinder, second parameter was the diameter ratio of cylinder pair. The results from the particle image velocimetry, PIV technique showed that the presence of the outer cylinder effect the maximum values of turbulence intensity in a good direction. In general manner, the vortices on each side of the cylinder were affected on diameter ratio, D/d whatever the porosity of outer cylinder is. Finally, they agreed that the calculation of the drag and lift coefficients also might help to understand the effect of the presence of the porous outer cylinder.

Another experimental study done by Gözmen, Akilli, and Şahin (2013) in order to control the flow downstream of a circular cylinder. They used a porous outer cylinder which had diameter of D = 75mm. Eight different porous value were used as follows β=0.4, 0.5, 0.6, 0.65, 0.7, 0.75, 0.8 and 0.85. In order to fully understand the effect of porosities on the vortex formation and turbulence statistics, such a wide range and frequently close values had been used. The description of porosity was defined as the ratio of the gap area on the body to the whole-body surface area. While experiments were being carried out, the free stream velocity, the Reynolds number, Re and the inner cylinder diameter kept constant. They founded that, among the all porosity values, the porosity of outer cylinder β=0.7 had better effect on controlling the flow than other porosity values. Compared to the case where only bare cylinder was used, a 70% reduction in the presence of the outer cylinder was obtained.

In addition to the experimental studies, Valipour, Rashidi, Bovand, and Masoodi (2014) made remarkable analyzes numerically in this area. Numerical models consist of porous diamond-square cylinders exposed to two dimensional and steady flow. At the conclusion, the experimental results compared based on

Darcy's number effect with the wake length and pressure coefficient showed a tendency to decrease when the Darcy numbers increased.

Mimeau et al. (2014) performed numerical and passive control technique study with porous coating around a two-dimensional semi-circular cylinder. Vortex-penalization method which allows to compute simultaneously the three fluid-porous-solid media was chosen for calculation. Their expected effects could be considered as follows; alter the vorticity generation of the boundary layer as well as vortex shedding as a result of this reduce drag coefficient and forces and also vortex induced vibration. They conducted experiments at transitional Reynolds number as Re = 550 and highly transitional regime at Re = 3000. They designated mainly two parameters. Firstly, porous layer permeability (λ) $\lambda = 1$ represent high permeability, 10, 10^2, 10^3 represent low permeability and third value of $\lambda = 0$ used for uncontrolled case secondly, porous layer thickness (τ). Their first result showed that bigger λ has more effect than low λ. The results showed that intermediate permeability with thin layer thickness conclude better drag reduction and they also added in real practice intermediate porous ring on the edge wall will be easy and low cost.

Pinar et al. (2015) conducted an experimental research in shallow water. Their research materials were perforated circular cylinder which has different porosity ratio (β). They defined β as the ratio of open area to the whole surface area of the cylinder and set the range of β for this study as $0.1 \leq \beta \leq 0.8$. In order to understand the effect of β on the flow structure in detail, other parameters preferred to keep constant the Reynolds number, which was calculated according to the free stream velocity U and the diameter of the perforated cylinder (D). Bare cylinders were used to refer to the results from the experiments and the results were compared using velocity and vorticity contours, turbulence kinetic energy and Reynolds stress values. It was noted that β with a range of $0.4 \leq \beta \leq 0.8$ was more effective in suppressing Karman Vortex Street, but it emphasized that the effect of

reducing the drag coefficient of the perforated circular cylinder should also be examined.

A typical passive control technique study which published last year and examined the effect of an independent from inner cylinder, perforated external control element in controlling flow control were done by Oruç, Akilli, and Sahin (2016). The PIV technique was used to extract results like other studies conducted at the same university. As a result of experiments with three different Re numbers, flow control was undoubtedly achieved and at the same time elongation in vorticity layers. They also reported that decrease in the Turbulent Kinetic Energy and Reynolds Shear Stress values measure in the wake region.

2.1.3. Control of Vortex Shedding by Splitter Plate

As a passive control approach and due to its simple geometric configuration, the use of a splitter plate arranged in the bluff body wake has attracted significant attention in the past. Vortex shedding downstream of a circular cylinder and the wake suppression effectiveness of the splitter plate was made in the early experimental studies of Roshko, conducted in the mid-1950s (Roshko, 1954). His experimental work was performed at Re = 14 500 and demonstrated that a plate of length 5D (where D was the cylinder diameter) attached at the cylinder base was able to completely suppress the vortex shedding. Consequently, the splitter plate led to an increase in the base pressure and a reduction in the drag force. He also observed that, as the plate (of length D) was located downstream at distances of less than 4D, it worked effectively on the cylinder wake to decrease the Strouhal frequency and to increase the base pressure.(Roshko, 1954)

Bearman (1965) experimentally examined the wake flow behind a two-dimensional bluff body model fitted with a wake splitter plate with a base/height up to 4. He found that the distance of the fully formed vortex from the model base was inversely proportional to the base pressure coefficient. Furthermore, he

categorized the flow into five regimes, according to the different wake behaviors along with the increase in the length of the splitter plate.

Since those early studies, many researchers focused their efforts on the effect of control plates on the aerodynamic features, wake structures (typically, behind circular or square cylinders) and the underlying flow mechanisms that were essential for wake control (Akilli et al., 2005; Anderson & Szewczyk, 1997; Apelt & West, 1975; Apelt et al., 1973; Gerrard, 1966; Nakamura, 1996; Ozono, 1999; Unal & Rockwell, 1988)

Gerrard (1966) studied a mechanism of vortex generation, size, frequency, formation and effect on the cylinder at $Re_D = 2x10^4$ behind a circular cylinder. Explained the effect of the splitter plate on the frequency of vortex shedding in terms of the frequency-determining mechanisms in the vortex-formation region and the shear layer diffusion length. From his study, he showed that the Strouhal number decreased when the length of the splitter plate was smaller than d, but it increased for D<L<2D. He also showed that the swirling formation zone was under a strong elongation in the presence of a SP and that two modes of swirling formation could appear according to the length of the separating element and its distance from the model.

Apelt et al. (1973) and Apelt and West (1975) conducted a series of experiments to investigate the effect of the splitter plate on the flow characteristics by measuring the pressure distribution, the vortex shedding frequency and the flow visualizations. Their results showed that the splitter plates were able to remarkably reduce the drag force, to increase the base pressure, to narrow the wake width and to change the Strouhal number. Moreover, the flow mechanisms of wake modification were found to vary for ‘short’ and ‘long’ plates. The ‘short’ plates operated to progressively stabilize the separation points and reduced the wake width with increasing plate length. Additionally, the trailing edge of the ‘short’ plates provided a fixed formation point for the vortices. However, the ‘long’ plates inhibited the interaction of the separated shear layers and reduced the roll-over

effect of the vortices. With increased plate length, the ‘long’ plates eventually were able to eliminate the vortices from crossing the wake centerline.

Unal and Rockwell (1988) divided the wake region into two separate regions: the pre-vortex formation region and post-vortex formation region. They found that the strength of absolute instability of the near wake was substantially controlled by the wake–plate interactions. Pressure Using an extended splitter plate, Nakamura (1996) experimentally investigated the vortex shedding from the bluff bodies of various cross-sectional shapes. He observed that the wake dynamic was characterized by the impinging shear layer instability, where the Strouhal number increased stepwise with increasing splitter plate length.

Kwon and Choi (1996) investigated the vortex shedding behavior behind a circular cylinder and effect of the splitter plate on vortex shedding at Reynolds numbers of 80-160. They showed that for $Re_D \geq 120$ the shedding frequency changed similarly as just described, whereas for $Re_D \leq 100$ the shedding frequency monotonically decreased as the plate length increased. They attributed the increased shedding frequency at L >D in the case of $Re_D \geq 120$ to a generation of the secondary vortex at the tip of the splitter plate. This secondary vortex near the tip of the splitter plate may also be a strong source of the flow-induced noise.

Anderson and Szewczyk (1997) found that the use of a splitter plate was able to reduce the level of three- dimensionality in the vortex formation region by stabilizing the transverse flapping of the separated shear layers; furthermore, it decreased the momentum thickness of the shear layer by approximately 45% in comparison to the plain cylinder configuration.

Experimental work by Nakamura (1996) included single-layer instability and how vortex shedding were shaped when an extended plate was added to the bluff bodies such as circular, semicircular section with and without a rectangular block , In general, they used four different bodies and a splitter plate was added to

each body. The dimensions used for the circular cylinder can be listed as follows; the diameter of the circular cylinder (D) was 20 mm and the thickness of the plate was 2 mm, while the length of the cylinder was calculated, dimensions takes from center of cylinder. All the other three models tested had a cross-flow dimension D of 1 cm. They founded that in systems with bluff bodies with different geometries and associated splitter plates, the vortex shedding depends on the number of Strouhal number (St), but on the contrary the Reynolds number (Re) and section geometry were weakly connected.

Ozono (1999) observed that the use of a short thin plate could cause the Strouhal number to exceed the natural vortex shedding frequency of plain cylinder for some range of the gap between the cylinder base and the plate tip. The mechanism behind this observation was identified as the shear layer separated from the gap side, which was forced to flow into the gap by the insert of the splitter plate, intensifying interactions in the nearer wake (Ozono, 1999).

Akilli et al. (2005) experimentally investigated the effect of detached splitter plates with varying positions on the suppression of vortex shedding in shallow water with PIV techniques. Velocity vector field and corresponding vorticity contours and streamline topology and Reynolds stress concentrations were used to explain the characteristics of the flow. They conducted experiments with different thickness splitter plates, have a length of 50 mm, which was equal to the diameter of the cylinder *(D)*. Gap distance between the base of the cylinder and the leading edge of the splitter plate ranged from 0 to 2*D*. Time-averaged velocity vector fields for various cases of gap ratio *(G/D)* and plate thickness ratio *(T/D)* were used to understand the effect of plate thickness on the suppression of vortex shedding. Although, the splitter plate has a substantial effect on suppression of the vortex shedding for the gap ratio between 0 and 1.75*D*, no effect of the splitter plate was observed when the splitter plate was located at 2D location. They showed that altering the flow characteristic plate thickness had same effect. After passing

the splitter plate, the flow starts to oscillate with smaller frequency compared to the natural frequency of the bare cylinder.

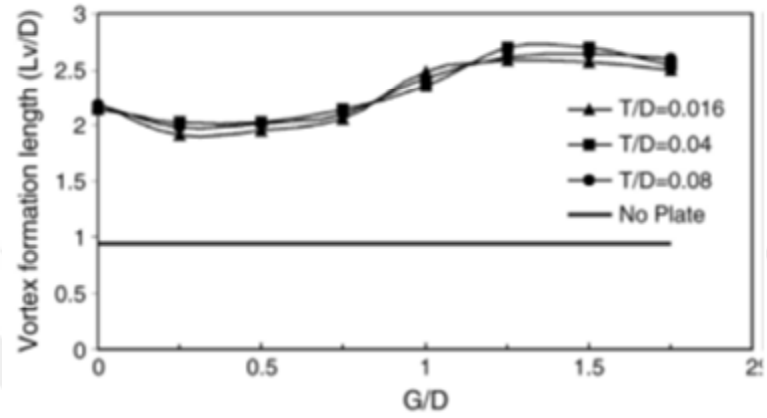

Figure 2.7 Variation of vortex formation length with gap ratio for three different splitter plate thickness.(Akilli et al., 2005)

Akilli, Karakus, Akar, Sahin, and Tumen (2008) investigated experimentally passive control of vortex shedding behind a circular cylinder by splitter plates of various lengths attached on the cylinder base in shallow water flow (Re=6300). At this study the length of the splitter plate was varied from L/D=0.2 to L/D=2.4 in order to see the effect of the splitter plate length on the flow characteristics. Instantaneous and time-averaged flow data clearly indicate that the length of the splitter plate has a substantial effect on the flow characteristics. They found the flow characteristics in the wake region of the circular cylinder sharply change up to the splitter plate length of L/D=1.0. and above this plate length, small changes occur in the flow characteristics.

Galvao et al. (2008) used vanes placed around the cylinder to control flow around a circular cylinder, reduce vortex-induced vibrations, and reduce drift coefficient. They experimentally realized this work by synchronizing a force

measurement system and a Particle Image Velocity Technique (PIV). First, with the aid of the two used vanes, we have reached the conclusion that the vibrations generated on the cylinder were completely eliminated and that the drag coefficient can be reduced to Cd = 0.5 for the sub-critical Reynolds values.

Assi, Bearman, and Kitney (2009) achieved suppression of cross-flow and in-line VIV of a circular cylinder, with resulting drag coefficients less than that for a fixed plain cylinder using two-dimensional control plates. He demonstrated how vortex-induced vibration can be practically eliminated by using free-to-rotate, two-dimensional control plates and further conclusion was that these devices achieve VIV suppression with drag reduction. He found the largest drag reduction to have a drag coefficient equal to about 60% of that for a plain, fixed cylinder over the Reynolds number range of the experiments, up to 30 000.

Shukla, Govardhan, and Arakeri (2009) investigated flow over a circular cylinder with a hinged-rigid splitter plate which typically made of 100μmm thickness two plastic sheets with a flexible plastic sheet of thickness 30μmm between them, as shown in Figure 2.8 by using PIV (Particle İmage Velocimetry) technique. D was the cylinder diameter, L was the splitter plate length.

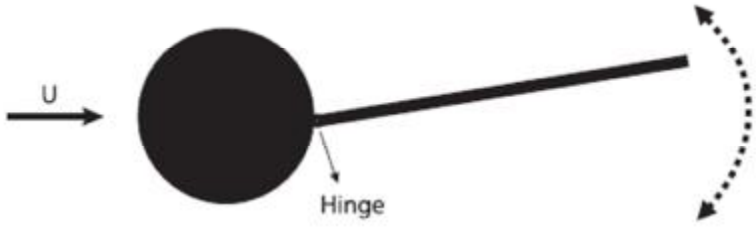

Figure 2.8 Schematic of cylinder with a hinged-rigid splitter plate. The rigid splitter plate was free to rotate about the hinge at the base of the cylinder (Shukla et al., 2009)

In their study they assigned main parameters were the Reynolds number (Re), splitter plate length to cylinder diameter ratio (L/D). On the other hand, the relative mass of the plate, and the stiffness and internal damping associated with

the hinge were not interested in this work and therefore these parameters consider as negligible. Hence, (L/D) and (Re) were the two effective dimensionless parameters. The momentary changes in the character and magnitude of the splitter plate oscillations may cause VIV problems. These experiments showed that the splitter plate length to cylinder diameter (L/D) ratio is important in determining the character and magnitude of the oscillations for the case of hinged splitter plate. They also realized from the experiments splitter plate oscillations increase with Reynolds numbers at low values of Re, and were found to reach a saturation amplitude level at higher Re. They concluded that at small splitter plate lengths ($L/D \leq 3.0$) the oscillations were periodic. If the splitter plate length increased beyond $L/D \geq 4.0$ plate oscillations began sudden changes which means became aperiodic but in small amplitudes. When the splitter plate length further increased $L/D \geq 5.0$ characteristic of splitter plate act like fixed-rigid splitter plate.

Gim, Kim, and Lee (2011) investigated the flow structure formed by placing control rods of different sizes immediately behind a circular cylinder with a particle imaging velocity measurement technique (PIV) in the water channel. Experiments were carried out for four different control rod sizes, with 50mm cylinder diameter for four different values ranging from 5000 to 20000 Reynolds numbers, and flow characteristics such as time average velocity field, turbulence intensity and Reynolds shear stresses were obtained. As a result, the cylinder trail was significantly influenced by the presence of the control rods, as a result of different interactions of the vortex pairs formed in the cylinder upper and lower regions, with the result that an optimum rod size for flow control and no Reynolds number value, different flow characteristics for each case were obtained.

Igbalajobi, McClean, Sumner, and Bergstrom (2013) In their present study, the effectiveness of a splitter plate was investigated for the flow around a circular cylinder at a Reynolds number of Re = 7.4 x 10^4. They used four type of cylinder aspect ratios AR = 9, 7, 5 and 3 to measure drag force coefficient and Strouhal number and five splitter-plate lengths, L/D = 1, 1.5, 2, 3, 5 and 7. For all

experiments, splitter plate placed on the centerline of wake and cylinders height kept constants and relative boundary layer thickness on the ground plane was always δ/D 1.5. They concluded that splitter plate is powerful drag reduction solution for infinite circular cylinder than the finite circular cylinder. Cylinder for AR = 9 with splitter plate length L/D = 1–3 has significant drag reduction (12% for the case of the infinite circular cylinder) was one of the important findings from this study of them. Besides of this finding when splitter plate became longer, drag coefficient increase slowly until the value that no splitter plate case.

Shukla, Govardhan, and Arakeri (2013) investigated experimentally the effect of flexible splitter plate on flow which was located in the wake of a circular cylinder. Plate can deform along its length when fluid-based forces act. They designated the parameter as the splitter plate length (L) and the flow speed (U), the flexural rigidity (EI) of the splitter plate for this study. The flexural rigidity (EI) indicate periodic traveling wave type deformations of the splitter plate with maximum tip amplitudes of the order of one-cylinder diameter. To understand the effect of EI they also designated dimensionless bending stiffness $K^* = EI/0{,}5\rho U^2 L^3$ where U was the free-stream velocity and L was the splitter plate length. If flow speed increase from small values, periodic plate oscillation with amplitude of about 0.5D which refer as mode I. When flow speed increase further the oscillation of splitter plate aperiodic with large variation in amplitude with time as a result higher flow speed, oscillation of splitter plate increases and became periodic again which refer as mode II. They founded that in periodic modes Strouhal number was about same (0.2) with no splitter plate case while frequencies of splitter plate motion were essentially lower in non-periodic regime. They concluded that from experiment results although shorter plates show significant differences, the splitter plate motions for varying splitter plate lengths indicate that plates that were substantially larger than the formation length of the plane cylinder wake have similar responses.

Gozmen, Akilli, and Sahin (2013) performed their experiments to control vortex shedding as they did in other studies such as(Gözmen et al., 2013). In previous articles, they also used the circular cylinder as a control body and a passive control method and the PIV technique as a control method. Differently, this work was used by the splitter plate alone. As shown in the Figure 2.9, the ratio of the circular cylinder diameter to the splitter plate length was taken as a main parameter (L/D) for experiments and second parameter was the height ratio (h_p/h_w) which means the ratio of the plate height to the water height. The Re number calculated according to the cylinder diameter was calculated as 6250. Control the vortex shedding separately, they found the L/D ratio to be 2 and h_p/h_w to be 1 as the most useful method. When evaluated alone, h_p/h_w ratio of 1 found as the most effective value but this value did not give the same effective and useful result in each plate length and when evaluated height ratio with plate length together, they observed the best ratio of h_p/h_w was 0.5 above all.

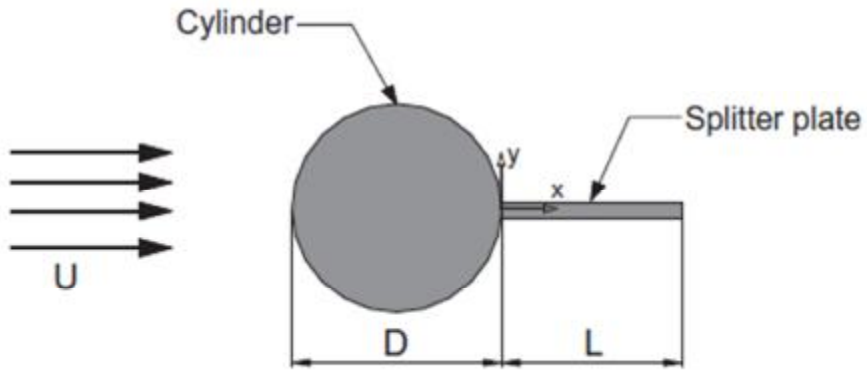

Figure 2.9 Parameter which used for experiments (Gozmen et al., 2013) Cylinder diameter D, length of plate L

Sarioglu (2017) studied experimentally vortex shedding formation behind square cylinder and conducted his experiments on subsonic wind tunnel. He used fixed splitter plate, which was located at the center of the back face of cylinder

Experiments have conducted at Reynolds number of $3x10^4$. The width of the plate and cylinder were chosen as 30mm and incidence angle of cylinder could rotate 0^o - 45^o. Pressure distribution. He found that near the angle of 13^o, although minimum drag coefficient was found, a sudden increase in the Strouhal number was encountered. When angle of incidence was zero, 20% decrease both drag coefficient and Strouhal number. He concluded from all experiments and findings drag reduction was minimum at about 13^o and reached its maximum value at about 20^o.

In recent years studies Gokturk Memduh Ozkan, Erhan Firat, and Huseyin Akilli (2017) examined the effect of splitter plates with various porosity ratios, which were located at a certain angle with respect to the flow, on the drift coefficient. They used two different test methods. The first part consists of dye experiments and the second part consists of PIV (Particle Image Velocimetry) experiments. Some parameters such as the diameter of cylinders and the Reynolds number (Re=5000) were kept constant in all experiments. The actual parameter to be investigated was porosity ratio (β). They explained β as the ratio of open surface area to the whole-body surface area. According to this definition values of β founded as β= 0.4, 0.5, 0.6, 0.7 and 0.8. As a result of the experiments performed, for the case β= 0.4, 0.5, 0.6, increased the drag coefficient acting on the cylinder even though it gave good results in preventing vortex shedding control. On the other hand, the situation was slightly different for β= 0.7, 0.8 in cases where plates with this permeability ratio were used, the success in preventing vortex shedding has not been achieved, but a good contribution has been made in terms of vibration and fluctuation acting on cylinder.

Gokturk M. Ozkan, Erhan Firat, and Huseyin Akilli (2017) used a perforated plate attached to fixed cylinder to control the vortex shedding at the same time to suppress and modify the two-dimensional flow structure around a stationary cylinder in the near future experimental work. Experiments in water they

used two different methods, PIV and flow visualization, as well as using the air tunnel to calculate the drift coefficient. The plate permeability (β) and the angle of the plate with the flow (θ) were selected as parameters in the experiments they made in the water and the purpose of the experiments made in the air tunnel was to find the effect of the drag coefficient of the plate on the drag coefficient of the stationary circular cylinder. When a perforated splitter plate was used it was seen that many results such as suppress vortex shedding and reducing the velocity fluctuations in the wake were obtained. From experimentally used splitter plate and angle combinations, plate permeability range $0.4 \leq \beta \leq 0.6$ and plate angle range $45° \leq \theta \leq 90$ °, reducing flow fluctuation, resulting in reduced turbulent kinetic energy and hence vortex induced vibrations. They also added some suggestion at the end of their study and it would be best to use in applications where the unsteady flow structure around the bluff bodies and the vortex induced vibration must be reduced to a great extent, using permeable plates with $0.4 \leq \beta \leq 0.6$ for $\theta \geq 30$ °, will give the best result, but it was also necessary to consider the increase in the drag coefficient.

2.2. Active Control Methods

2.2.1. Control of Vortex Shedding by Electrical Methods

With the simple cylinder model developed by Roshko Artana, Sosa, Moreau, and Touchard (2003) experimentally investigated the time average flow parameters of near wake using an electro hydrodynamic actuator. These experiments were carried out for the cases where the flow was perturbed steadily and the Reynolds number ranges between $2{,}300 < Re < 58{,}000$. Experiments were carried out in the air tunnel and using two electrodes both parallel to the cylinder axis. They concluded from experimental data, despite the fact that the effect of the actuator in the low Reynolds numbers has a noticeable effect on the near wake flow field, in the case of the high Reynolds number, the actuator has not much effect on the separation of the boundary layers.

Hyun and Chun (2003) tried to control the vortex generated by the flow in contact with the cylindrical surface in the experimental work they done using the ion wind method which was one of the active control methods. Ions were produced in strong electrical fields and the electric momentum of these ions was transferred to the fluid in the environment. So that a fluid movement was provided. This was called the ion wind. One of the parameters that they had tested was the distance between the electrode wire and the cylinder this was expressed as H. The other one was the angular values measured clockwise from the front stagnation point and these angle values were also shown as θ. Two wires were used except for the case where the angle is 180^{o}.As a result of the experiments carried out, it was observed that the ion wind was an effective way to control wake flow, vortex shedding and flow separation.

Thomas, Kozlov, and Corke (2008) used single dielectric barrier discharge plasma actuators (basic features of this type of actuator could be seen in the work of Enloe et al. (2004)) in order to control cylinder flow control, unsteady vortex shedding, and to reduce noise. In the study of $Re = 3.3x10^{4}$ value, both steady and unsteady operation were used. They noted that in both steady and unsteady, the results of the Karman vortex shedding were canceled, the turbulence levels in the wake were significantly reduced and the sound pressure levels were reduced by 13.3 dB. Although the unsteady actuator reduced total shedding pressure by 25%, steady actuator was suitable for sound control as unsteady body force increases the actuation frequency when unsteady actuator was used.

Mertz and Corke (2011) developed to acquire the dynamic structure of the local air ionization and vector distribution for unsteady body force which was the mechanism to achieve flow control. They used single dielectric barrier discharge plasma actuators (basic features of this type of actuator can be seen in the work of Enloe et al. (2004)) in order to control cylinder flow control, unsteady vortex shedding, and to reduce noise. They concluded that numerical experiments to

simulate the SDBD plasma actuator model using two flow simulations included an impulsively started plasma actuator in still air, and the flow around a circular cylinder in which plasma actuators were used to suppress the Karman vortex street. Experiments and numerical studies show that output results were in support of each other

2.2.2. Control of Vortex Shedding by Feedback Control Method

Feedback control method was an active method based on the principle of applying an actuator feedback from an appropriate sensor. In the early period Williams and Zhao (1989) were examples of the early use of the feedback method with the experimental setups they have arranged as an acoustic feedback of signals taken from hot-wires located in the wake of circular cylinder. Another in the early period study, Park et al. (1994) work was done using the principle of this feedback method. They used this two-dimensional Naiver Stokes equation to do this work to control Karman vortices around the circular cylinder at low Reynolds number. They have concluded that the use of a single feedback sensor and Reynolds number of Re = 60 values the vortex shedding was suppressed completely. On the other hand, when the position of the feedback sensor was fixed, the vortex shedding was suppressed by the increasing feedback gain α. The increasing feedback gain α was trying to disrupt the flow balance and Re = 80 and over has become unable to provide the desired control over the vortex shedding.

Using a nonlinear model Roussopoulos and Monkewitz (1996), they used the feedback method to control Karman vortices. The Re = 47 Reynolds numbers that were critical to the cylinder diameter, for long cylinders vortex shedding can only be suppressed at the spanwise location of the sensor even though the actuation occurs uniformly over the entire span.

Tao, Huang, and Chan (1996) have done visualization exercises to understand how the wake flow behind the cylinder were affected when the feedback method was used. They concluded that when no control method was

used, the resulting natural vortex street were suppressed when the feedback method was used. At the same time, the wavy streak lines converted to become almost a straight line. Also, the peak points indicated by the monitor probe were observed to fall off when using the feedback method.

Fujisawa et al. (2001) examined the vortex shedding behind the circular cylinder, made it at the moderate Reynolds numbers. The experimental work they conducted as a principle works according to the following event cycle. The feedback signal was generated using the velocity values of the cylinder wake with this signal the rotary cylinder oscillations were controlled. As a result of the experiments, velocity fluctuations and fluid forces were found to decrease in comparison to experiments in uncontrolled practice.

Fujisawa and Nakabayashi (2002) performed experimental study in order to control the vortex behavior behind the circular cylinder using feedback method with rotational oscillation. This method, which was classified as an active method, uses a neural network model. They explained that the purpose of this model was to maximize the performance of the feedback system. The results of the experiments could be summarized as a single sentence as experiments using the most favorable feedback control have shown that the lift force was suppressed by 70% and drag force reduced 16% compared to the case where it was compared with the fixed cylinder.

2.2.3. Control of Vortex Shedding Generating Secondary Flow

Seal and Smith (1999) studied effect of steady suction on turbulent flow junction and used Particle Image Velocimetry to visualize the flow pattern and collect data from downstream and cross-stream planes. The results show that both the sudden turbulent vortex and the surface interactions associated with it in the plane of symmetry could be weaken, can actively remove the presence of the turbulent necklace in symmetry plane and weakens the extensions of the vortex at the downstream. All effects achieved by the surface suction.

Tensi, Boué, Paillé, and Dury (2002) aimed to control of the flow around circular cylinder at Reynolds number of 105 (with respect to cylinder diameter) with method of unsteady blowing (synthetic jet). Synthetic jet performance was digitized by terms of delaying separation and altering drag coefficient. It was suggested that zero-mass-flux actuator types, which require little energy, could be used for further flow control around various bodies including airfoils.

W.-L. Chen et al. (2013) conducted experimental study on circular cylinder aimed suppress the vortex induced vibration by using one of the active methods which was suction flow control method. As shown on the Figure 2.10 experiments were conducted in a wind tunnel had test section 4.0m (width) x 3.0 m (height) with a length of 25m. Acrylic circular cylinder with spring mass system used for this study and on the cylinder has four suction holes has a diameter of 10 mm located at the lowest point of the cylinder. In a system where flow control was used or not used, Vortex Induced Vibration as well as vibration dynamics were quantified in terms of fluctuating pressure coefficients and aerodynamic force coefficients acting on the cylinder. Therefore, the parameters related to the flow, the suction flow rate and the success of control method were found quantitatively. For tests with different suction flow rates, the best control was not achieved either at very low or very high flow rates. Instead, maximum efficiency was obtained at the optimum suction rate compared to these values. The information from the test results shows that a steady suction flow control was a useful method for reducing and suppressing VIV.

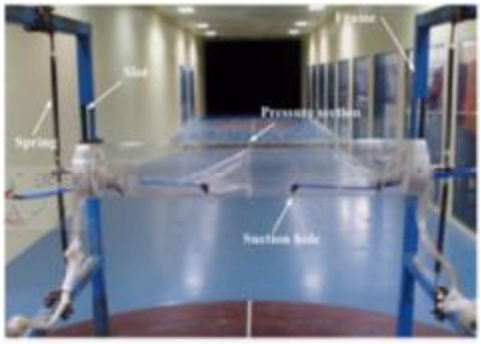

Figure 2.10 Experimental setup of a cylindrical cable model (W.-L. Chen et al., 2013)

2.2.4. Control of Vortex Shedding By A Magnetic Field

Magnetohydrodynamics (MHD) known and classified as active control method and also classified as a boundary layer control method. Basically; this method was related to the dynamics of magnetic field in medium which conducting electrical current. Any movement that occurred in the magnetic field creates electrical current. In the place where the magnetic field and current were, the unit volume of liquid was subjected to a fluid force known as Lorentz force. Since this force acts in the opposite direction to the flow, it not only slows down the flow rate and provides a certain balance in the flow but also have significant effect on the drag and lift forces acting on the body.

Mutschke et al. (1998) studied on circular cylinder wake control with magnetic field. They aimed to control 2-D and 3-D flow by performing numerical experiments on flow with different Re number. They concluded that 2-D flow could be stabilized and vortex shedding could be suppressed by using strong magnetic field. Z. Chen and Aubry (2005) aimed to develop a numeric algorithm for both wake control of circular cylinder and flow separation from cylinder in a water with low conductivity water consistency. This was achieved through the introduction of a Lorentz force in the azimuthal direction generated by an array of permanent magnets and electrodes located on the solid structure. With the use of a symmetric and static Lorentz force over the entire surface of the cylinder, the

vortex shedding behind the cylinder weakens and eventually disappears completely when the Lorentz force was sufficiently large. Sintu Singha (2011) aimed to control the vortex shedding on the circular cylinder placed in the middle of the channel and with the number of Re ranging from 50 to 250. They found that periodic vortexes at high Re values were completely eliminated if enough imposed magnetic field was applied.

3. MATERIAL AND METHOD

3.1. Experimental Arrangement

Increasing technological developments, especially in electric and electronic engineering, provide new measuring techniques. All measurement techniques have some advantages and disadvantages associated with the specific method. It was increasingly important not only to measure the mean values at a point in space, but also to measure and characterize turbulent and instantaneous values in the investigated flow field. Particle Image Velocimetry, PIV, was a non-intrusive technique used to measure an instantaneous two-dimensional velocity vector field under investigated area. The velocity was determined by measuring the displacement of particles in a flow field that was illuminated by a laser sheet.

3.1.1. Water Channel System

Experiments were carried out in a large-scale water channel located in the Fluid Mechanics Laboratory at Çukurova University. The model of water channel was shown in Figure 3.1. The channel has the following dimensions: a length of 8000 mm, width of 1000 mm, and a depth of 750 mm. The water channel test section was constructed of transparent Plexiglas with the thickness of 15 mm with upstream and downstream fiberglass reservoirs. A honeycomb screen arrangement was placed at the entrance of contraction in order to maintain the turbulence intensity below 0.1 %. The water velocity in the channel was adjusted by a centrifugal pump which can operate at different speeds with the help of a speed control unit.

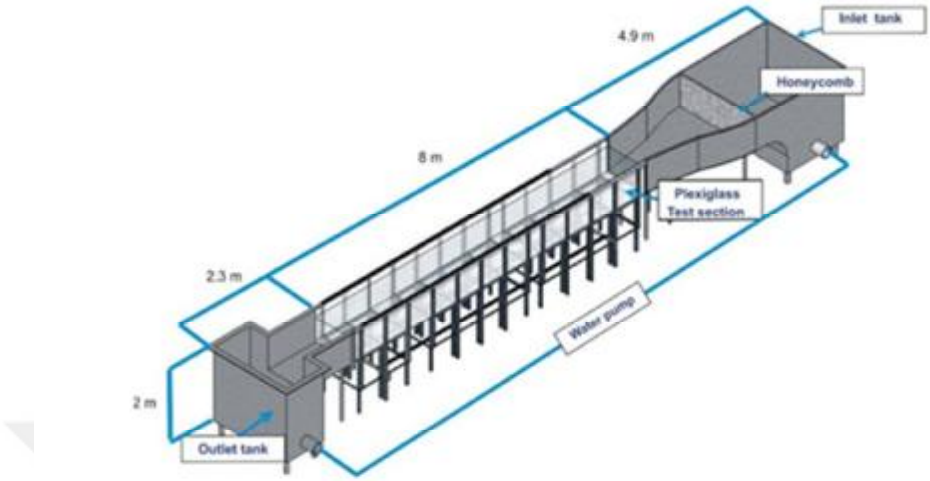

Figure 3.1 The model of water channel

Deep water experiments were carried out on a platform placed in the water channel. For experiments, the reason why the platform was chosen instead of the base of the channel was that the perforated outer cylinders and perforated plates used in the experiments were fixed with the help of an apparatus connected to the plexi-glass plate on the platform (this platform has to be connected to the channel

base if the platform has not been made) was set with the apparatus. The length of this platform was 2300mm, the width was 980mm, and the height of the platform base from the bottom of the water channel was adjusted to be 220mm with the upper plexi-glass layer (Figure 3.2).

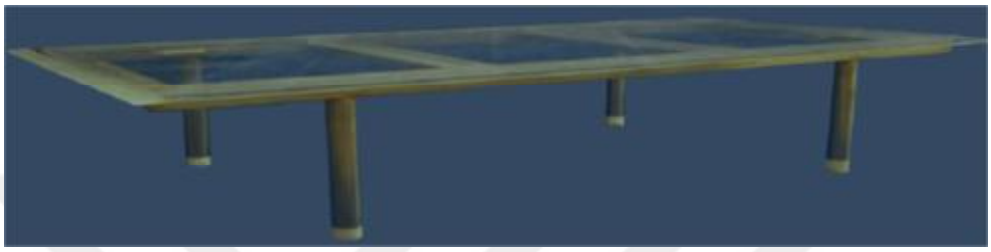

Figure 3.2 The platform where placed in the water channel to create deep water flow and adjust the Reynolds number, Re as desired

3.2. Experiment and Measurement Technique

3.2.1. Flow Visualization Techniques

The dye-injection flow visualization experiments were conducted in a largescale water channel. The cylinder model (D_i = 50 mm) was constructed of a type of acetyl polymer called Delrin which was a highly versatile engineering polymer. The outer meshed cylinders (control elements) with diameter, D_o of 125 mm was constructed of chrome-nickel screens having different porosities. The cylinder was located at 5.5m from the entrance of the water channel. Reynolds number was kept constant Re =5000.

The method to be applied in dye experiments was as follows; light sensitive dye (Fluorescent Paint, Rhodamine 6G or Rhodamine B) was mixed with water to form a solution. The dye solution was transparent in daylight. However, the dye was visible when it was illuminated by a laser in a dark environment. In the dark, the dye and hence the flow structure was made visible. The dye color was green, red and yellow colors depending on the laser and the color. A continuous type laser (Spectra Physics) unit was used during the dye experiments as shown in Figure 3.4. The dye solution prepared in a container and dye came from a

container, which were located 75 cm above the free surface of the water channel and went through a plastic tube. Dye visualization technique aimed to visualize flow by spreading some amount of Rhodamine type dye that shines under the continuous laser light in the desired flow field. The video camera which was SONY HD-SR1 was used to capture the instantaneous video images of the vortex flow structures. Digitized images were enhanced for analysis using Picture Motion Browser program. The video images were then analyzed to obtain images representative of the flow structure for each experimental situation. Each experiment was recorded for approximately three minutes. However, in some critical situations this time increased to 15 minutes. The dye visualization technique offered no numerical analysis or data to use but showed a brief demonstration of the flow that gives an idea about the flow field and the vortices. A brief demonstration of the dye visualization setup is shown in Figure 3.3.

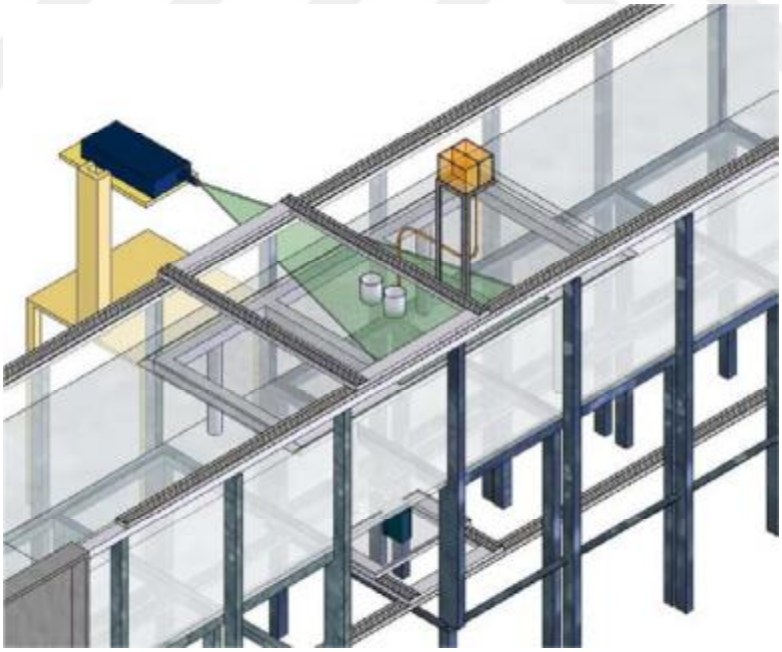

Figure 3.3 Overview of dye visualization technique in water channel

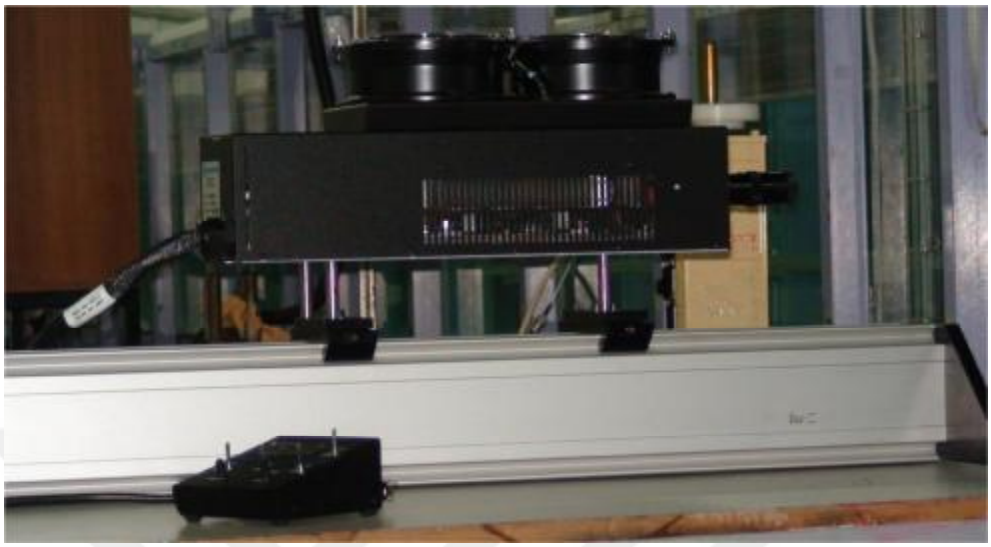

Figure 3.4 Continuous laser used for experiments.

3.2.2. Particle Image Velocimetry (PIV) Techniques

Particle Image Velocimetry (PIV) was a numerical measurement technique used to simultaneously determine the velocities at many points in a flow field. The technique involved seeding the flow field, illuminating the region under investigation and capturing two images of that region in rapid succession. From the displacement of the tracer particles, provided that the time interval between image captures was known, a velocity vector map could be calculated in the flow field. The theory of PIV was introduced by Landreth and Adrian (1988) in the late 1980s with the first experimental implementations following shortly afterwards (Keane & Adrian, 1990). At the stage, due to hardware limitations, a single photographic frame was multiplying exposed and analyzed using an auto-correlation technique. However, improved speed of photographic recording soon allowed images to be captured on separate frames for analysis by cross-correlation. The introduction of digital camera technology to PIV enabled the direct recording of particle images (Willert & Gharib, 1991), at the expense of reduced resolution, resulting in the development of digital PIV (Jerry Westerweel, Dabiri, & Gharib, 1997). As well as

these hardware advances, many new algorithms developed in the last decade, increasing the accuracy and speed of PIV analysis. One key advantage of the PIV technique over other conventional techniques such as LDV or hotwire anemometry was ability to obtain instantaneous flow-field information was important for probing the structure of turbulent flow fields. (Meinhart & Adrian, 1995; J Westerweel, Draad, Van der Hoeven, & Van Oord, 1996)

3.2.2.1. Principle of PIV

Particle Image Velocimetry (PIV) was a measurement technique for obtaining instantaneous whole field velocities. It was based on the well-known equation

$$\text{Speed} = \text{Distance} / \text{Time}$$

In PIV the property actually measured was the distance traveled by particles in the flow field within a known time interval. These particles were added to the flow and known as seeding. Different types of seeding particle were used depending on the nature of the flow for PIV experiments. The type of seeding particle was chosen to follow the flow, and in order to detect their movement, an area of the flow field was illuminated by a light-sheet. The light-sheet, which was generated by a laser and a system of optical components, was not continuous/permanent, but pulsed to produce a stroboscopic effect, freezing the movement of the seeding particles. The time between the light pulses was the denominator in the equation above. To detect the position of the illuminated seeding particles, a CCD-camera (CCD = Charge Coupled Device) was positioned at right angles to the light-sheet, and particle positions will appear as light specks on a dark background on each camera frame. The pulsing light-sheet and the camera were synchronized so that particle positions at the instant of light pulse number 1 were registered on frame 1 of the camera, and particle positions from

pulse number 2 were on frame 2. (Older generations of CCD cameras couldn't switch frames fast enough, so both the first and the second pulse of the light sheet was recorded on the same camera frame).

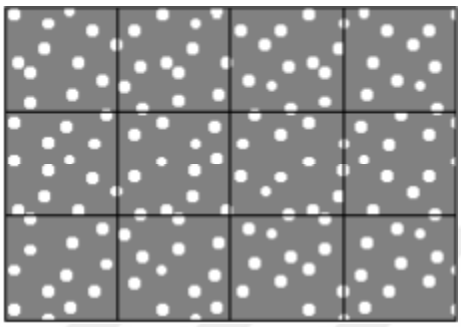

Figure 3.5 Interrogation areas

The camera images were divided into square regions called interrogation areas or interrogation regions, and for each of these interrogation areas the image from the first and the second pulse of the light-sheet were correlated to produce an average particle displacement vector. Doing the same process for all interrogation regions produce a vector map of average particle displacements. Dividing with the known time between the two images captured, the displacement vectors were converted into a map of so-called raw velocity vectors. Then validation algorithms can be applied to the raw vector maps, so that outliers, the term for erroneous vectors, can be detected and removed. In the Flow Map PIV system, for reasons of experimental reproducibility, the raw vector map was archived and a new validated vector map was output, and further analysis could produce streamlines, vorticity and so on.

From the basic principles the following main topics of PIV emerge:

- Seeding
- Illumination
- Cameras

- Synchronization
- Correlation
- Validation and further analysis

3.2.2.2. Image Acquisition

The flow under investigation was illuminated by laser sheet and images of the illuminated flow field were captured and stored for later analysis. In Figure 3.6, typical experimental arrangement for PIV measurements was demonstrated.

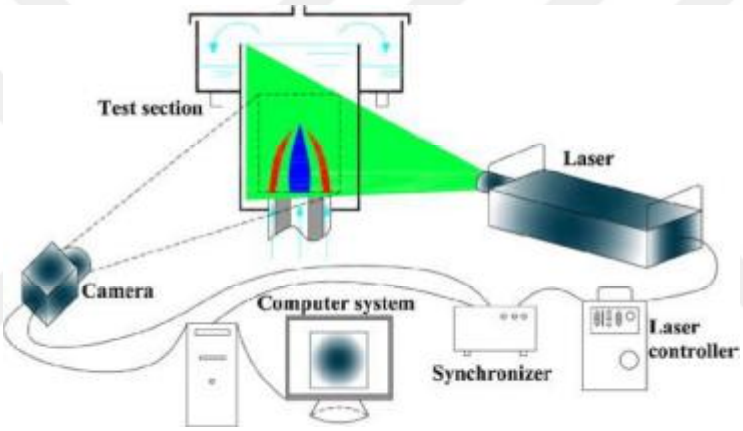

Figure 3.6 Typical experimental arrangement for PIV measurements

3.2.2.3. Seeding

Seeding particles were added to the flow for tracing the velocity field by means of recording the particle images with a camera. Therefore, the size, number, distribution and tracking ability of the particles and their images were very important. Moreover, Particle size and density, and fluid density and viscosity, determine the effects of buoyancy and inertia. Exact neutral buoyancy was difficult to achieve, but particles must remain suspended throughout an experiment.

As the seeding of flow field was explained, we should mention Stokes number. The Stokes Number which provides a measure of particles' ability to track

the flow field and the limiting of Stokes number depends on the flow and the occurrence of considerable accelerations or decelerations.

Stokes number was defined as the ratio of the response time of a particle to the characteristic time of the flow field;

$$S_k = \frac{\tau_p}{\tau_f} \tag{3.1}$$

Here, τ_f was determined by the ratio of the diameter of particle to fluid velocity.

$$S_k = \frac{\tau_p . U_\infty}{d_{particle}} \tag{3.2}$$

The response time of a particle was given by

$$\tau_p = \frac{\rho_{particle} . d_{particle}^2}{18 \rho_{fluid} . \vartheta_{fluid}} \tag{3.3}$$

At this equation, $\rho_{particle}$ and $d_{particle}$ show particle density and particle diameter as ρ_{fluid} indicates fluid density.

For acceptable accuracy of tracing, the particle response time should be faster than the smallest time scale of the flow. Smaller Stokes numbers present better tracing accuracy; for S_k >> 1, particles will detach from a flow especially where the flow decelerates abruptly. For S_k << 1, particles follow fluid streamlines closely. If S_k << 1, tracing accuracy errors were below 1%. The Stoke Number for this study was calculated about 1.83×10^{-4}

In general, the seeding in water was easier than in air. For water applications, typically polystyrene, polyamide or hollow glass spheres shedding which were in the range 5 mm to 100 mm were used. Any particle that follows the flow satisfactorily and scatters enough light to be captured by the CCD camera can be used. The number of particles in the flow was important to obtain a good signal peak in the cross-correlation. As a rule of thumb, 10 to 25 particles should be seen in each interrogation area.

3.2.2.4. Illumination

To illuminate the flow field, lasers were used as illumination sources since they can produce a pulsed, collimated and monochromatic light beam that can be easily formed into a thin light sheet. The PIV illumination method involves important criteria as following:

- The duration of the illumination light pulse should be sufficiently short so that the motion of the particles was “frozen” during the pulse exposure in order to avoid blurring of the images.
- Time delay between the illumination pulses should be long enough to enable the displacement between the images of the tracer particles to be determined with sufficient resolution and short enough to avoid particles with an out-of-plane velocity component leaving the light sheet between subsequent illuminations.
- The light power should be sufficiently high to ensure the intensity of scattered light from the seeding particles was such that images of them can be recorded on the used camera in PIV system.

The most common device used for PIV experiments was the solid-state frequency-doubled Nd: YAG laser that emits light with a wavelength of 532 nm. It produces pulse energies ranging between 10 mj and 1 j. With its very short pulse duration (5-15 ns) this instrument was practically suited to illuminate flows without any limit on the flow speed. However, the repetition rate of a YAG-laser was typically 10-50 Hz, which causing the major limitation of Nd: YAG based systems in carrying out time-resolved experiments except for very low-speed ($v < 0.2$ m/s) flows. (Tropea & Yarin, 2007)

3.2.2.5. Image Capturing

Full-frame progressive scan interline transfer CCD camera, also called as cross-correlation CCD-camera was used to acquire two single exposed images with a time separation of the order of microseconds. The basic working principle was that the image exposed by the first laser pulse was transferred very quickly to light hidden areas on the CCD-chip. Each pixel has its own storage site in immediate vicinity of the light sensitive pixel area. Both images were transferred to the computer after the second exposure. Only a few double-images can be taken per second owing to fact that a lot of data has to be transferred in computer.

Proper seeding of the flow with tracer particle was important to obtain accurate PIV measurements. The particles should be as small as possible in order to follow closely the flow. However, the seeding particles should not be too small since very small particles don’t scatter enough light. Additionally, the camera and the laser pulse should be synchronized in order to capture the images accurately.

3.2.2.6. Image Evaluation

Image evaluation consists of pre-processing, interrogation, data analysis and post processing. Particle image velocimetry processing basically defines the distance that the particles have moved in the time between laser illuminations in photographic based or laser pulses in digital PIV. In order to determine this

distance, the most common methods were particle tracking or correlation. There were many correlation methods such as auto-correlation, one-frame cross-correlation and two-frame cross correlation. The differences in these correlation techniques were the image window areas for the first and second images. In the auto-correlation, the same image window was used for both first and second images window. In the one-frame cross-correlation, the second image window was offset in the flow direction from the first image on the same window. The processing of the one-frame cross-correlation depends on the amount of overlap between the first and second image windows. In two-frame cross correlation, the first image window located on the first frame and the second image window was located on the second frame. Both interrogation windows in time delay have the same coordinate. In this study, cross-correlation technique was used to determine the distance when particles move in the period of specified time of two laser illuminations. The cross correlation of each pair of interrogation areas was obtained using Fourier transform operator. After interrogating the images in this way and generating the vector map, post-processing was carried out to validate the data and to improve the vector map resolution and accuracy. Using this vector map, vorticity and Reynolds stress contours and streamline topology can be obtained.

In order to determine incorrect vectors from interrogation, the resulting vector field obtained from FLOWMAP software and the corresponding boundaries of objects were examined using program. These types of vectors can exist when an incorrect particle correlation was made near boundaries or within shadow regions. To eliminate incorrect vectors, vector validation software called CLEANVEC was used. The software CLEANVEC contains four statistical filters designed for incorrect vectors removal

3.2.2.7. PIV Parameters used in this study

The experiments were performed and the measured data were processed using Dantec Dynamics PIV system and FLOW MANAGER Software installed on

a computer. The measurement field was illuminated by a thin and an intense laser light sheet by using a pair of double-pulsed Nd:YAG (yttrium aluminum garnet) laser units each having a maximum energy output of 120 mJ at 532 nm wavelength.

The image capturing was performed by an 8-bit cross-correlation charge-coupled device (CCD) camera having a resolution of 1008×1016 pixels, equipped with a Nikon AF Micro 60 f / 2.8D lens. In the image processing, 32×32 rectangular interrogation pixels were used and an overlap of 50% was employed. A total of 3844 (62×62) velocity vectors were obtained for an instantaneous velocity field at a rate of 15 frames/ s. The plan view of measuring planes covered the downstream of the cylinder with the area of 200mm x 200mm for all configurations and the image magnification was 0.0709 mm/pixel. The laser sheet was oriented parallel to the bottom surface of the water channel and the experiments were carried out at the mid- plane of the water height. Water heights were taken to be 50mm. The time interval between pulses was 1.75 ms for all experiments and the thickness of the laser sheet illuminating the measurement plane was approximately 2 mm. The time interval and the laser sheet thickness were selected such that the maximum number of particles in the interrogation window was obtained. The number of particles in an interrogation area was in between 20 and 25. The uncertainty in velocity relative to depth averaged velocity was about 2% in the present experiments. The water was seeded with 12 μm diameter hollow glass sphere particles. The instantaneous images were captured, recorded, and stored in order to obtain averaged-velocity vectors and other statistical properties of the flow field. Spurious velocity vectors (less than 3%) were removed using the local median-filter technique and replaced by using a bilinear least square fit technique between surrounding vectors. The velocity vector field was also smoothed to avoid dramatic changes in the velocity field using the Gaussian smoothing technique. The vorticity value at each grid point was calculated from the circulation around the eight neighboring points. All

experiments were carried out above a platform, having a length of 2300mm to obtain fully developed shallow flow conditions.

3.3. Experimental Model

3.3.1. Definition of the Porosity of The Outer Cylinder and The Splitter Plate

In present study, permeable cylinders constructed from chrome-nickel wire mesh were used as a passive control method of vortex shedding downstream of a circular cylinder (inner cylinder). In this study, the effects of the porosity of outer cylinder and the porosity of the splitter plate were investigated. Porosity was defined as the ratio of the gap area on the body to the whole-body surface area. Porosity value was calculated by using the following formula including wire diameter and distance between two wires. It was shown in Figure 3.7.

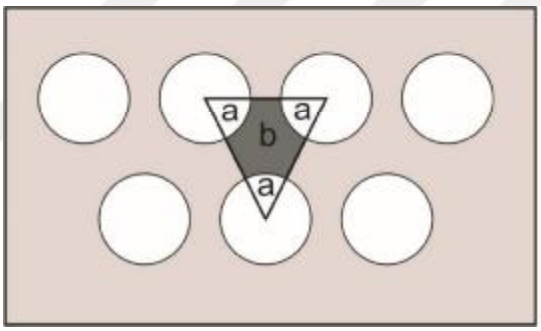

$$\beta = \frac{3a}{3a+b}$$

Figure 3.7 Calculation of the Porosity, β

Both the outer cylinder and the plate had a porosity because of that preventing they intermix with each other, the symbol, β_p were used when referring to the plate porosities, while the symbol, β_c were used when referring to the outer cylinder porosities. Three different wire meshes were used corresponding to three values of porosity as β = 0.3, 0.5, 0.7 for all elements of experiments (outer cylinder and splitter plate) The diameters of permeable outer cylinder for each porosity were constant as 125mm. Considering the fact that the diameter of the inner cylinder was 50mm, the diameter ratio of the inner cylinder to the outer

cylinder, D_i/D_o become D_i/D_o = 0.4. In order to investigate the effect of the porosities of the outer cylinder and splitter plate, the diameter ratio of cylinder pair was kept constant as D_i/D_o= 0.4 for all experiments. During the experiments the inner cylinder and perforated outer cylinder were positioned in a way that they were concentric. The outer cylinder was positioned towards downstream direction, in a concentric way and in near wake region of the inner cylinder.

In order to investigate the effect of porosity on the unsteady flow structure created inner region of the inner cylinders, outer cylinders of three different porosities were used as β_c = 0.3, 0.5, 0.7. The perforated outer cylinders were obtained by perforating d = 5mm diameter holes on 1 mm stainless steel plates and then bending the plates. Spring length of the perforated half and quarter outer cylinders were respectively.

There were two different parameters that are used to examine the effect of the presence of the plate on the flow structure. The first parameter was the plate porosity (β_p) which have three different value as β_p = 0.3, 0.5, 0.7 same as the outer cylinder. The second was the angle of the splitter plate which have five different angles as α = 60°, 90°, 120°, 150°, 180°. The placement of the cylinder pair and splitter plate represented in Figure 3.10. A view of the experimental setup was presented in Figure 3.8 and Figure 3.9. All measurements were done on the plan view for water heights of h_w= 50mm, laser sheet was located parallel to the bottom of the water channel at heights of h_L=25mm for each case.

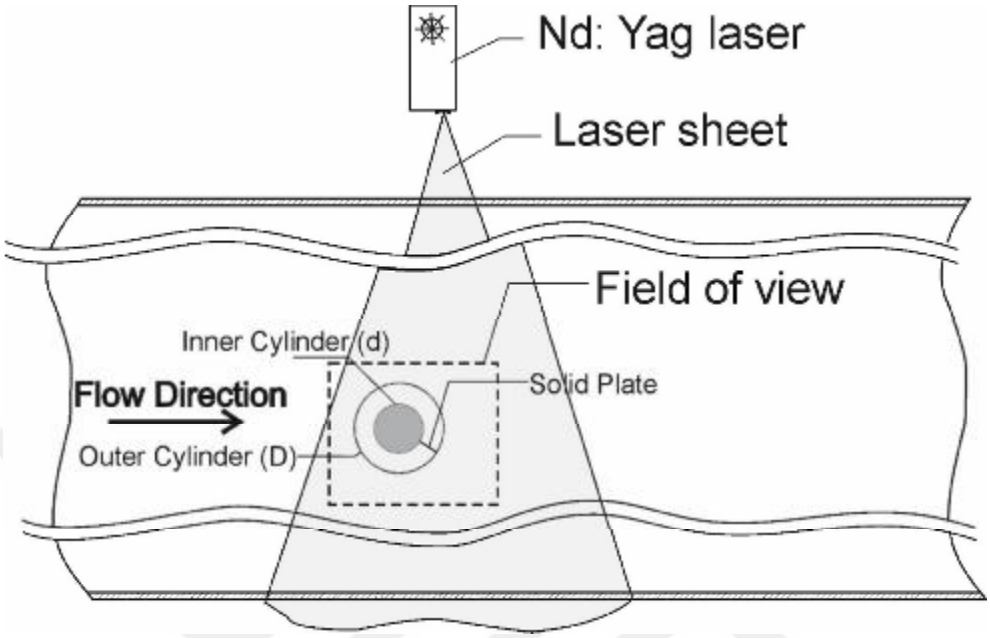

Figure 3.8 Plan view of the system

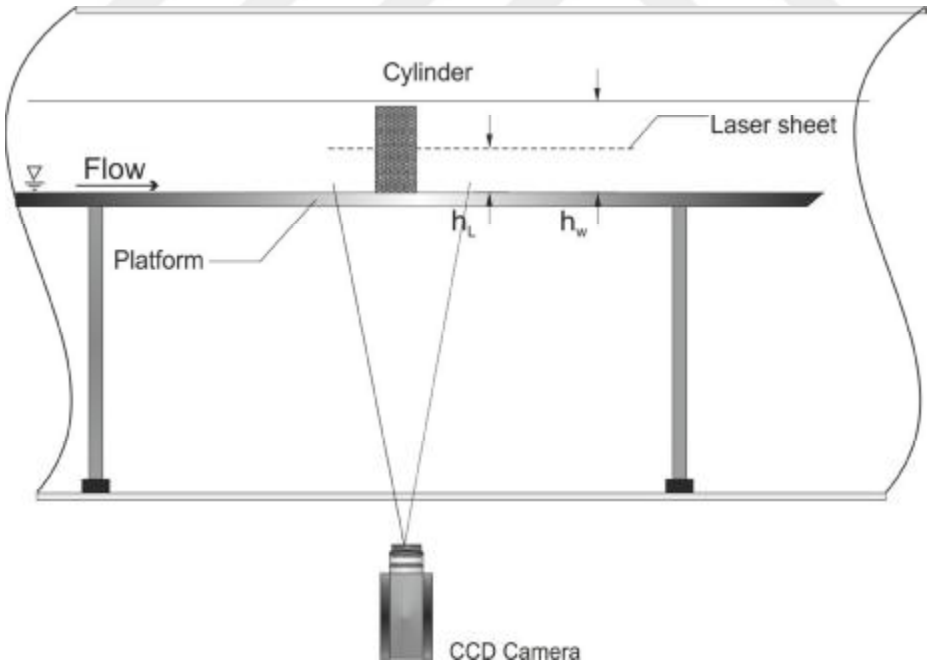

Figure 3.9 Overview of experimental system for side view

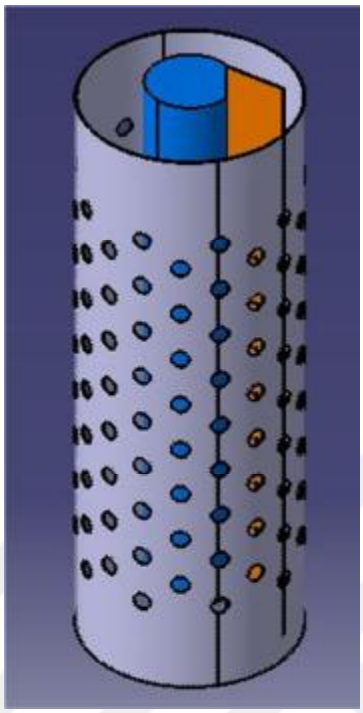

Figure 3.10 Overview of inner cylinder, outer cylinder and splitter plate

4. RESULT AND DISCUSSION

4.1. Inner Cylinder Results

Before the outer cylinder and the splitter plate are used as control members, it is appropriate to examine the behavior of the flow structure downstream of the inner cylinder. For this purpose, the time average vorticity contours <ω> and the time average streamlines <ψ> are presented in Figure 4.1. These images were obtained from 1000 instantaneous images from PIV technique. Since, (Roshko, 1954) Karman Vortex Street formation occurs in downstream of the cylinder as mentioned in the introduction causes plenty of undesired problems on cylinder such as velocity fluctuations. The high vorticity magnitudes in transverse direction can be seen close to the shear layer of cylinder in the first image of Figure 4.1. These time averaged vorticity magnitude forms symmetrical and as can be seen getting closer to each other in the wake region. When second image of Figure 4.1is examined, as can be seen that the time averaged streamlines form F_1 and F_2 focal points near the inner cylinder. Focal points occur behind the cylinder form symmetrical as expected.

Turbulent kinetic energy (TKE) of cylinder was also calculated. Assuming that the flow is 2D and taking the third component of velocity equal to the half of ($\overline{u'u'}$ + $\overline{v'v'}$) (Sheng, Meng, & Fox, 2000), then TKE formula resulting in the following expression.

$$TKE = \frac{3}{4} [\, \overline{u'u'} + \overline{v'v'} \,]$$

TKE increase in downstream direction starting from the base of the cylinder and reach their peak values of 0.44. Then, it starts to decrease progressively through the downstream direction.

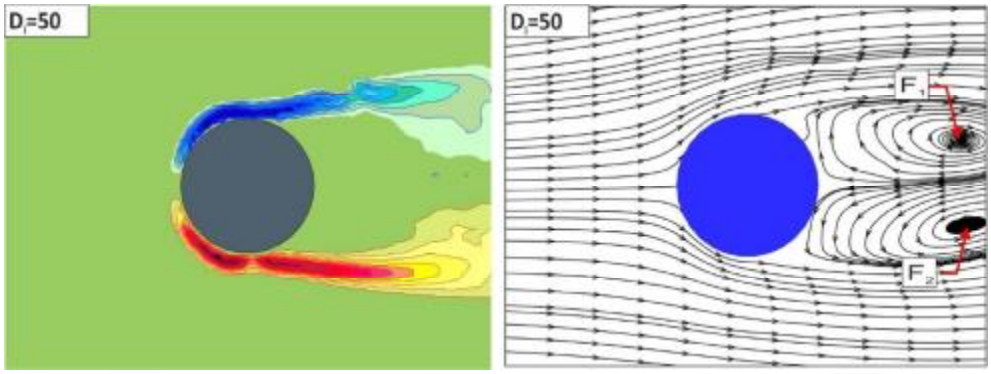

Figure 4.1 Time-averaged vorticity contours and corresponding streamline topology for the inner cylinder

4.2. Dye Visualization Experiments Results

The dye visualization experiments were performed prior to the PIV experiments to obtain a quantitative understanding of the flow behavior in the annular region. Rhodamine 6G, the fluorescent molecules were used for the dye visualization experiments and results were examined to investigate especially area close to the annular region. One of the objectives of the thesis to control the possible vortex pairs that form in the annular region and the vortex breakages that follow. The most obvious parameter in this case was D_i/D_o = 0.4, which is the diameter ratio of the cylinder pair. First of all, it must be noted that the quality of the dye visualization appearance increases as the porosity ratios increase due to the holes on the outer cylinder surface, and the illumination for low porosity ratios such as β_c = 0.3 appears to be insufficient than the β_c = 0.5 and the β_c = 0.7 cylinders. For this reason, the direction and behavior of the flow in annular region is shown with red arrows obtained by watching and following the videos of all experimental cases. Here the dashed outer line presents the perforated outer cylinder located concentrically around the inner cylinder. When the outer cylinder has a β_c = 0.3 porosity ratio, less amount of the flow enters though the outer cylinder holes than the cylinder with β_c = 0.5 and β_c = 0.7. The same result can be

observed when the splitter plate is used in a similar approach. The instantaneous flow visualization images of only perforated cylinder and the inner-outer cylinder pair are given in the Figure 4.2. In the use of only $\beta_c = 0.3$ cylinder, it is seen that the flow that directed to rear side of perforated cylinder forms the jet-like structure. The $\beta_c = 0.5$ cylinder gives similar jet flow structure in downstream of cylinder as $\beta_c = 0.3$. This similarity is an indicator the porosity of the outer cylinder, β_c has dominant effect on the flow characteristic in annular region. When the porosity value increased to $\beta_c = 0.7$ as shown in last line of Figure 4.2. it is clearly observed that jet-like structure did not occur at rear side of perforated cylinder. The expression of $\beta_c = 0.3$ outer cylinders behaves almost like a solid cylinder (no holes) therefore this cylinder is not very efficacious on controlling the vortex pair in the annular region. Furthermore, it is expected that the vorticity concentration and the turbulence values will be low at $\beta_c = 0.3$ outer cylinder than $\beta_c = 0.5$ and $\beta_c = 0.7$. In the second column of Figure 4.2, instantaneous flow images of the cylinder pair are presented. An incoherent but persistent vortex pair is observed within the annular region downstream of the inner cylinder which might increase the turbulence within this region.

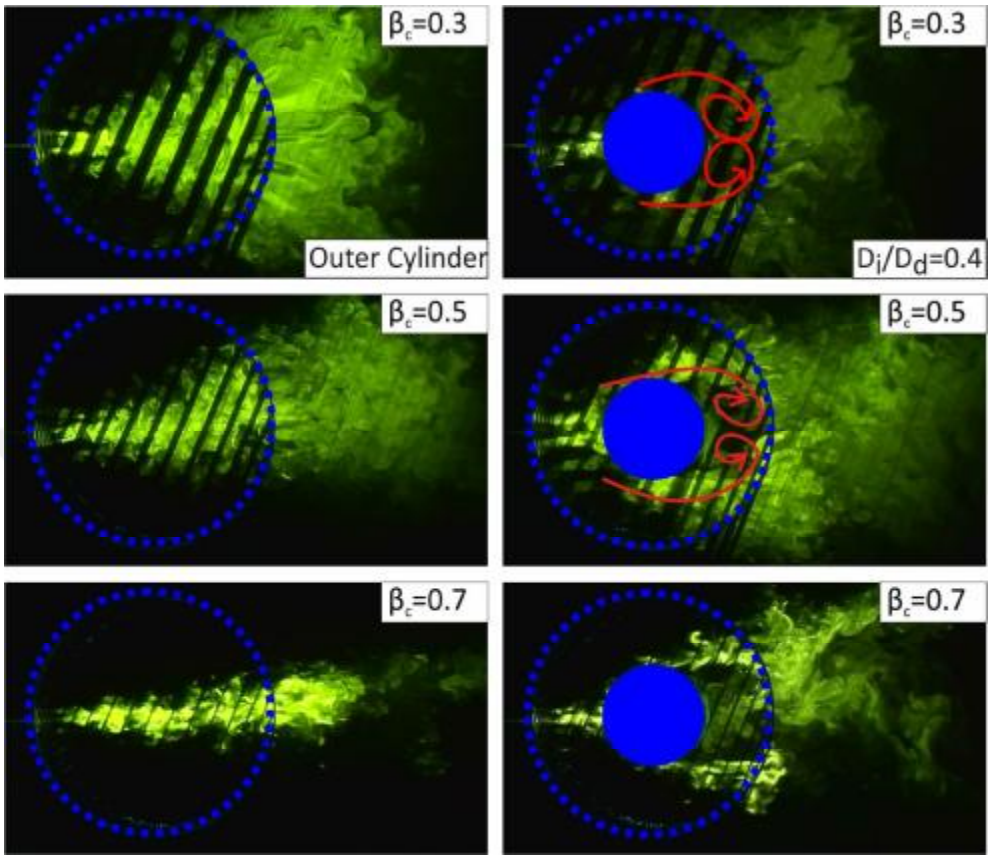

Figure 4.2 The flow visualization images of the inner-outer cylinder pair corresponding to the diameter ratio of D_i / D_o = 0.4 with no plate

Because the outer cylinder is not effective alone in suppressing the vortex pairs in the annular region, there still would be unsteady loadings on the inner cylinder. To get rid of this undesirable effect on the inner cylinder, a splitter plate is located in between cylinder pair. The instantaneous flow images obtained from dye experiments for the β_c = 0.3 cylinder are shown in Figure 4.3. In figure, each column shows different plate porosity ratios (β_p = 0.3, β_p = 0.5 β_p = 0.7) while each row shows the plate angles. At the low plate angle, β_p = 0.3 plate diverted some of the flow towards the upper side of the inner cylinder. This condition strengthens the shear layer at that side of the inner cylinder and causes it to flow with a

stronger momentum. As the plate angle increases (α = 150° and 180°), this effect on the upper side of the inner cylinder decreases. Consequently, the presence of perforated plates only causes the resulting flow structure in annular region to be asymmetrical.

It can be seen from the flow images of Figure 4.3, the plate angle α = 150° separates the vortex pair and prevents interaction of shear layer in downstream of the inner cylinder. The prevention of this interaction is considered to be a good situation to reduce the vortical fluctuations in the annular region, but it will be more practical to obtain more quantitative results for this angle. For all plate porosity ratios, the plate angle α = 180° separates the vortex pairs from each other. At the other plate angles ($60° \leq \alpha \leq 120°$), the flow through the splitter plate in the lower shear layer and the upper shear layer of the cylinder forms vortex pair in downstream of the inner cylinder. But again, it will be useful to consider the turbulence intensity in the annular region. The last two columns in Figure 4.3 present the flow visualization images of the β_p = 0.5 and 0.7 plates. Once the flow images are examined, it is understood that for almost all the plate angles, the vortex pair occurs in the downstream of the cylinder which is directly related to the flow rate passing through the plates. However, it should not be forgotten that this result is only given by examining the dye visualization experiments. Furthermore, dye experiments give solid evidence that plate porosity is an important parameter for the flow structure in annular region.

The experiments carried out for a porosity ratio β_c = 0.3 cylinder revealed that this porosity ratio is not sufficient to control the vortex shedding in downstream of the inner cylinder therefore the next porosity parameter of the outer cylinder of the process is shifted to β_c = 0.5. Practically, this porosity value is thought to pass through the holes almost half of the flow from the perforated outer cylinder. Thus, in the applied flow control method, the predominance of the outer cylinder on the flow structure is expected to decrease. The instantaneous flow images for the β_c = 0.5 outer cylinder are shown in Figure 4.4.

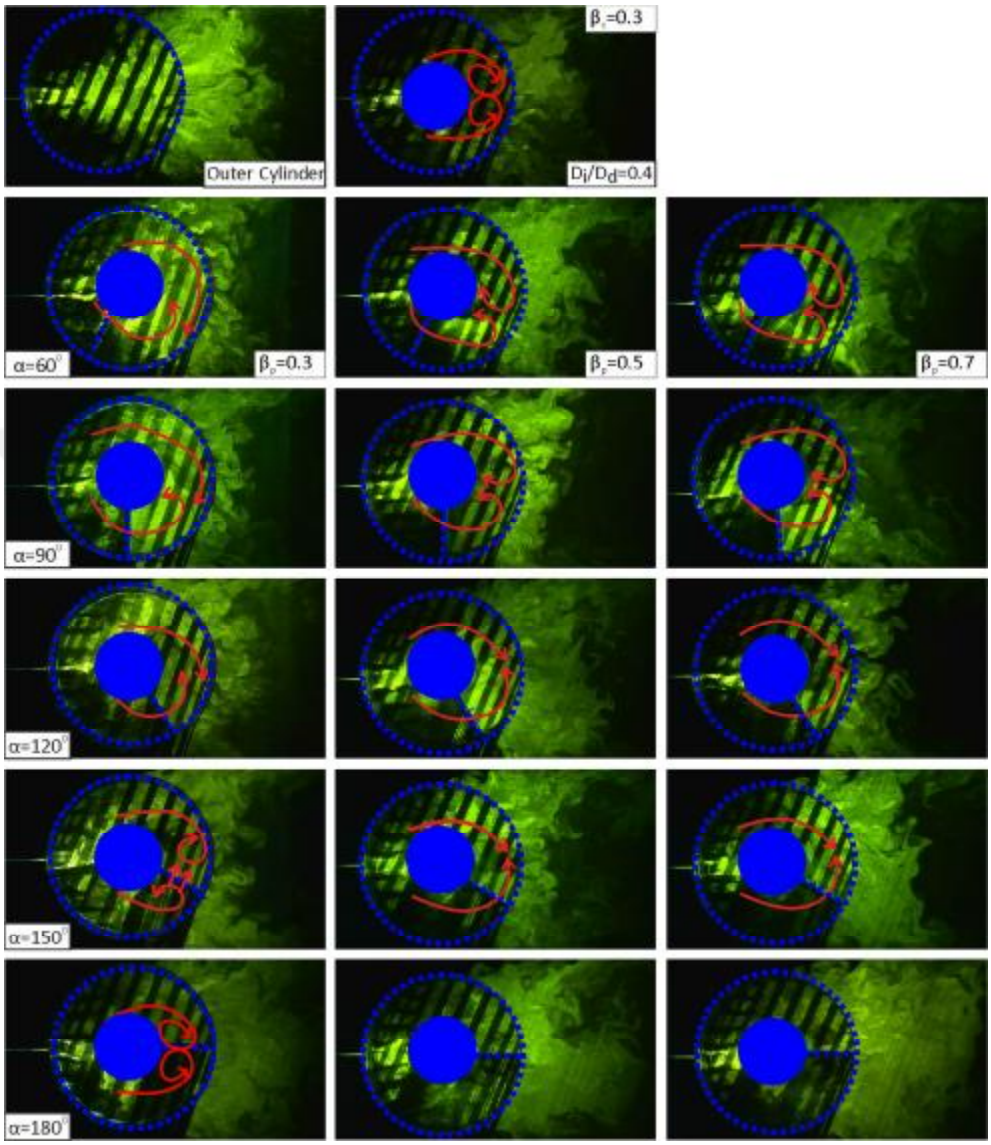

Figure 4.3 Instantaneous flow visualization images of the porosity of the outer cylinder, β_c = 0.3 with three different porosities of the splitter plate β_p = 0.3, β_p = 0.5, β_p = 0.7 at five different plate angles

The top row of the Figure 4.4 shows the flow images for the β_c = 0.5 outer cylinder without splitter plate. It was seen that the vortex pair in the annular region occurs in a similar manner to that caused by β_c = 0.3 outer cylinder. It is observed from the flow images of the first column of Figure 4.4 that the β_p = 0.3 plate is almost blocking the flow through the holes and directing this flow towards the upper side of the annular region. Due to the difficulty of the flow's passing through, more fluid and higher momentum is formed in the upper region of inner cylinder. Therefore, the flow enters the dead flow region and causes a high-intensity vortex in the upper side of inner cylinder, especially at the α = 90° and 120° plate angles. The plate porosity β_p = 0.3 at α = 180° plate angle is slightly different because the vortices formed downstream of inner cylinder for all plate porosities have interaction problems with each other. The reason of this problem is the lack of holes in the splitter plate. Apart from these, there is no significant change in other flow structures. As the plate porosity (β_p) increases, the flow through the holes of plate penetrates in the downstream of the inner cylinder more quantities and that the possible vortex pair does not interfere with each other. The last two column of Figure 4.4 presents the flow images for the β_p = 0.5 and 0.7 plate. Especially at low plate angles (α = 60° and 90°), unlike the β_p = 0.3 plate, the flow is not force towards the upper side of annular region. For this reason, even though there are small-scale vortices in the annular region, they do not have the size and momentum to interact with each other. For the plates angles α = 60° and 90°, almost identical vortices and interaction between these vortices are obtained for both β_p = 0.5 and 0.7 plate. However, when the plate angle is increased to α = 120° and 150°, there is a difference in the resulting flow structure in downstream of the inner cylinder, the β_p = 0.5 plate porosity passes some of the flow and blocks some of them. This flow, which cannot pass through the splitter plate forms a smaller vortex in front of the plate than the always occurring vortices in downstream of the inner cylinder. The interaction of the vortex pair in the annular region continuous as the plate angles α = 60° and 90°. When the perforated plates

are brought to the angle $\alpha = 180°$, the vortices formed in downstream of the inner cylinder does interacted with each other because of the separation effect of the plate on the vortices that formed in the upper and lower side of the inner cylinder. In addition, the jet-like flow formation behind the outer cylinder can also be observed for all plate porosities.

The Figure 4.5 gives the flow visuals of the $\beta_c = 0.7$ outer cylinder. It is expected that the velocity of the free flow acting on the inner cylinder will increase as the perforated outer cylinder porosity increases by one step, so that the vortices that form in the annular region is more or less interfere with the splitter plate use. It is seen from the first column of the Figure 4.5 that the flow which is leave the outer cylinder, is redirected in the annular region. This reverse flow can be observed for all $\beta_c = 0.7$ outer cylinder experiments. The vortices formed for the $\alpha = 120°$and $\alpha = 150°$ plate angles are shown with red arrows in the second column of Figure 4.5 ($\beta_p = 0.5$ plate). At the $\alpha = 120°$ plate angle, the flow passes on the upper side of the inner cylinder tends to leave the annular region instead of make vortices. Therefore, at this time, the vortices at the lower side is larger than the upper side. A particularly complex flow structure also has been observed for $\alpha = 150°$ plate angle. A small vorticity concentration occurs in front of the splitter plate.

It is noteworthy that the flow in the dead flow zone enters the low velocity region which is formed behind the plate (for $\beta_p = 0.3$). For this reason, even though some of the flow is blocked by the splitter plate which is located the lower side, a significant portion of the flow is directed to upward of the inner cylinder.

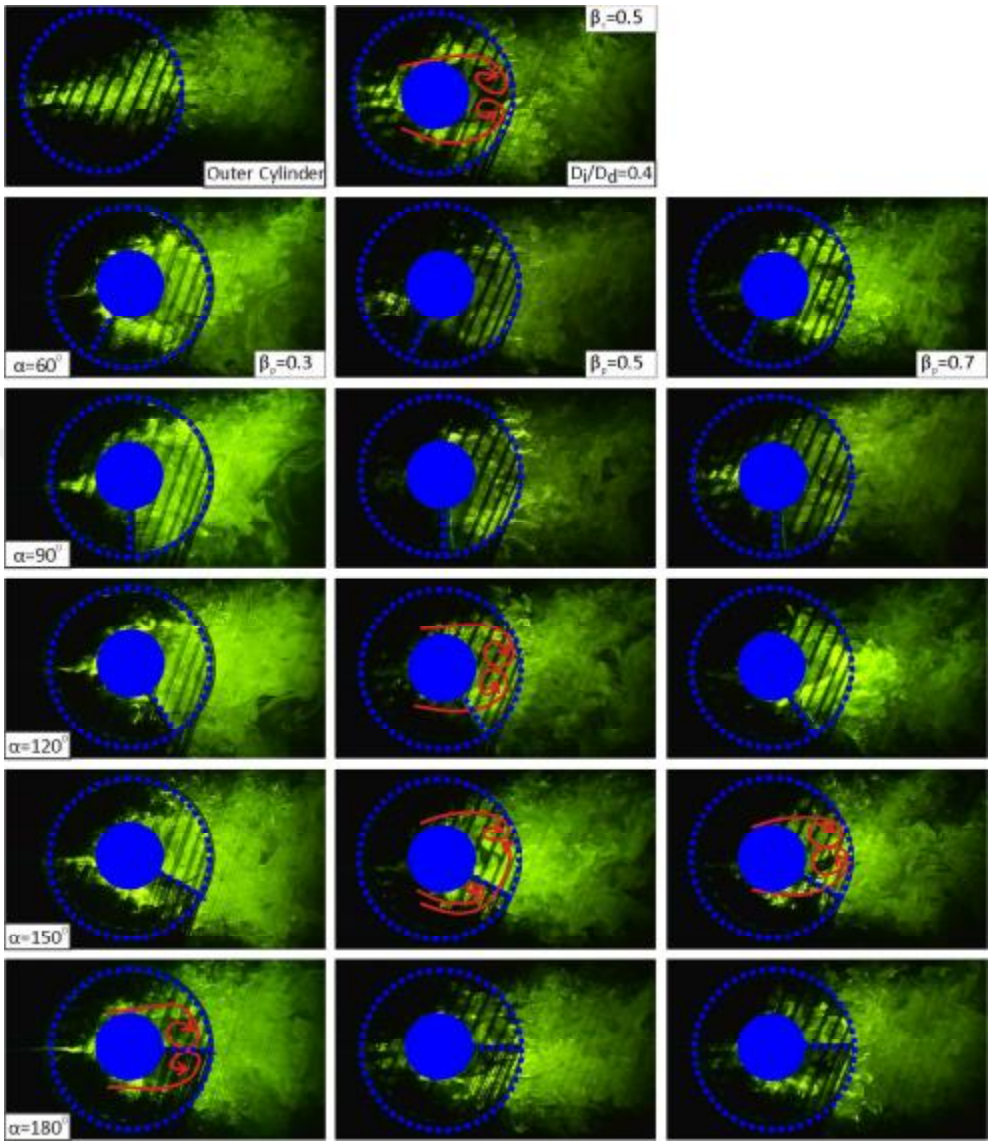

Figure 4.4 Instantaneous flow visualization images of the porosity of the outer cylinder, $\beta_c = 0.5$ with three different porosities of the splitter plate $\beta_p = 0.3$, $\beta_p = 0.5$, $\beta_p = 0.7$ at five different plate angles

Thus, the higher momentum has been placed at the upper side of the annular region. As a result, the vortices form by the upper shear layer easily enter the dead flow region, causing the vortex interaction and vortex breakage. This observation means that the control may work well for these parameters. Last two column of Figure 4.5 shows the effect of plates with porosity of $\beta_p = 0.5$ and $\beta_p = 0.7$ on the flow structure in the annular region. It has been observed that for the a = 60° plate angle, the vortex is formed just behind the inner cylinder. On the other hand, the vortices with $\beta_p = 0.5$ have asymmetric structure and the $\beta_p = 0.7$ plate is relatively symmetrical, which is directly related to the amount of flow which passes through the plate.

In general, using a high porosity plate instead of low porosity would allow the flow to the other side of the plate depending on the porosity ratio, rather than blocking the flow. In first place it is obvious that the flow can easily pass through the plate when using high porosities.

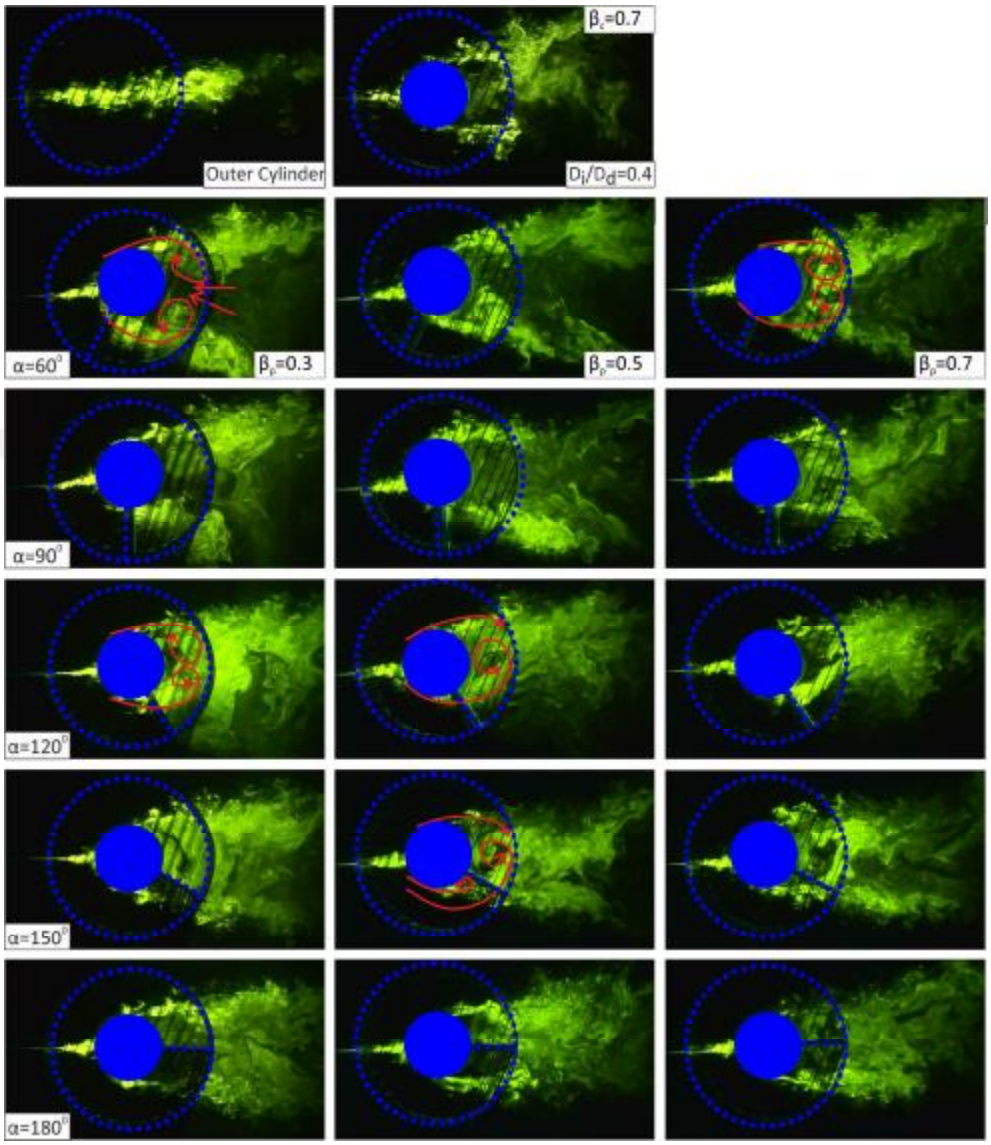

Figure 4.5 Instantaneous flow visualization images of the porosity of the outer cylinder, $\beta_c = 0.7$ with three different porosities of the splitter plate $\beta_p = 0.3$, $\beta_p = 0.5$, $\beta_p = 0.7$ at five different plate angles

4.3. PIV Experiments Results

The first observations were obtained in the light of the dye visualization experiments. But these observations were not enough to fully understand the flow structure in the annular region. By using the PIV measurement technique, it was aimed to obtain the numerical data about the vorticity concentration in the annular region and to investigate the flow structure in this region in further detail. In order to compare the influence of the splitter plate on the flow structure downstream of the inner cylinder, only the perforated outer cylinder (no inner cylinder with diameter D_i = 50mm) and the cylinder pair as the control element was examined. The time average streamline topologies $<\psi>$ and the time average vorticity contour $<\omega>$ are shown in Figure 4.6 for the outer cylinder diameter ratio, $D_i / D_o = 0.4$. As can be seen from the streamlines $<\psi>$, in the absence of the inner cylinder (first column of the Figure 4.6), the outer perforated cylinder with the porosity of βc = 0.3 results in circulations indicated by F_1 and F_2 foci points in the upper and lower parts of the outer cylinder. With increasing the porosity of the outer cylinder to β_c = 0.5, the outer cylinder starts to lose its influence on the flow inside of the cylinder due to the increase in the number of holes or porosity, βc of the perforated outer cylinder, and the focal points formed for the outer cylinder porosity, β_c = 0.3 lose its effects on the upward side and decrease its vorticity intensity on the downward side of the cylinder. When the outer cylinder porosity is increased to the value of β_c = 0.7, it was observed that the focal points that formed either side of the outer cylinder, does not occur and the fluid continue to flow through the outer cylinder holes. It is thought that these focal points presence are effective to the flow characteristics in the annulur region where it is desired to control the flow behivour, and it is already thought that the undesirable vibrations the cylinder and sound generation due to this vortex shedding. The level of vibraiton and sound generation even increases more when the perforated cylinder with β_c = 0.3 is used.

In the case of cylinder pair use together which is shown in the second column of the Figure 4.6, it is seen that the circulation or foci point symbolized by

F_1 and F_2 are formed immediately downstream of the inner cylinder in the region between cylinder pair (annular region) for all porosities. These circulations and focal points show that at all porosities of the perforated outer cylinder for D_i / D_o = 0.4, a non-uniform flow region are formed downstream of the inner cylinder. It is also assessed that the third focal point, F_3 which is observed from the streamline topology at the porosity of the cylinder, β_c = 0.3 originated from the outer cylinder. The circulation which originated from the outer cylinder at the upper side of the this cylinder indicated by F_1 in the first image of Figure 4.6 loses its visibility when the inner cylinder is added. This is because the PIV laser sheet fails to illuminate the exact position which this focal point at the upper side of the inner cylinder form due to the presence of the inner cylinder. For the porosity of the outer cylinder β_c = 0.3, the flow separated from the inner cylinder and travels through the cylinder wall contacting the inner surface of perforated cylinder and finally the focal points F_1 and F_2 occur. At the outer perforated cylinder with low porosities such as β_c = 0.3, the flow separated from the inner cylinder is limited to the annular region due to the low number of holes on the outer cylinder.

In the case of the perforated outer cylinder with the porosity of β_c = 0.7, the outer cylinder begins to lose its effects on flow characteristics throught the annular region due to the high value of the porosity, β of the outer cylinder, and non-permanent vortex shedding originating from the inner cylinder begins to occur. In the second column of Figure 4.7, the experimental results show that the vorticity magnitude along the shear layer of the inner cylinder increases with the increasing the outer cylinder porosity, β_c. An increase of vorticity magnitude is obvious when the porosity of the perforated plates in increased. The dye visualization also demonstrates that the flow in the annular region is more vortical due to the high rate of porosity, β. It was also seen from the dye visualization observations that the flow rate which moves in the annular region through the holes of the cylinder is directly proportional to the outer cylinder porosity. On the other hand, the continuous flow structure due to the holes on the outer cylinder is obviously seen in

front of the inner cylinder. In this case, the front face of the inner cylinder is exposed to a non-continuous flow. When the perforated outer cylinder with the porosity of $\beta_c = 0.3$ is used, the total amount flow which affects aerodynamics of the inner cylinder. As the outer cylinder's porosity, β_c gets, smaller for example less than 0.5, distances between holes become higher causing dead flow regions between these jet streams. A strong shear layers between the dead flow zones and the jet flows take places. A well defied reverse flows occur around the jets. Entrainment between dead flow regions and jet streams occur causing high rate of turbulence and three-dimensional vortical flow structures between the inner and the outer cylinders. As Şahin and Ward-Smith (1990) indicated that in the absence of flow-control devices the flow leaves the diffuser in the form of an axial-jet surrounded by a large region of reversed flow, The installation of a single perforated plate of 50% porosity simply increases the cross section of the jet.

As a result, the outer cylinder with the porosity of $\beta_c = 0.3$ has a negative effect on the flow structure in the annular region, because this perforated cylinder with low porosity, $\beta_c = 0.3$ allows less flow rate through the outer cylinder holes than the outer cylinder with the porosities of $\beta_c = 0.5$ and $\beta_c = 0.7$.

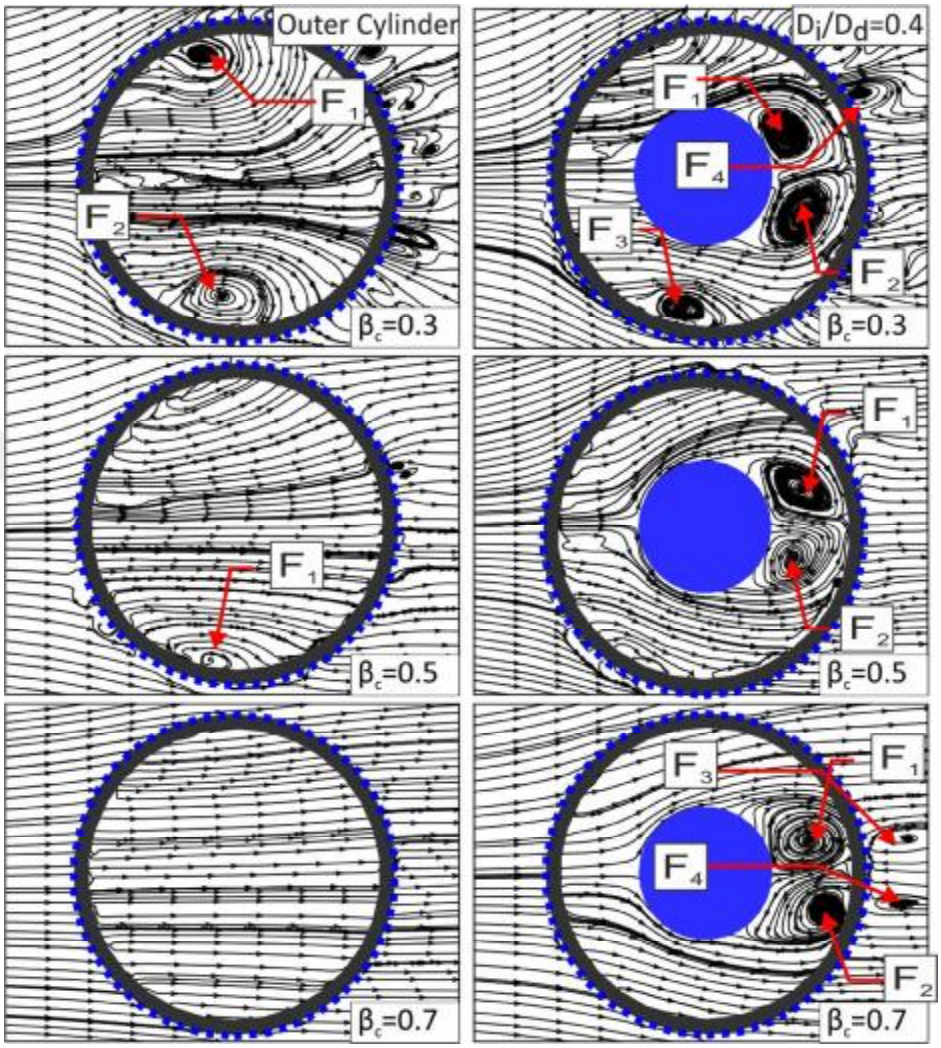

Figure 4.6 Time average streamline topologies <ψ> for the case of the inner and outer cylinder

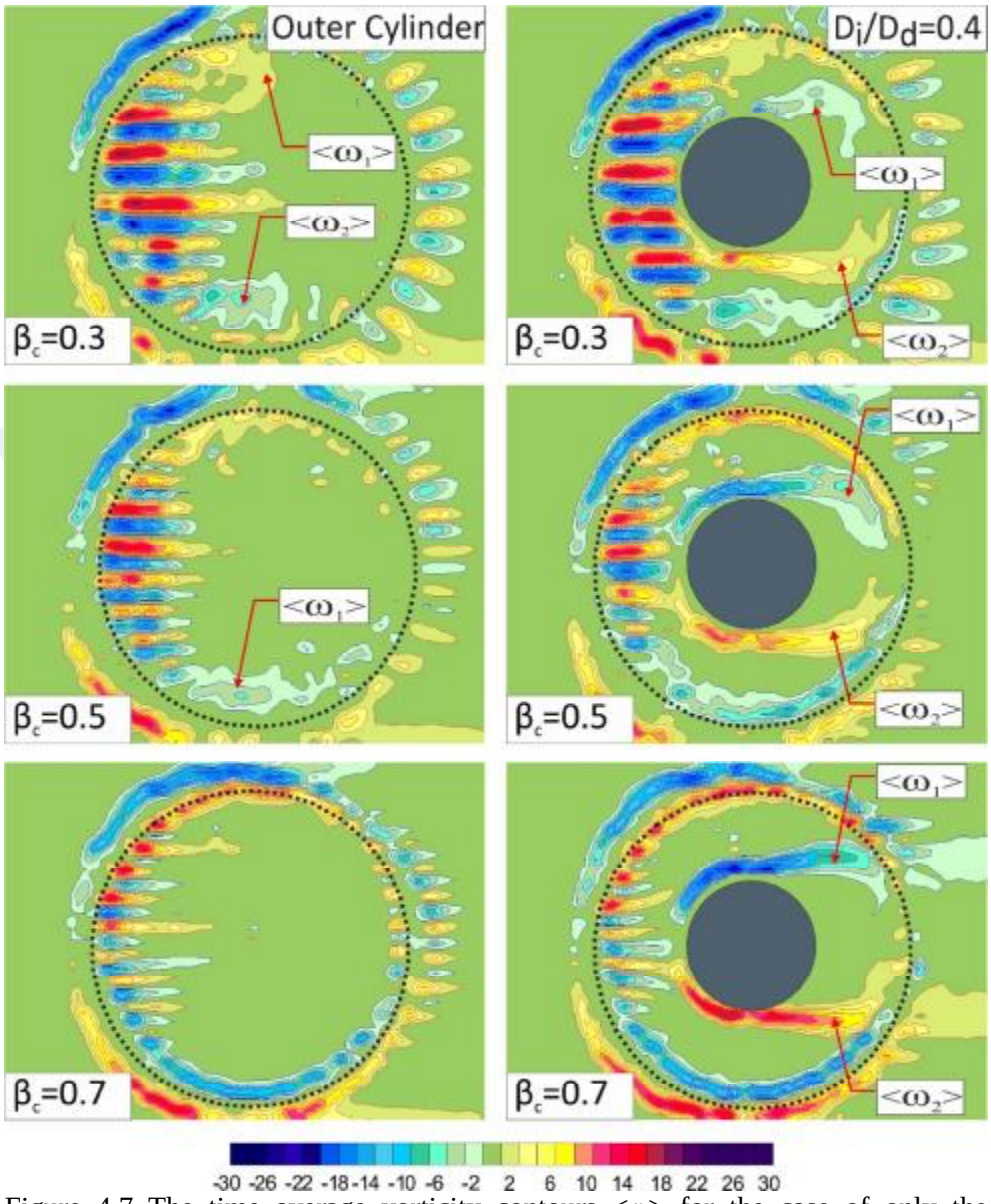

Figure 4.7 The time average vorticity contours <ω> for the case of only the perforated outer cylinder

In order to cover the gap region between inner and outer cylinder completely and to prevent possible vortex formation and vibrational effect on the inner cylinder, splitter plates (The plate attached the inner and outer cylinder) were placed in the region between two cylinders. After examining the effect of perforated cylinder on the flow characteristics in the annular region, it was decided to combine the splitter plate to control the flow structures further. In this case the splitter plate was located between the inner and outer cylinders. The existence of the splitter plate as well as the angle of the plate were examined in this study. The time average streamline topologies $<\psi>$ and time average vorticity contours $<\omega>$ for the outer cylinder with following porosities, $\beta_c = 0.3$, $\beta_c = 0.5$ and $\beta_c = 0.7$ are illustrated in Figure 4.8 -

Figure 4.13. The outer cylinder and splitter plate porosities were kept constant, but the splitter plate locations were gradually changed in the case of the splitter plate experiments. Similar experiments were repeated by changing the splitter plate porosity, β_p. The time-averaged streamlines $<\psi>$ and the time-averaged vorticity contour for the outer cylinder with porosity $\beta_c = 0.3$ are illustrated in Figure 4.8 and Figure 4.9 respectively. In these figures, each column shows the porosity of the splitter plate, $\beta_p = 0.3, 0.5, 0.7$ and each row shows the angle of the splitter plate, $\alpha = 60°, 90°, 120°, 150°, 180°$.

The last two column of Figure 4.8 indicates the streamline topology $<\psi>$ of the plate with porosities of $\beta_p=0.5$ and $\beta_p=0.7$, it has been observed from the images that the flow which enters the annular region through the outer cylinder holes form vorticity concentrations on both the lower and the upper sides of the inner cylinder similar to the case where no splitter plate is used. These vorticity concentrations can be observed on the shoulders of outer cylinder when the porosity of the perforated cylinder is taken as $\beta_c = 0.3$. Unlike the above description when the porosity of the splitter plate such as $\beta_p=0.3$ is used with the plate angle of $\alpha = 60°$ 90° and 120°, flow characteristic in the area between the cylinder pair begin to change.

This change can be explained as follows; the flow which enters the annular region through the outer cylinder holes cannot pass through the porosity of the plate β_p=0.3 with sufficient amount therefore some part of the flow directed the upper side of the inner cylinder. As a result, instead of the focal points, F_1 and F_2 form in the separated flow region of the inner cylinder, a larger focal point F_1 is formed at the plate angles α = 60° 90° and 120°. This larger focal point, F_1 can easily be observed if you look at first three rows of the first column in figure. The larger focal point, F_1 differs than the other porosity of plates, β_p measurements and the vorticity magnitude at the upper side of the inner cylinder is increased due to the plate existence. The circulation which occurs at the bottom side of the outer cylinder (indicated by F_3) forms only at the porosity of the outer cylinder, β_c = 0.3 and this circulation clearly visible at all plate angles except the plate angle, α = 60°. The reason for not seeing this circulation at the plate angles, α = 60° is that the splitter plate corresponds to the location of this circulation. This circulation which forms (illustrated by focal point, F_3) at the bottom side of the outer cylinder with the porosity of β_c = 0.3, and found to have originated from the outer cylinder itself felt its effect at all plate angles. This circulation in the annular region is a sign of not serving the main purpose of manipulation of the fluctuations of velocity components and vibration of the inner cylinder by creating the extra circulation in area between the inner and outer cylinder. While keeping the porosity of the outer cylinder β_c = 0.3, if the porosity of the plate increases to β_p = 0.5 at the plate angles α = 60° 90° and 120°, the same larger focal F_1 as the porosity of plate β_p = 0.3 formed in the upper side of the inner cylinder. The formation of circulation in the lower side of the inner cylinder is smaller than the upper side of the cylinder. When the plate angle is set to α = 150° the circulation in the lower side of the inner cylinder shows a behavior of downsizing because of the plate comes to the location where the circulation is formed. But in these parameters, as mentioned above, it seems that the circulation which originates from the outer cylinder with porosity of β_c = 0.3 stand still same. For the highest plate angle used for this study, α = 180°,

the splitter plate acts as a separator between the vortices that formed immediately downstream of the inner cylinder with different sizes and sometimes interacting with each other.

If the porosity of the plate increases to $\beta_p = 0.7$, the smaller scale focal points F_1 and F_2 occurs instead of a single large focal point F_1 at downstream of the inner cylinder in five angles of the plate. The circulation which originating from the outer cylinder with the porosity of $\beta_c = 0.3$ remains the same at the porosity of plate $\beta_p = 0.7$. When the results are examined in general, although the porosity of outer cylinder, β_c is changed throughout the experimental measurements, all porosity of the plate with the plate angle, $\alpha = 180°$ ensures that the vortices denoted by focal point F_1 and F_2 are symmetrical at downstream of the inner cylinder. The plate angle $\alpha = 60°$ is an exception for the circulation caused by the outer cylinder because of the splitter plate location. Consequently, this observation strengthens the notion that increasing the porosity is more effective in controlling the flow structure, as noted in the dye visualization experiments.

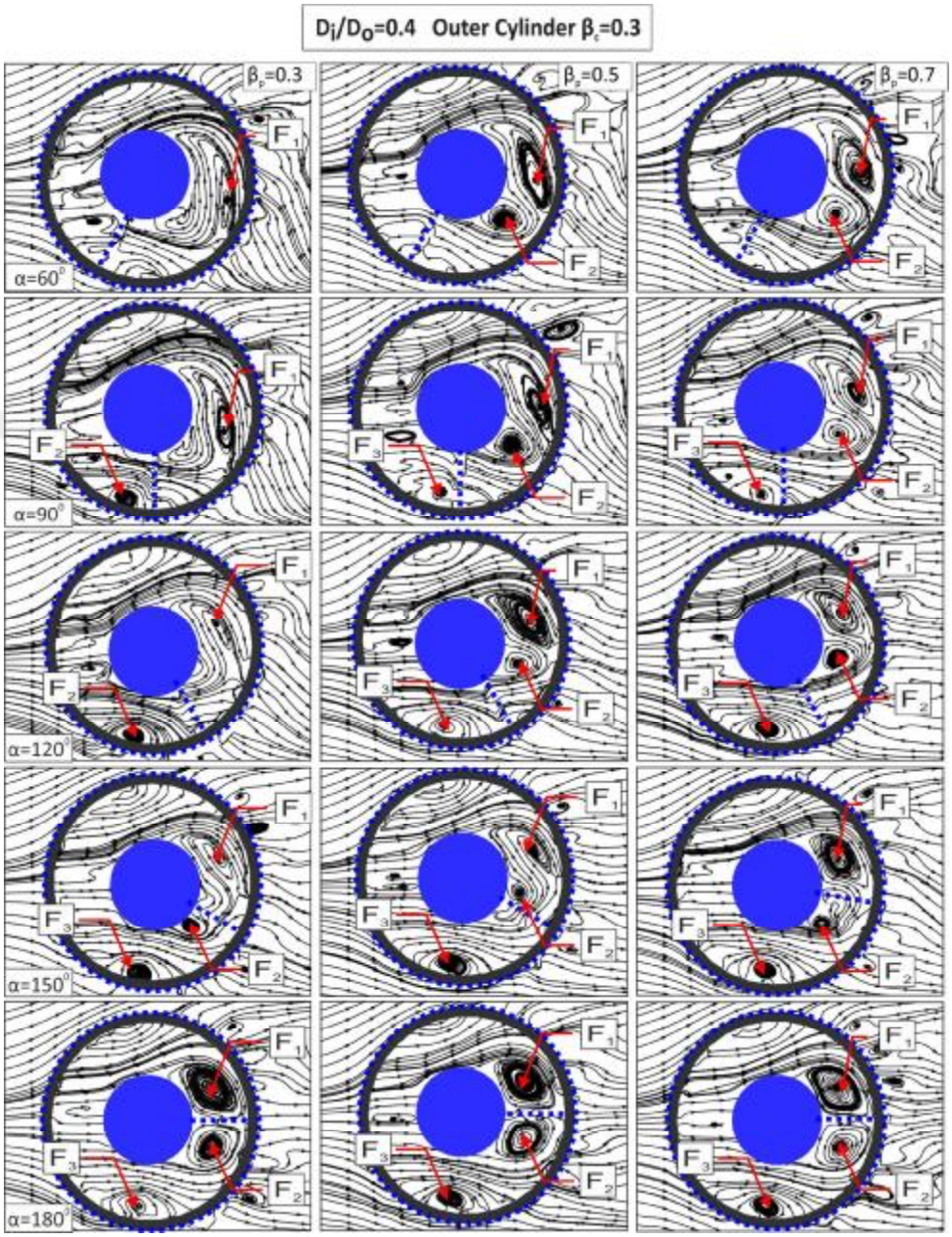

Figure 4.8 Time average streamline topologies <ψ> of the porosity of the outer cylinder, $\beta_c = 0.3$ with three different porosities of the splitter plate $\beta_p = 0.3$, $\beta_p = 0.5$, $\beta_p = 0.7$ at five different plate angles

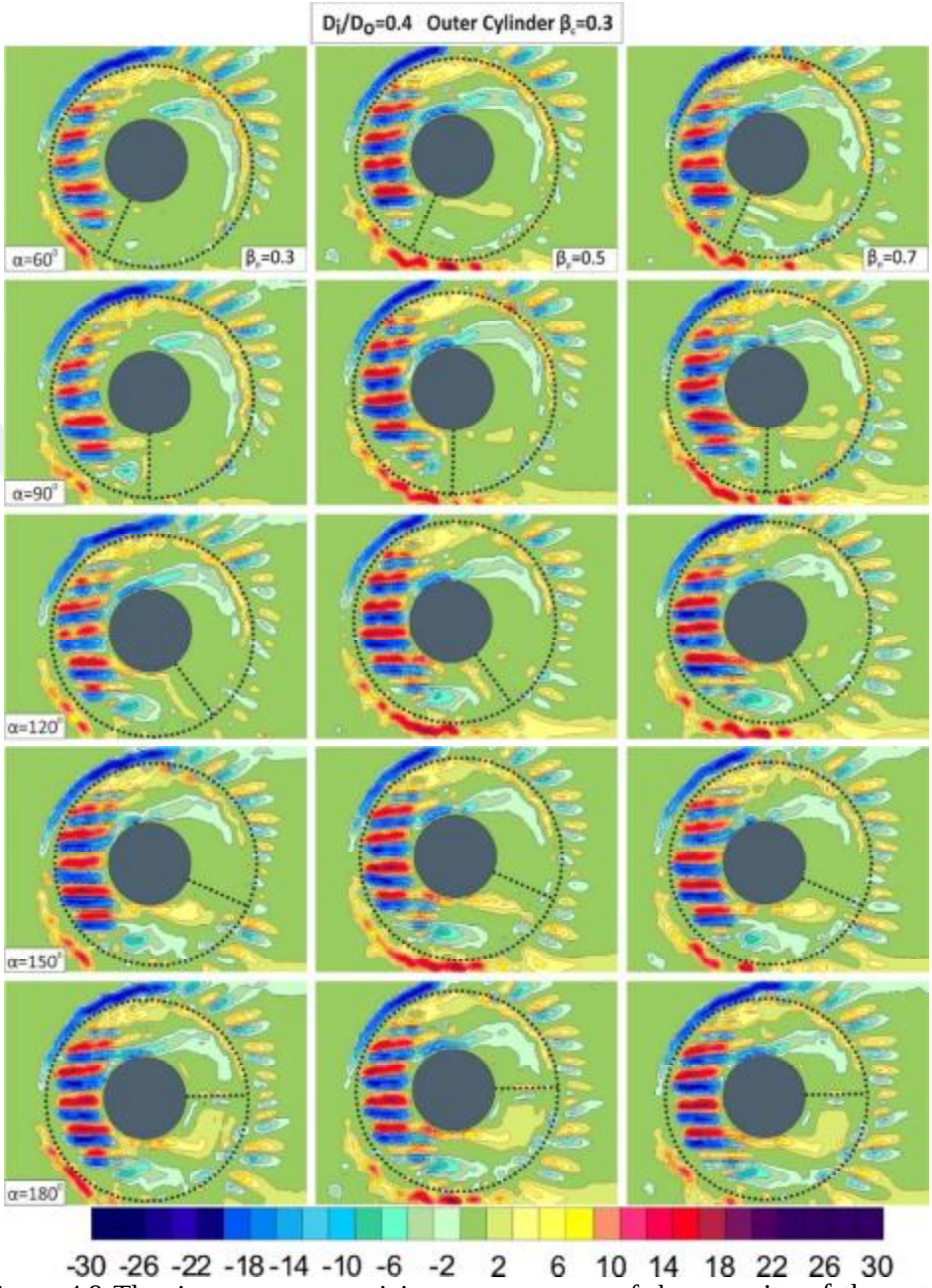

Figure 4.9 The time average vorticity contours <ω> of the porosity of the outer cylinder, $\beta_c = 0.3$ with three different porosities of the splitter plate $\beta_p = 0.3$, $\beta_p = 0.5$, $\beta_p = 0.7$ at five different plate angles

The time-averaged streamline topologies <ψ> and time-averaged vorticity contour <ω> obtained from the PIV experiments for the outer cylinder with porosity of $\beta_c = 0.5$ are illustrated in Figure 4.10 and Figure 4.11. In the figures, the porosity of the plate $\beta_p = 0.5$ is illustrated at five different angle of the plate α = 60°, 90°, 120°, 150°, 180°. If the results are examined that the outer cylinder is better for controlling the flow structure in annular region than the outer cylinder with porosity $\beta_c = 0.3$. This situation can be understood from the disappearance of the circulation which forms in the lower side of the outer cylinder. Differently from the porosity of the outer cylinder $\beta_c = 0.3$, a small vorticity concentration at the plate angle $\alpha = 150°$ forms. If the vorticity magnitudes at this plate angle are examined, it can be seen clearly that the plate at angle $\alpha = 150°$ prevent the interaction of vortices between in the upper and lower side of the inner cylinder. When the plate angle increases to $\alpha = 180°$, the vorticity concentration in downstream of the inner cylinder separated from each other.

The time-averaged streamline topologies <ψ> and time-averaged vorticity contour for the outer cylinder with the porosity of $\beta_c = 0.7$ are illustrated in Figure 4.12 and

Figure 4.13. In the figures, the rows show the porosity of the plate $\beta_p = 0.3$, 0.5, 0.7 respectively and the lines show the change of the plate angle α = 60°, 90°, 120°, 150°, 180°. From the streamline topologies, the focal points F1 and F2 are observed immediately downstream of the inner cylinder for the porosity of outer cylinder $\beta_c = 0.7$ at every plate angle. This vortex pair which form in annular region have very similar behavior with each other independently from the porosity of plate. When this porosity of outer cylinder measurement is carefully studied, it has been observed that the splitter plate has slightly effect on the structure of vortices form in annular region. The plate angle $\alpha = 150°$ again shows the success of separating the interaction of vortices formed downstream of the inner cylinder. The jet-like structure due to openness on the outer cylinder in front of the inner cylinder can easily be seen in

Figure 4.13. The vorticity magnitude of this jet structure decreases as the porosity of the outer cylinder, β_c increases. The jet-like flow structure can be defined that as the case where the flow velocity at the outlet of the perforated outer cylinder is greater than the free stream velocity of flow.

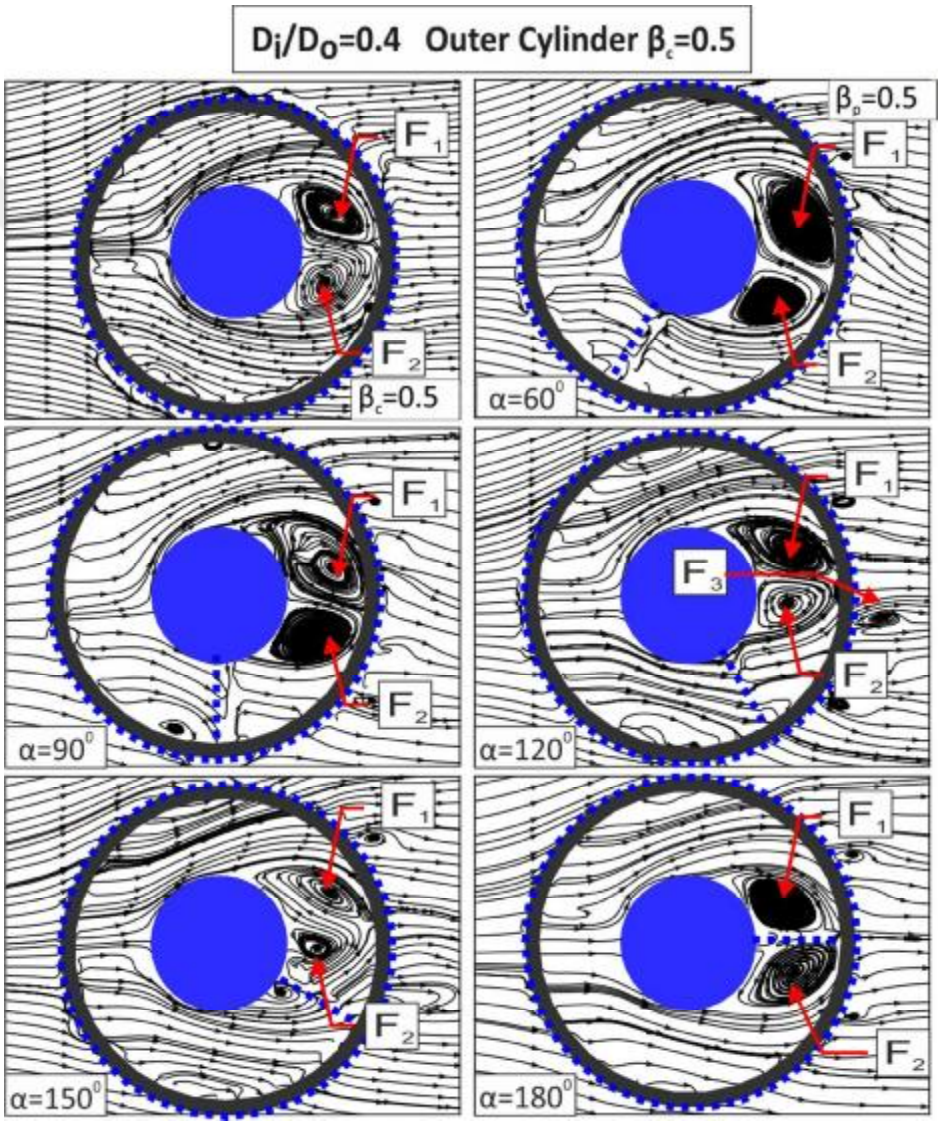

Figure 4.10 Time average streamline topologies <ψ> of the porosity of the outer cylinder, β_c = 0.5 with the porosity of the splitter plate β_p = 0.5 at five different plate angles

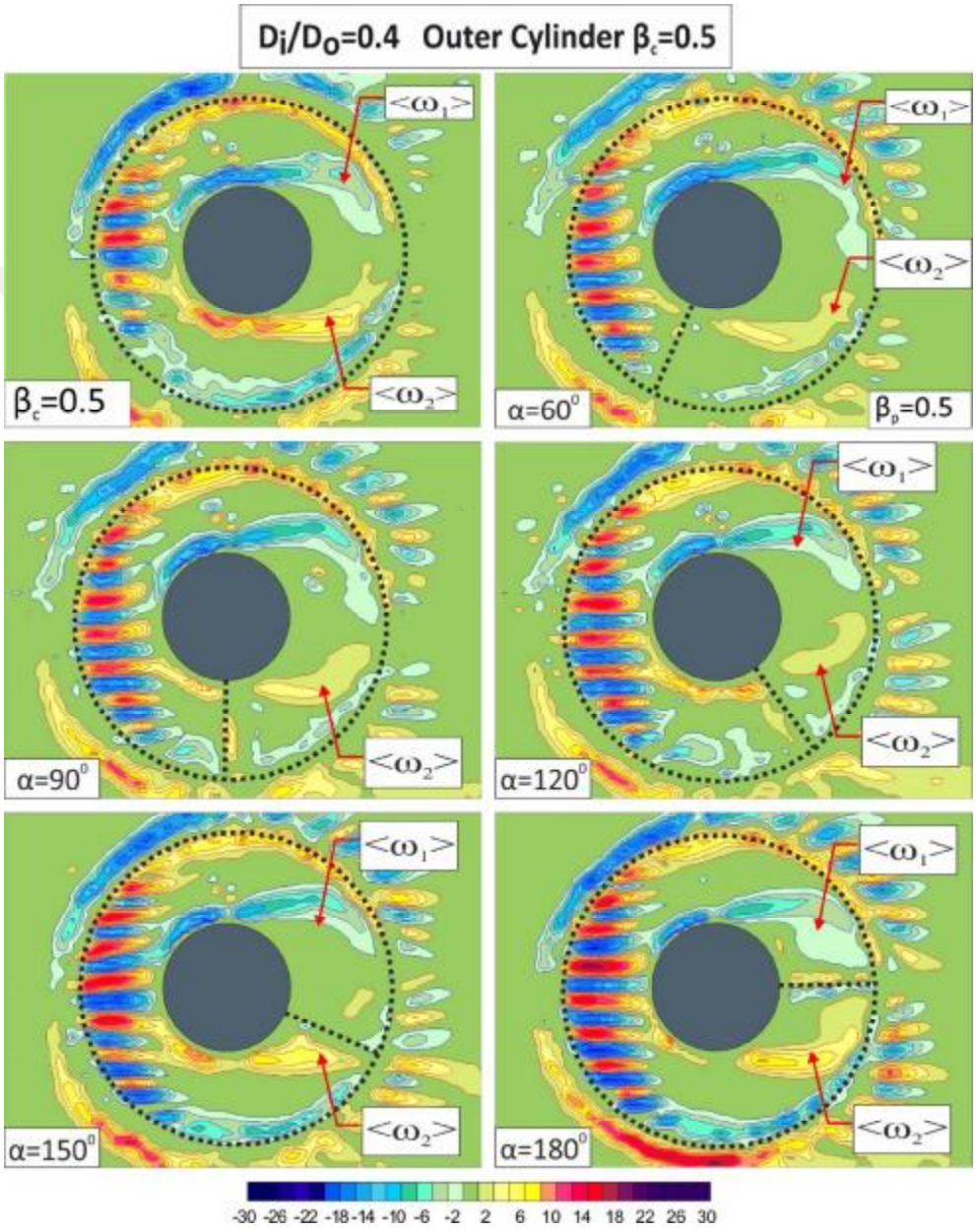

Figure 4.11 The time average vorticity contours <ω> of the porosity of the outer cylinder, β_c = 0.5 with the porosity of the splitter plate, β_p = 0.5 at five different plate angles

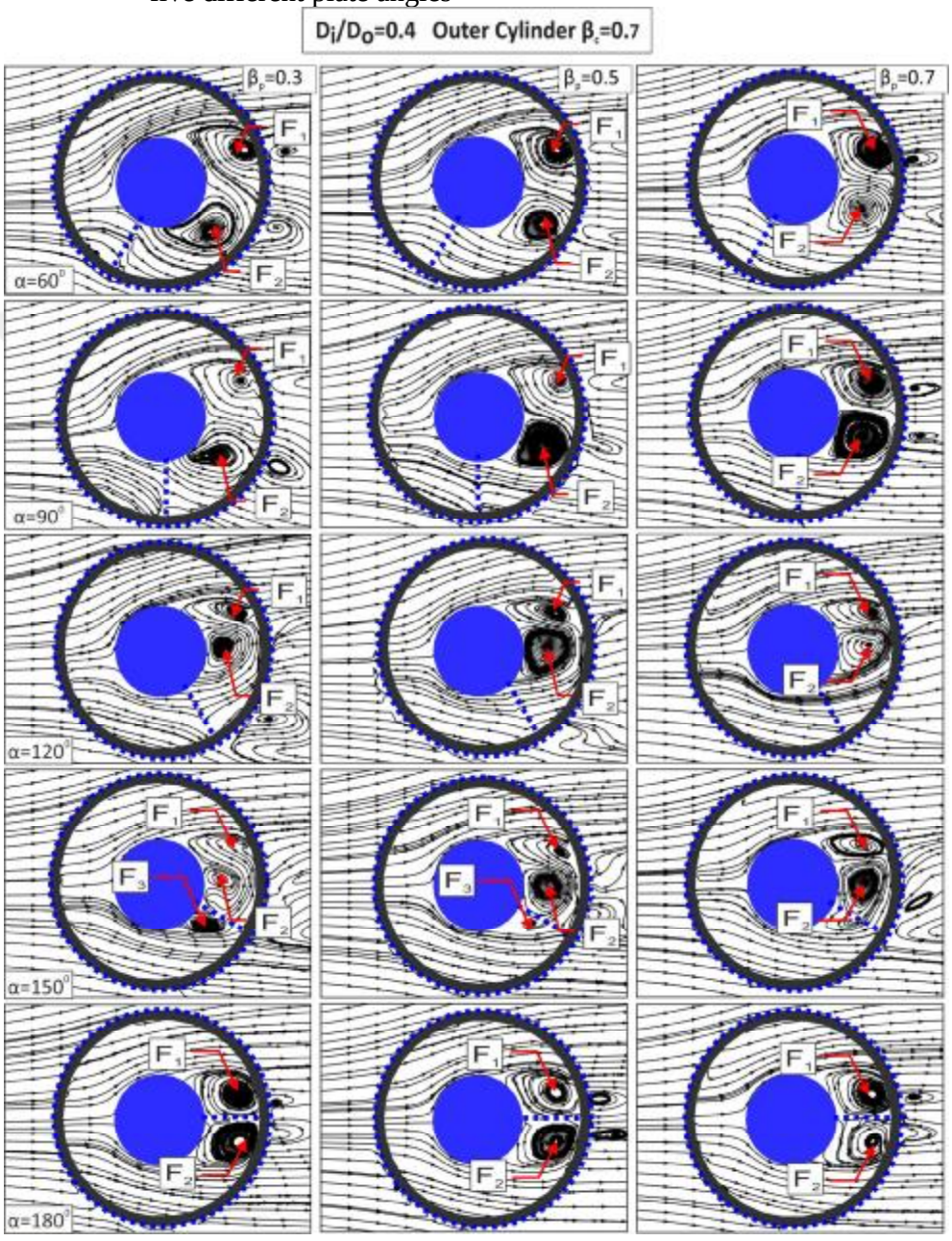

Figure 4.12 Time average streamline topologies <ψ> of the porosity of the outer cylinder, $\beta_c = 0.7$ with three different porosities of the splitter plate $\beta_p = 0.3$, $\beta_p = 0.5$, $\beta_p = 0.7$ at five different plate angles

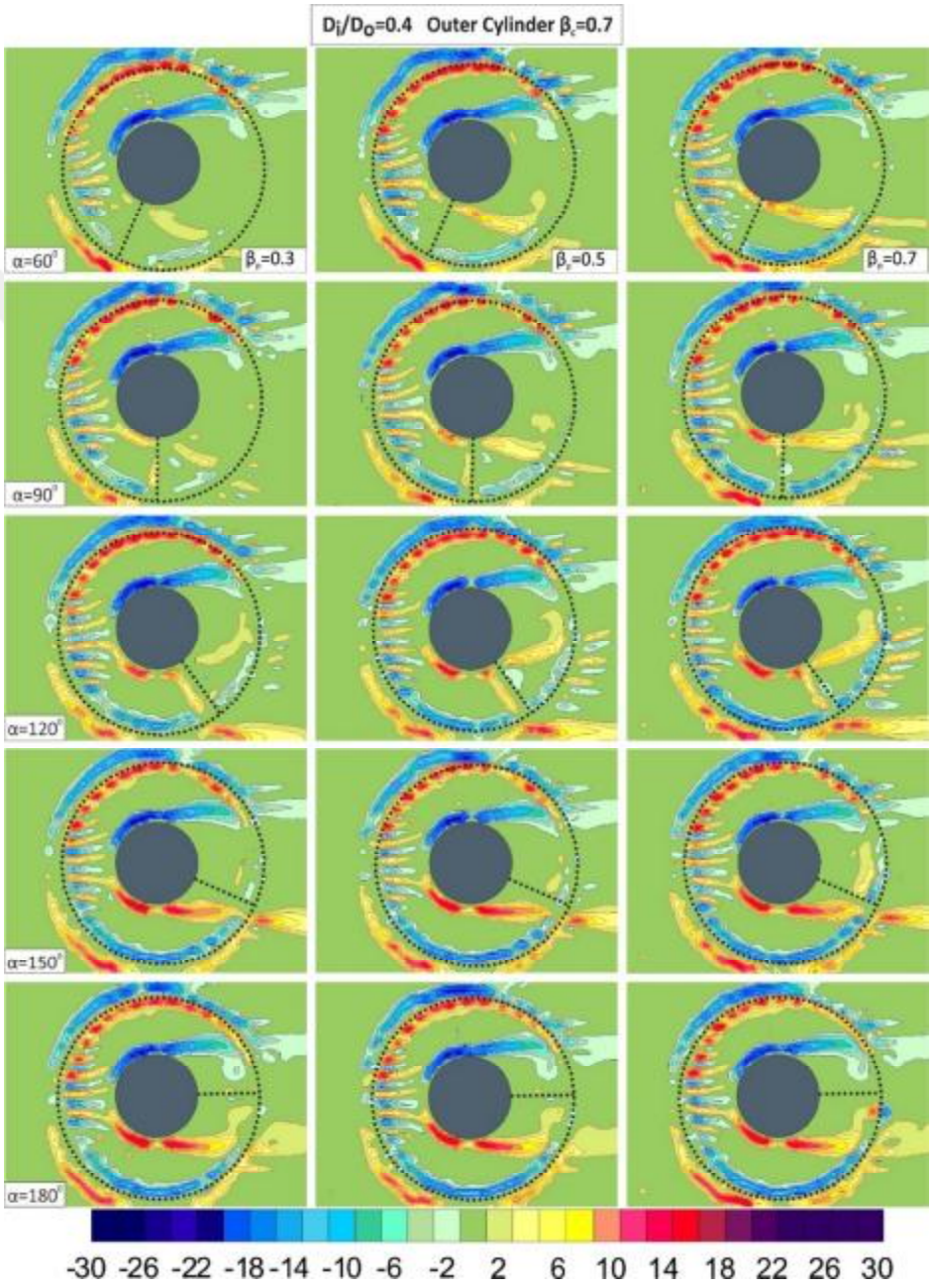

Figure 4.13 The time average vorticity contours <ω> of the porosity of the outer cylinder, $\beta_c = 0.3$ with three different porosities of the splitter plate $\beta_p = 0.3$, $\beta_p = 0.5$, $\beta_p = 0.7$ at five different plate angles

4.4. Turbulence Kinetic Energy Results

As a result of experiments with the particle image velocimetry measurement technique, the flow structure was tried to be interpreted with the aim of determining the parameters which are effective to control the continuous flow structure form in downstream of the inner cylinder. For this purpose, the time average streamline topologies <ψ> and time average vorticity contours <ω> are examined. In general perspective, the results which obtained from dye and PIV technique for the various porosities of the splitter plate are quite similar to the case where only the cylinder pair without the splitter plate is used. For example; the focal points F_1 and F_2 were formed in the separated flow region of the inner cylinder for the porosity of outer cylinder $\beta_c = 0.7$, in this case the outer cylinder is used both with the splitter plate and without this plate at almost all angles. In order to control the unsteady structure of the flow downstream of the circular cylinder, it is necessary to reduce the intensity of Turbulent Kinetic Energy especially in the annular region. Accordingly, it is not possible to say that the control parameters are completely effective or ineffective by looking only at these focal points. Although the focal points are formed in area between the cylinder pair, there may be a decrease in the turbulence values. Therefore, the comparative TKE values are presented below in graphical form. In order to make comparisons for the TKE values, the dashed line is used in graphs for the TKE value of only the cylinder pair presence. The turbulence Kinetic Energy is calculated in our work because it gives more general information about the turbulence level that the flow has. The TKE_{max} is calculated using the following formula.

$$TKE = \frac{1}{2}\left[\overline{u'u'} + \overline{v'v'} + \overline{w'w'}\right]$$

Assuming isotropic flow, the third fluctuating velocity component can be estimated by a 2D approximation (Sheng et al., 2000), namely the third component has been supposed to be equal to the half of [$\overline{u'u'} + \overline{v'v'}$], then the TKE can be calculated with the following expression;

$$TKE = \frac{3}{4} [\, \overline{u'u'} + \overline{v'v'} \,]$$

In the following figures, the TKE_{max} values occurring in the separated flow region of the inner cylinder and the variation of the control parameters are given in two-dimensional graphs. As a result of analysis of these graphs, the effect of the control parameters on the turbulence level of the flow formed in downstream of the inner cylinder is investigated. The Figure 4.14 shows that the variation of the maximum values of the turbulent kinetic energy stresses in the annular region at different porosity of the plate, β_p, and the plate angles, α. In the graphs, the diameter ratio of the cylinders $D_i / D_o = 0.4$ and the porosity of the outer cylinder, $\beta_c = 0.3$ are kept constant. The dashed line on the graph is drawn as a control element to express the received TKE_{max} value for the case where the splitter plate is not used and at the same porosity of the outer cylinder, β_c. The TKE_{max} for the only inner cylinder (no control) was founded at 0.044. The TKE_{max} value is found as 0.0274 when the outer cylinder with porosity of $\beta_c = 0.3$ is used as the control element. Adding the porosity of the outer cylinder $\beta_c = 0.3$ resulted in a 38% reduction in the TKE_{max} intensity. But it should not be forgotten that this reduction on TKE was predicted from the result of dye visualization experiments and this situation was explained because of the lack of flow through the outer cylinder holes. When the perforated plate and the perforated outer cylinder are used together for controlling the unsteady structure in annular region, the TKE_{max} value on the

upper side of the inner cylinder is below the level which showed with the dashed line on the graph until the plate angle $\alpha = 150°$. After the plate angle $\alpha \geq 150°$ for the porosity of the outer cylinder $\beta_c = 0.3$, the TKE_{max} values approaches to the value which founded for no plate situation. The higher TKE value is obtain at the plate angle $\alpha = 180°$ for the all porosity of the plate compare to the no plate case.

For the parameter where the outer cylinder with porosity of $\beta_c = 0.3$ and the plate with the porosity of $\beta_p = 0.3$ is used at the plate angle $\alpha = 90°$ shows a noticeable decrease in the TKE_{max} value. Better results for the current outer cylinder, a reduction of 29% in the peak value of TKE is achieved for the plate with porosity of $\beta_p = 0.5$ at $\alpha = 60°$. A common outcome that can be subtracted from the Figure 4.14 is that presence of the plate for the outer cylinder with porosity of $\beta_c = 0.3$ succeed in decreasing the TKE_{max} value.

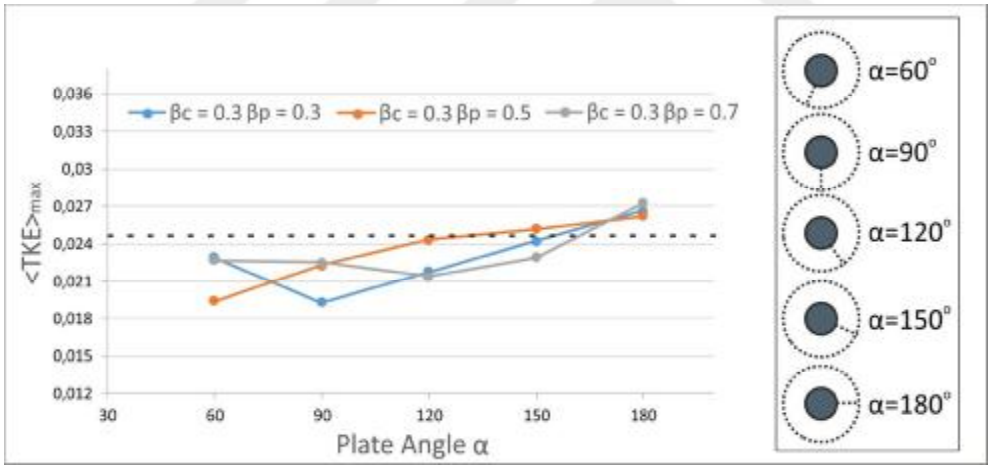

Figure 4.14 The effect of porosity of the plate "β_p" with changing the plate angles on the TKE_{max} for the outer cylinder with the porosity of $\beta_c = 0.3$

The maximum value of TKE generated downstream of the inner cylinder is measured to be 0.0323 when the outer cylinder with a porosity of $\beta c = 0.7$ without the splitter plate is used as the control element.

Figure 4.15 shows the change of the TKE_{max} values with the plate angle. The dashed line on the Figure 4.15 indicates the TKE_{max} value when only the cylinder pair are present (no plate). When the outer cylinder with porosity $\beta_c = 0.7$ at plate angle $\alpha = 60°$ is used for all porosity of plate, the maximum value of TKE_{max} is above the TKE_{max} obtained from the cylinder pair case. That's why $\alpha = 60°$ for all porosity plate is not recommendable parameter for the outer cylinder with porosity of $\beta_c = 0.7$. The combined use of the porosity of the plate $\beta_p = 0.7$ and the porosity of outer cylinder $\beta_c = 0.7$ has the positive effect on decreasing the TKE_{max} values at plate angles $\alpha = 90°, 120°, 150°, 180°$. For this combined parameter the 10% reduction has obtained at the plate angle $\alpha = 90°$. On the other hand, the use of the outer cylinder with porosity $\beta_c = 0.7$ with porosity of the plate $\beta_p = 0.3$ is considered ineffective in term of the TKE_{max} values because at all plate angles the TKE_{max} values bigger than the reference line which is shown with the dashed line. It has been determined from the figure that the increasing the plate angle to $\alpha = 150°$ slightly effect on the TKE_{max} values and the maximum reduction at this angle is calculated 6%. But this effect does not reach the TKE_{max} values obtained from the outer cylinder with porosity of $\beta_c = 0.3$. Therefore, the use of the plate with the porosity of the outer cylinder $\beta_c = 0.7$ can be consider ineffective for decreasing the TKE_{max} values as well as decreasing fluctuations in the wake of cylinder.

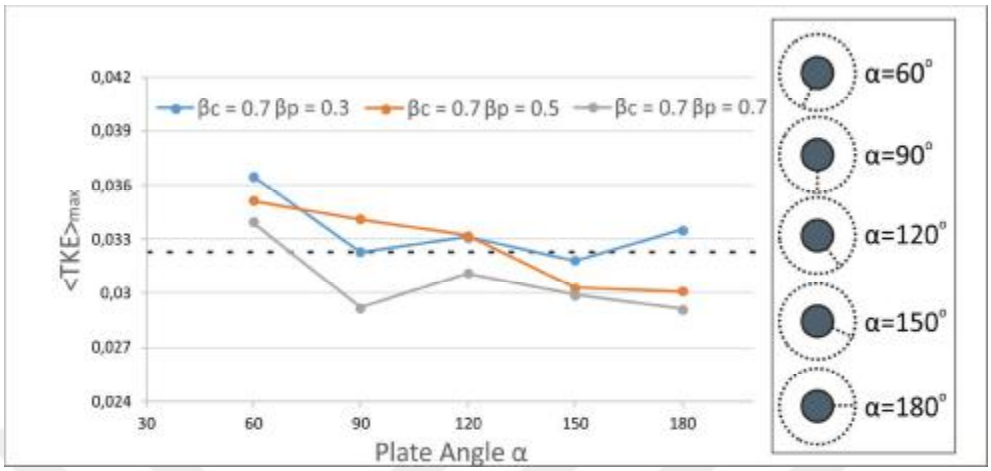

Figure 4.15 The effect of porosity of the plate "β_p" with changing the plate angles on the TKE_{max} for the outer cylinder with the porosity of $\beta_c = 0.7$

It is more appropriate to see the effect of the porosity of the outer cylinder by holding the porosity of the plate constant. For this purpose, the TKE_{max} value of the plate with porosity of $\beta_p = 0.5$ and also values which cylinder pair for three different porosities are illustrated in the Figure 4.16. The dashed lines are added to the graph to make it easier to compare the TKE_{max} values. Each specific color represents the TKE_{max} value obtained from the cylinder pair. For example, the orange curve gives the changing of the TKE_{max} values with the porosity of the outer cylinder $\beta_c = 0.7$, while the orange dashed line gives the TKE_{max} values of cylinder pair at same porosity but without the splitter plate. As it can be seen clearly in the Figure 4.16, as the porosity of the outer cylinder increases, the increase in the TKE_{max} values is observed. In other words, the porosity of the outer cylinder proportional to the TKE_{max}. At the high plate angles especially at the angle $\alpha = 150°$, the opposite situation of the above explanation occurs. The TKE_{max} values for the outer cylinder with the porosity of $\beta_c = 0.5$ at the plate angle $\alpha = 150°$ is lower than the outer cylinder with the porosity of $\beta_c = 0.3$. For the current study, a reduction of 13% in the maximum value of TKE is achieved for the splitter plate ($\beta_p = 0.5$, $\alpha = 150°$). At the plate angle of $\alpha = 150°$ can be advisable for controlling

the shear layer interaction for the upper and lower side of the inner cylinder. Since the interactions of the shear layers can be prevented or moved farther away from the cylinder wake, consequently resulting in decreased fluctuations in the near wake. According to all figures and the results, it can be concluded that the porosity of the outer cylinder has remarkable effect on lowering the TKE_{max} values in near wake of the inner cylinder. In general, the perforated outer cylinder with low porosities, β_c such as $\beta_c = 0.3$ and $\beta_c = 0.5$ are better for diminish the TKE_{max} value. On the other hand, the porosities of the plate are less effective in reducing the TKE_{max} than the porosity of the outer cylinder.

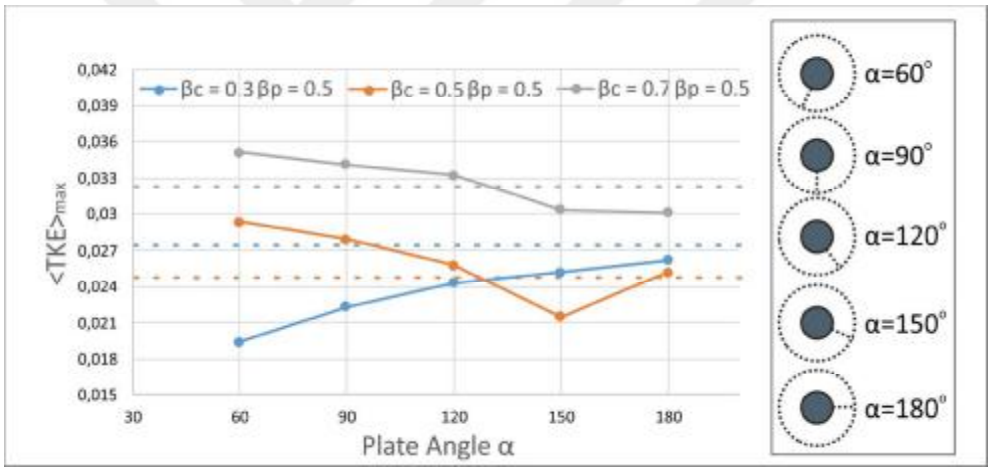

Figure 4.16 The effect of the porosity of the outer cylinder "β_c" on the TKE_{max} for the plate with the porosity of $\beta_p = 0.5$

5. CONCLUSION

The dye-injection flow visualization and Particle Image Velocimetry (PIV) technique were used to decrease undesired turbulence intensities, prevent a well-defined vorticity concentration, fluctuations of velocity components and vortex shedding in swirling motion along the cylinder surface causing the cylinder to vibrate. Under a high frequency of vortex shedding during wing storm this vibration generates sound. In order to avoid this vibration a bare cylinder was surrounded with the perforated cylinder. A quantitatively and qualitatively results were obtained experimentally for the inner cylinder with diameter of 50 mm (D_i) with concentric the perforated outer cylinder with the diameter of 125 mm (D_o).

In order to reduce the turbulence intensity acting on the inner cylinder and control the flow entering between the cylinder pair, mainly three different most effective parameters were used.

The dye visualization experiments showed that for the outer cylinder with the porosity of $\beta_c = 0.3$, the flow struggle to enter the annular region with sufficient amount, so that the flow at the exit of the outer cylinder cannot have sufficient momentum. Streamline shows that the larger focal point, F_1 occurs on the upper side of the inner cylinder when the outer cylinder with the porosity of $\beta_c = 0.3$ and the plate with the porosity of $\beta_p = 0.3$ used together. The time averaged streamline showed that using the perforated outer cylinder and the splitter plate did not create important difference on vortex formation in annular region. For almost all cases a focal point F_1 and F_2 occurred immediately downstream of the inner cylinder. However, the time averaged vorticity magnitudes had prominent effect on the flow structure.

In general, the vorticity magnitude increased proportional to the porosity of the outer cylinder, β_c. As it can be seen clearly in Figure 4.16, when the porosity of the outer cylinder increases, the TKE_{max} values also increased in the annular region. The perforated outer cylinder with low porosities, β_c such as $\beta_c = 0.3$ and $\beta_c = 0.5$

are better for diminishing the TKE_{max} value. Accordingly, the porosity of the outer cylinder has remarkable effect on lowering the TKE_{max} values in near wake of the inner cylinder. On the other hand, it can be concluded that the porosities of the plate are less effective in reducing the TKE_{max} than the porosity of the outer cylinder. The most beneficial porosity of the plate is found to be $\beta_p = 0.5$. Therefore chosing the plate with porosity of $\beta_p = 0.5$ for control the unsteady flow structure may be advisable. In comprasion with the bare cylinder case, when the porosity of the plate, $\beta_p = 0.5$ at the plate angle of $\alpha = 150°$ used with the porosity of the outer cylinder $\beta_c = 0.5$, the maximum value of TKE in annular reigon is reduced by 52%. This reduction could be considering the most effective effect for this study. Furthermore, the plate angle $\alpha = 150°$ has a trend as decreasing the maximum value of TKE for the outer cylinder with the porosities of $\beta_c = 0.5$ and 0.7. Thus, the plate angle, $\alpha = 150°$ can be advised within the aid of a complete elimination of upper and lower shear layer interactions in the annular region.

Diversification of further research and parameters can be used to increase the effectiveness of the present control method. In addition, since the region between the cylinder pair is examined in this study, it may be useful to examine the vorticy consentration that occur downstream of these cylinders. Examination of the drag coefficient (C_d) values may also be useful for understanding the detailed effects of the combined use of the outer cylinder and plate.

REFERENCES

Achenbach, E. (1971). Influence of surface roughness on the cross-flow around a circular cylinder. *Journal of Fluid Mechanics, 46*(2), 321-335.

Achenbach, E., & Heinecke, E. (1981). On vortex shedding from smooth and rough cylinders in the range of Reynolds numbers 6× 10 3 to 5× 10 6. *Journal of Fluid Mechanics, 109*, 239-251.

Akilli, H., Karakus, C., Akar, A., Sahin, B., & Tumen, N. F. (2008). Control of vortex shedding of circular cylinder in shallow water flow using an attached splitter plate. *Journal of Fluids Engineering, 130*(4), 041401.

Akilli, H., Sahin, B., & Filiz Tumen, N. (2005). Suppression of vortex shedding of circular cylinder in shallow water by a splitter plate. *Flow Measurement and Instrumentation, 16*(4), 211-219.

Allen, D., & Henning, D. (2001). *Surface roughness effects on vortex-induced vibration of cylindrical structures at critical and supercritical Reynolds numbers.* Paper presented at the Offshore Technology Conference.

Anderson, E., & Szewczyk, A. (1997). Effects of a splitter plate on the near wake of a circular cylinder in 2 and 3-dimensional flow configurations. *Experiments in Fluids, 23*(2), 161-174.

Apelt, C., & West, G. (1975). The effects of wake splitter plates on bluff-body flow in the range 10 4< R< 5× 10 4. Part 2. *Journal of Fluid Mechanics, 71*(01), 145-160.

Apelt, C., West, G., & Szewczyk, A. A. (1973). The effects of wake splitter plates on the flow past a circular cylinder in the range 10 4< R< 5× 10 4. *Journal of Fluid Mechanics, 61*(01), 187-198.

Artana, G., Sosa, R., Moreau, E., & Touchard, G. (2003). Control of the near-wake flow around a circular cylinder with electrohydrodynamic actuators. *Experiments in Fluids, 35*(6), 580-588.

Assi, G. R. S., Bearman, P. W., & Kitney, N. (2009). Low drag solutions for suppressing vortex-induced vibration of circular cylinders. *Journal of Fluids and Structures, 25*(4), 666-675.

Bearman, P. (1965). Investigation of the flow behind a two-dimensional model with a blunt trailing edge and fitted with splitter plates. *Journal of Fluid Mechanics, 21*(02), 241-255.

Bearman, P., & Harvey, J. (1993). Control of circular cylinder flow by the use of dimples. *AIAA journal, 31*(10), 1753-1756.

Berger, E. (1967). Suppression of vortex shedding and turbulence behind oscillating cylinders. *The Physics of Fluids, 10*(9), S191-S193.

Bernitsas, M. M., & Raghavan, K. (2008). *Reduction/suppression of VIV of circular cylinders through roughness distribution at 8× 103< Re< 1.5× 105.* Paper presented at the ASME 2008 27th International Conference on Offshore Mechanics and Arctic Engineering.

Bernitsas, M. M., Raghavan, K., & Duchene, G. (2008). *Induced Separation and Vorticity Using Roughness in VIV of Circular Cylinders at 8× 103< Re< 2.0× 105.* Paper presented at the ASME 2008 27th International Conference on Offshore Mechanics and Arctic Engineering.

Bhattacharyya, S., Dhinakaran, S., & Khalili, A. (2006). Fluid motion around and through a porous cylinder. *Chemical Engineering Science, 61*(13), 4451-4461.

Bruneau, C.-H., & Mortazavi, I. (2006). Control of vortex shedding around a pipe section using a porous sheath. *International Journal of Offshore and Polar Engineering, 16*(02).

Bruneau, C.-H., Mortazavi, I., & Gilliéron, P. (2008). Passive control around the two-dimensional square back Ahmed body using porous devices. *Journal of Fluids Engineering, 130*(6), 061101.

Bruneau, C. H., & Mortazavi, I. (2004). Passive control of the flow around a square cylinder using porous media. *International Journal for Numerical Methods in Fluids, 46*(4), 415-433.

Chang, C.-C., Ajith Kumar, R., & Bernitsas, M. M. (2011). VIV and galloping of single circular cylinder with surface roughness at 3.0×104≤Re≤1.2×105. *Ocean Engineering, 38*(16), 1713-1732.

Chen, W.-L., Xin, D.-B., Xu, F., Li, H., Ou, J.-P., & Hu, H. (2013). Suppression of vortex-induced vibration of a circular cylinder using suction-based flow control. *Journal of Fluids and Structures, 42*, 25-39.

Chen, Z., & Aubry, N. (2005). Active control of cylinder wake. *Communications in Nonlinear Science and Numerical Simulation, 10*(2), 205-216.

Ekmekci, A., & Rockwell, D. (2011). Control of flow past a circular cylinder via a spanwise surface wire: effect of the wire scale. *Experiments in Fluids, 51*(3), 753-769.

Enloe, C., McLaughlin, T. E., VanDyken, R. D., Kachner, K., Jumper, E. J., Corke, T. C., . . . Haddad, O. (2004). Mechanisms and responses of a single dielectric barrier plasma actuator: geometric effects. *AIAA journal, 42*(3), 595-604.

Fujisawa, N., Kawaji, Y., & Ikemoto, K. (2001). Feedback control of vortex shedding from a circular cylinder by rotational oscillations. *Journal of Fluids and Structures, 15*(1), 23-37.

Fujisawa, N., & Nakabayashi, T. (2002). Neural network control of vortex shedding from a circular cylinder using rotational feedback oscillations. *Journal of Fluids and Structures, 16*(1), 113-119.

Gabbai, R., & Benaroya, H. (2005). An overview of modeling and experiments of vortex-induced vibration of circular cylinders. *Journal of Sound and Vibration, 282*(3-5), 575-616.

Galvao, R., Lee, E., Farrell, D., Hover, F., Triantafyllou, M., Kitney, N., & Beynet, P. (2008). Flow control in flow–structure interaction. *Journal of Fluids and Structures, 24*(8), 1216-1226.

Gao, Y., Fu, S., Wang, J., Song, L., & Chen, Y. (2015). Experimental study of the effects of surface roughness on the vortex-induced vibration response of a flexible cylinder. *Ocean Engineering, 103*, 40-54.

Gerrard, J. (1966). The mechanics of the formation region of vortices behind bluff bodies. *Journal of Fluid Mechanics, 25*(02), 401-413.

Gim, O.-S., Kim, S.-H., & Lee, G.-W. (2011). Flow control behind a circular cylinder by control rods in uniform stream. *Ocean Engineering, 38*(17-18), 2171-2184.

Gozmen, B., Akilli, H., & Sahin, B. (2013). Passive control of circular cylinder wake in shallow flow. *Measurement, 46*(3), 1125-1136.

Gözmen, B., Akilli, H., & Şahin, B. (2013). Vortex control of cylinder wake by permeable cylinder. *J. Faculty Eng. Arch, 28*, 77-85.

Hyun, K., & Chun, C. (2003). The wake flow control behind a circular cylinder using ion wind. *Experiments in Fluids, 35*(6), 541-552.

Igbalajobi, A., McClean, J. F., Sumner, D., & Bergstrom, D. J. (2013). The effect of a wake-mounted splitter plate on the flow around a surface-mounted finite-height circular cylinder. *Journal of Fluids and Structures, 37*, 185-200.

Kawamura, T., Takami, H., & Kuwahara, K. (1986). Computation of high Reynolds number flow around a circular cylinder with surface roughness. *Fluid Dynamics Research, 1*(2), 145-162.

Keane, R. D., & Adrian, R. J. (1990). Optimization of particle image velocimeters. I. Double pulsed systems. *Measurement science and technology, 1*(11), 1202.

Kiu, K. Y., Stappenbelt, B., & Thiagarajan, K. P. (2011). Effects of uniform surface roughness on vortex-induced vibration of towed vertical cylinders. *Journal of Sound and Vibration, 330*(20), 4753-4763.

Kwon, K., & Choi, H. (1996). Control of laminar vortex shedding behind a circular cylinder using splitter plates. *Physics of Fluids, 8*(2), 479-486.

Landreth, C., & Adrian, R. (1988). *Measurement and refinement of velocity data using high image density analysis in particle image velocimetry.* Paper presented at the 4th International Symposium on Applications of Laser Anemometry to Fluid Mechanics.

Leclerc, E., Sagaut, P., & Mohammadi, B. (2006). On the use of incomplete sensitivities for feedback control of laminar vortex shedding. *Computers & Fluids, 35*(10), 1432-1443.

Lim, H.-C., & Lee, S.-J. (2002). Flow control of circular cylinders with longitudinal grooved surfaces. *AIAA journal, 40*(10), 2027-2036.

Meinhart, C. D., & Adrian, R. J. (1995). On the existence of uniform momentum zones in a turbulent boundary layer. *Physics of Fluids, 7*(4), 694-696.

Merrick, R., & Bitsuamlak, G. (2008). *Control of flow around a circular cylinder by the use of surface roughness: A computational and experimental approach.* Paper presented at the 4th International Conference Advances on Wind and Structures (A WAS08).

Mertz, B. E., & Corke, T. C. (2011). Single-dielectric barrier discharge plasma actuator modelling and validation. *Journal of Fluid Mechanics, 669*, 557-583.

Mimeau, C., Mortazavi, I., & Cottet, G.-H. (2014). Passive flow control around a semi-circular cylinder using porous coatings. *International Journal of Flow Control, 6*(1).

Mutschke, G., Shatrov, V., & Gerbeth, G. (1998). Cylinder wake control by magnetic fields in liquid metal flows. *Experimental Thermal and Fluid Science, 16*(1), 92-99.

Nakamura, Y. (1996). Vortex shedding from bluff bodies with splitter plates. *Journal of Fluids and Structures, 10*(2), 147-158.

Oruç, V. (2017). Strategies for the applications of flow control downstream of a bluff body. *Flow Measurement and Instrumentation, 53*, 204-214.

Oruç, V., Akilli, H., & Sahin, B. (2016). PIV measurements on the passive control of flow past a circular cylinder. *Experimental Thermal and Fluid Science, 70*, 283-291.

Ozkan, G. M., Firat, E., & Akilli, H. (2017). Control of Vortex Shedding Using a Screen Attached on the Separation Point of a Circular Cylinder and Its Effect on Drag. *Journal of Fluids Engineering, 139*(7), 071107.

Ozkan, G. M., Firat, E., & Akilli, H. (2017). Passive flow control in the near wake of a circular cylinder using attached permeable and inclined short plates. *Ocean Engineering, 134*, 35-49.

Ozkan, G. M., Oruc, V., Akilli, H., & Sahin, B. (2012). Flow around a cylinder surrounded by a permeable cylinder in shallow water. *Experiments in Fluids, 53*(6), 1751-1763.

Ozono, S. (1999). Flow control of vortex shedding by a short splitter plate asymmetrically arranged downstream of a cylinder. *Physics of Fluids, 11*(10), 2928-2934.

Park, D., Ladd, D., & Hendricks, E. (1994). Feedback control of von Kármán vortex shedding behind a circular cylinder at low Reynolds numbers. *Physics of Fluids, 6*(7), 2390-2405.

Pinar, E., Ozkan, G. M., Durhasan, T., Aksoy, M. M., Akilli, H., & Sahin, B. (2015). Flow structure around perforated cylinders in shallow water. *Journal of Fluids and Structures, 55*, 52-63.

Rashidi, S., Hayatdavoodi, M., & Esfahani, J. A. (2016). Vortex shedding suppression and wake control: A review. *Ocean Engineering, 126*, 57-80.

Rodríguez, I., Lehmkuhl, O., Piomelli, U., Chiva, J., Borrell, R., & Oliva, A. (2016). Numerical simulation of roughness effects on the flow past a circular cylinder. *Journal of Physics: Conference Series, 745*(3), 032043.

Roshko, A. (1954). *On the drag and shedding frequency of two-dimensional bluff bodies. Tech.* Retrieved from

Roussopoulos, K., & Monkewitz, P. A. (1996). Nonlinear modelling of vortex shedding control in cylinder wakes. *Physica D: Nonlinear Phenomena, 97*(1), 264-273.

Ruck, B., Klausmann, K., & Wacker, T. (2012). *The flow around circular cylinders partially coated with porous media.* Paper presented at the AIP Conference Proceedings 4.

Sarioglu, M. (2017). Control of flow around a square cylinder at incidence by using a splitter plate. *Flow Measurement and Instrumentation, 53*, 221-229.

Seal, C., & Smith, C. (1999). The control of turbulent end-wall boundary layers using surface suction. *Experiments in Fluids, 27*(6), 484-496.

Sheng, J., Meng, H., & Fox, R. (2000). A large eddy PIV method for turbulence dissipation rate estimation. *Chemical Engineering Science, 55*(20), 4423-4434.

Shukla, S., Govardhan, R. N., & Arakeri, J. H. (2009). Flow over a cylinder with a hinged-splitter plate. *Journal of Fluids and Structures, 25*(4), 713-720.

Shukla, S., Govardhan, R. N., & Arakeri, J. H. (2013). Dynamics of a flexible splitter plate in the wake of a circular cylinder. *Journal of Fluids and Structures, 41*, 127-134.

Sintu Singha, K. P. S. (2011). Control of vortex shedding from a circular cylinder using imposed transverse magnetic field. *International Journal of Numerical Methods for Heat & Fluid Flow, 21*(1), 32-45.

Şahin, B., & Ward-Smith, A. (1990). Effect of perforated plates on wide-angle diffuser-exit velocity profiles. *Journal of Wind Engineering and Industrial Aerodynamics, 34*(2), 113-125.

Tao, J., Huang, X., & Chan, W. (1996). A flow visualization study on feedback control of vortex shedding from a circular cylinder. *Journal of Fluids and Structures, 10*(8), 965-970.

Tensi, J., Boué, I., Paillé, F., & Dury, G. (2002). Modification of the wake behind a circular cylinder by using synthetic jets. *Journal of Visualization, 5*(1), 37-44.

Thomas, F. O., Kozlov, A., & Corke, T. C. (2008). Plasma actuators for cylinder flow control and noise reduction. *AIAA journal, 46*(8), 1921.

Tropea, C., & Yarin, A. L. (2007). *Springer handbook of experimental fluid mechanics* (Vol. 1): Springer Science & Business Media.

Unal, M., & Rockwell, D. (1988). On vortex formation from a cylinder. Part 2. Control by splitter-plate interference. *Journal of Fluid Mechanics, 190*, 513-529.

Valipour, M. S., Rashidi, S., Bovand, M., & Masoodi, R. (2014). Numerical modeling of flow around and through a porous cylinder with diamond cross section. *European Journal of Mechanics - B/Fluids, 46*, 74-81.

Weier, T., & Gerbeth, G. (2004). Control of separated flows by time periodic Lorentz forces. *European Journal of Mechanics - B/Fluids, 23*(6), 835-849.

Westerweel, J., Dabiri, D., & Gharib, M. (1997). The effect of a discrete window offset on the accuracy of cross-correlation analysis of digital PIV recordings. *Experiments in Fluids, 23*(1), 20-28.

Westerweel, J., Draad, A., Van der Hoeven, J. T., & Van Oord, J. (1996). Measurement of fully-developed turbulent pipe flow with digital particle image velocimetry. *Experiments in Fluids, 20*(3), 165-177.

Willert, C. E., & Gharib, M. (1991). Digital particle image velocimetry. *Experiments in Fluids, 10*(4), 181-193.

Williams, J. F., & Zhao, B. (1989). The active control of vortex shedding. *Journal of Fluids and Structures, 3*(2), 115-122.

Williamson, C. H. (1996). Vortex dynamics in the cylinder wake. *Annual review of fluid mechanics, 28*(1), 477-539.

Wolfe, D., & Ziada, S. (2003). Feedback control of vortex shedding from two tandem cylinders. *Journal of Fluids and Structures, 17*(4), 579-592.

Zdravkovich, M. (1981). Review and classification of various aerodynamic and hydrodynamic means for suppressing vortex shedding. *Journal of Wind Engineering and Industrial Aerodynamics, 7*(2), 145-189.

Zdravkovich, M. (1997). Flow around circular cylinders volume 1: fundamentals. *Oxford University Press, Oxford, 19*, 185.

Zhao, M., & Cheng, L. (2010). Finite element analysis of flow control using porous media. *Ocean Engineering, 37*(14-15), 1357-1366.

Zhou, B., Wang, X., Gho, W. M., & Tan, S. K. (2015). Force and flow characteristics of a circular cylinder with uniform surface roughness at subcritical Reynolds numbers. *Applied Ocean Research, 49*, 20-26.

CURRICULUM VITAE

Arda YENİÇUN. He finished Danişment Gazi Anatolian High School in Adana and after the graduation he entered in Mechanical Engineering Department of Cukurova University. He graduated as a Mechanical Engineer from the university in June 2013 and completed his military service in May, 2015.